Escuela de
Ingeniería y Arquitectura
Universidad Zaragoza

Efficient Simultaneous Localisation And Mapping in Large and Complex Environments

Cesar Dario Cadena Lerma

Thesis submitted in fulfillment of the requirements for the degree of Doctor of Philosophy in Computer Science and Systems Engineering

Supervised by José Neira Parra

Computer Science and Systems Engineering Department

Escuela de Ingeniería y Arquitectura

Universidad de Zaragoza

September, 2011

Efficient Simultaneous Localisation And Mapping in Large and Complex Environments

by

Cesar Dario Cadena Lerma

Submitted in fulfillment of the requirements for the degree of Doctor of Philosophy in Computer Science and Systems Engineering

Computer Science and Systems Engineering Department

Escuela de Ingeniería y Arquitectura

Universidad de Zaragoza

September, 2011

Abstract

Finding its way in the environment in which a robot operates is a basic problem that must be solved for true autonomy. There are two main aspects to this problem, known as Simultaneous Localization and Mapping (SLAM): (1) the continuous problem of estimating the location of elements of interest for the robot, and (2) the discrete problem of finding correspondences between measurements of the sensor that the robot uses to perceive its environment and the elements already in the map. In this thesis we address these two aspects of SLAM.

The estimation problem is classically solved with a filtering approach with satisfactory solutions for environments of limited size. But as the operating environments grow, basic filtering approaches are no longer an option because of their high computational cost and loss of precision. There has been great progress in advancing filtering algorithms in this sense. In this thesis we intend to push filtering algorithms further forward. We propose a highly scalable filtering algorithm, also conceptually simple to implement. The Combined Filter SLAM algorithm (CF SLAM) is a judicious combination of Extended Kalman (EKF) and Extended Information Filters (EIF) that can be used to execute highly efficient SLAM in large environments.

CF SLAM is always more efficient than any other EKF or EIF algorithm: filter updates can be executed in as low as $\mathcal{O}(\log n)$ as compared with the linear cost of the currently most efficient filtering algorithms. In the worst cases, updates are executed in linear time for CF SLAM as compared with the quadratic cost for all others. In addition to its computational cost savings, CF SLAM does not include approximations (apart from linearisations) and requires only linear memory with respect to the size of the environment.

The estimation process in SLAM is subordinated to the constraints imposed by the detected correspondences between sensor observations, and thus the algorithm that solves the correspondence must be robust. This problem is usually referred to as the data association problem. In this thesis, we address a central data association problem: detecting that the robot is revisiting a previously visited place. This problem is known as loop closing or place recognition.

We propose a place recognition algorithm for SLAM systems that works with image and 3D sensors. Our algorithm considers both appearance and geometric information of points of interest in the image and 3D data. Both near and far scene points provide information for the recognition process. Hypotheses about loop closings are generated using a fast appearance technique based on the bag-of-words (BoW) method. Our main contribution is in the verification stage, using conditional random fields (CRFs). We build on CRF-matching with two main novelties: we use both image and 3D geometric information, and we carry out inference on a Minimum Spanning Tree (MST), instead of a densely connected graph. Our results show that MSTs provide an adequate representation of the problem, with the additional advantages that exact inference is possible and the computational cost of the inference process is limited.

We evaluate our proposals in a several publicly available datasets of indoor and outdoor static and dynamic urban environments, using stereo cameras and 3D laser sensors. We compare with other methods in the state of the art to illustrate the improvements in computational cost and robustness of the methods proposed.

Resumen

El conocimiento de autolocalización en el entorno en que un robot opera es un problema básico a solucionar para lograr una verdadera autonomía. Hay dos aspectos principales de este problema, conocido como Simultaneous Localisation And Mapping (SLAM): (1) el problema de estimación continua de la ubicación de los elementos de interés para el robot, y (2) el problema discreto de encontrar correspondencias entre medidas del sensor que el robot utiliza para percibir el entorno y los elementos ya incluidos en el mapa. En esta tesis nosotros abordamos estos dos aspectos del SLAM.

Clásicamente el problema de estimación ha sido resuelto con un enfoque de filtrado, con soluciones satisfactorias para entornos de tamaño limitado. Pero, a medida que los entornos de operación crecen en escala, los enfoques básicos de filtrado no son más una opción debido a su alto costo computacional y pérdida de precisión. Ha habido un gran progreso en mejorar los algoritmos de filtrado en este sentido. En esta tesis, nuestra intención es avanzar aún más allá en los enfoque de filtrado. Proponemos un algoritmo de filtrado altamente escalable y conceptualmente simple de implementar. El Combined Filter SLAM (CF SLAM) es una cuidadosa combinación de los filtros extendidos de Kalman (EKF) y de Información (EIF) que puede ser usado para ejecutar SLAM muy eficientemente en entornos grandes.

CF SLAM es siempre más eficiente que cualquier otro algoritmo basado en EKF o EIF: las actualizaciones del filtro pueden ser realizadas en un orden tan bajo como $\mathcal{O}(\log n)$ en comparación con el costo lineal de los algoritmos más eficientes actuales. En el peor de los casos, CF SLAM ejecuta las actualizaciones en tiempo lineal, en comparación con el costo cuadrático de los demás. Además de sus ventajas en eficiencia, CF SLAM no realiza aproximaciones (aparte de linealizaciones) y sólo requiere memoria lineal con el tamaño del ambiente modelado.

El proceso de estimación está supeditado a las restricciones que imponen las correspondencias entre observaciones del sensor, por lo cual el algoritmo que resuelve las correspondencias debe ser tan robusto como sea posible. Este problema generalmente se denomina el problema de asociación de datos. En esta tesis hemos abordado un problema central en la asociación de datos: detectar que el robot está revisitando un lugar previamente visitado. Este problema es conocido como cerrado de bucles o reconocimiento de lugares

Proponemos un algoritmo de reconocimiento de lugares para sistemas de SLAM que funciona con sensores visuales y tambin 3D. El algoritmo considera tanto la información de apariencia como la geométrica de los puntos de interés de la imagen, así como los puntos tanto cercanos como lejanos al sensor. Nos apoyamos en un método basado en bag of words (BoW) para una eficiente generación de candidatos y hacemos nuestro principal aporte en la etapa de verificación de éstos con un método basado en los conditional random fields (CRFs). Nuestro CRF-matching tiene dos novedades principales, el uso de información de imagen y de geometría 3D, y la definición de la estructura del grafo con un minimum spanning tree (MST), lo que nos permite llevar a cabo una inferencia eficiente y exacta.

Evaluamos nuestras propuestas en un gran número de datasets de acceso público de entornos urbanos de interiores y exteriores, y estáticos y dinámicos, usando cámaras estéreo y sensores de 3D con láser. Mostramos comparaciones cuantitativas con otros métodos en el estado del arte e ilustramos las ventajas de cada una de nuestras contribuciones.

Contents

List of Abbreviations

AM	Active Matching
ATE	Absolute Trajectory Error
BoW	Bag of Words
BP	Belief Propagation
CF SLAM	Combined Filter SLAM
CI	Consistency Index
CI-Graph	Conditional Independent Graph
CRF	Conditional Random Field
D&C	Divide & Conquer
DoF	Degree of Freedom
DP-SLAM	Distributed Particle SLAM
EC	Epipolar Constraint
EIF	Extended Information Filter
EKF	Extended Kalman Filter
ESDF	Exactly Sparse Delayed-State Filter
FAB-MAP	Fast Appearance Based Mapping
GC	Geometrical Checking
GT	Ground Truth

HMM	Hidden Markov Model
I-SLSJF	Iterated SLSJF
IC	Individual Compatibility
ICP	Iterative Closest Point
IF	Information Filter
iSAM	incremental SAM
JCBB	Joint Compatibility Branch and Bound
jEIF	joining with EIF
KF	Kalman Filter
LIDAR	Light Detection And Ranging
MAP	Maximum A Posteriori
MB	Markov Blanket
MEMM	Maximum Entropy Markov Model
MRF	Markov Random Field
MST	Minimum Spanning Tree
NEES	Normalised Estimation Error Squared
NN	Nearest Neighbour
PCA	Principal Component Analysis
PR	Place Recognition
PTAM	Parallel Tracking And Mapping
RANSAC	Random Sample Consensus
RJC	Randomised Joint Compatibility
RMSE	Root Mean Squared Errors

RSLAM	Relative SLAM
SAM	Smoothing And Mapping
SEIF	Sparse EIF
SIFT	Scale Invariant Feature Transform
SLAM	Simultaneous Localisation And Mapping
SLAMIDE	SLAM In Dynamic Environments
SLSJF	Sparse Local Submap Joining Filter
SPA	Sparse Pose Adjustment
SSE	Sum of Squared Errors
SURF	Speed Up Robust Feature
TSAM	Tectonic SAM

Chapter 1

Introduction

1.1 Motivation

What does the world look like? Where am I? The answer to these two fundamental questions is the first step in building an autonomous robot able to navigate safely and effectively in an unknown environment. Answering these questions at the same time is known as simultaneous localisation and mapping (SLAM): a robot estimates its position with respect to a simultaneously mapped environment.

Mapping the environment has a direct and critical influence on basic robotic tasks, such as collision avoidance and path planning, and also in non-autonomous applications such as teleoperation in unknown and risky areas. The real world is complex, irregular, and dynamic. Furthermore, available sensors usually provide noisy measurements, and robots must operate robustly in this complex world.

To navigate reliably, mobile robots must also know where they are in the environment. In order to localise itself, a robot needs access to relative and absolute measurements both about its motion and about the environment surrounding the robot. Given this information, the robot should determine its location as accurately as possible.

Over the past two decades mobile robotics research in the simultaneous localisation and map building problem has been very active. Nowadays most robots operate in controlled and limited environments and are expensive. There are only a few examples of low-cost robots with limited use at home, like the Roomba vacuum cleaner.

Of course, the quality of the mapping and pose estimation depends on the quality of the sensors, but as the robot operates in larger and more complicated environments, the limiting factor becomes *algorithmic*: the amount of computational effort required to process sensor observations grows quickly with the number of observations and size of the environment. Conventional stochastic solutions to SLAM, which involve the computation of covariance matrices, are in general of complexity $\mathcal{O}(n^2)$ in the number of features (or landmarks) in the map.

Much effort has been made to reduce the complexity of the *estimation process* (or back-end) in SLAM algorithms. However, that is not enough for solving the problem, it is mandatory to also solve *data association*, the front-end. Association of sensor measurements with map features becomes difficult as errors in position estimations increase. Reliable detection and association of landmarks plays a major role in autonomous localisation and mapping.

The most of current outdoor robotic platforms are based on sensors that provide geometric (range and bearing) information. Although these sensors are accurate, they only provide geometric profiles of objects which are, in general, insufficient for recognition. Imaging sensors provide richer information such as texture, and, in most cases, are less expensive than ranging sensors. Appearance information has the difficulty of interpretation, but it also gives a complementary point of view to purely geometric information. In addition to the latter, these kind of sensors have almost unlimited range, which has the inconvenience of increasing the difficulty of managing the information of far-field objects, but also opens the opportunity for using such information.

Another major problem when performing localisation and mapping in large outdoor environments is reliable data association. As the uncertainty over the position of landmarks and vehicle grows, correct associations can be very difficult. If an incorrect data association hypothesis is accepted and introduced in the estimation process, the estimation may become inconsistent, and this can compromise the correctness of the map. The detection of revisited places, or loop closure, in SLAM is also a significant issue when a robot follows a long path. Without closing the loop, the uncertainty of the robot grows unbounded, making the map less precise and further associations more difficult.

In this thesis we are concerned advance the state of the art by making SLAM systems *more efficient* (so they can handle larger environments) and *more robust* to sensor noise and ambiguity.

1.2 The Estimation problem

Since the mid 80s, SLAM has been widely addressed using different approaches, see (Bailey and Durrant-Whyte 2006; Durrant-Whyte and Bailey 2006) for a comprehensive review. Researchers have devoted much effort to develop algorithms to improve the computational efficiency of SLAM in large scale environments. We find work in Extended Kalman filters (EKF) and Extended Information filters (EIF) (Dissanayake et al. 2001; Thrun et al. 2005), particle filters (Burgard et al. 1996; Thrun 2002), nonlinear optimization (Grisetti et al. 2007a; Olson et al. 2006), and sparse linear algebra (Dellaert and Kaess 2006), to name a few.

The earliest formulation for SLAM was the EKF of Smith et al. (1988). Although it is very popular, its limiting computational properties are well known (Thrun et al. 2005). Given a map of n features, the classical EKF SLAM algorithm has a cost of $\mathcal{O}(n^2)$ per update step.

One important contribution has been the idea of splitting the full map into local maps and then putting the pieces back together in some way. Decoupled Stochastic Mapping (Leonard and Feder 2001), Constant Time SLAM (Leonard and Newman 2003) and the ATLAS system of Bosse et al. (2004) are local mapping solutions close to constant time, although through approximations that reduce precision. Map Joining of Tardós et al. (2002) and the Constrained Local Submap Filter of Williams et al. (2002) are exact solutions (up to linearisation) that require periodical $\mathcal{O}(n^2)$ updates. Map Joining builds the map by joining a sequence of independent local submaps with EKF. This leads to a more consistent map in addition to computational savings. The Constrained Local Submap Filter is a technique similar to Map Joining.

Belonging to the group of exact solutions with submapping, two recent algorithms have provided important reductions in computational cost: D&C SLAM of Paz et al. (2008) has an amortised cost $\mathcal{O}(n)$ per step, and Sparse Local Submap Joining (SLSJF) SLAM of Huang et al. (2008a) reports a cost $\mathcal{O}(n^{1.5})$ per step in the worst case. D&C SLAM introduces an improved method of managing the submaps which postpones expensive joining operations of large maps. SLSJF takes advantage of the sparsity of the information form to reduce the computational complexity.

Recently proposed, the CI-Graph (Pinies et al. 2009) is an algorithm in which the local maps are conditionally independent. CI-Graph keeps the submaps separate, but additionally, it takes into account that information may be shared between submaps, breaking their independence. A spanning tree topology is used to handle environments with many loops. The price for keeping the conditional independence between submaps is some overhead in the size of the submaps: all the extra components added in different submaps in order to keep the conditional independence and to propagate the information in updates. However, CI-Graph reduces memory requirements when exploring an environment as it does not need to maintain all covariance matrix entries. The authors empirically obtained a cost per step close to linear in the worst case.

Exact solutions also include incremental Smoothing and Mapping (iSAM) of Kaess et al. (2008) and Tectonic SAM of Ni et al. (2007), and their more recent and efficient versions: iSAM2 (Kaess et al. 2011) and TSAM2 (Ni and Dellaert 2010), respectively. These solutions keep the full trajectory and all features in the state vector and use the square root of the information matrix to efficiently solve the SLAM problem. Using also the information form, Frese (2006) proposed the Treemap, which captures the sparse structure of the system using a tree representation. Each leaf in the tree is a local map and the consistency of the estimation is achieved by sending updates to the local maps through the tree. This is a very efficient algorithm but it is not exact: where there are many overlapping features, it uses a weak link breakage policy in order to prune edges and thus maintain the tree structure. Under topological restrictions on the environment, Treemap has a cost $\mathcal{O}(\log n)$ per step. However, if the map has many local connections, the size of the local maps can be very large and their updates become computationally expensive, as shown by Konolige et al. (2010b). In this thesis we aim at further reducing the computational complexity of EKF and EIF-based algorithms, without any sacrifice of precision or accuracy.

The SLAM problem has also been addressed using particle filters (Thrun 2002). The particle filter keeps a number k of possible locations of the robot, and computes an alternative map for each. The most efficient SLAM algorithms based on particle filters factorise the problem so that only the vehicle location is represented with a set of particles, and have a cost $\mathcal{O}(nk)$ per step (Eliazar and Parr 2004; Grisetti et al. 2007b; Montemerlo et al. 2003; Törnqvist et al. 2009). In FastSLAM (Montemerlo et al. 2002) each particle represents a distinct hypothesis of the vehicle trajectory and has its own EKF associated with it to estimate the map. The particles are dispersed according to the motion model in order to create a proposal distribution. Each particle is then weighted and re-sampled according to the measurements model. Montemerlo et al. (2003) refine the algorithm, FastSLAM 2.0, by modifying the proposal distribution to improve the richness of particles in the most likely regions of the posterior distribution. The DP-SLAM of Eliazar and Parr (2004) is an algorithm analogous to FastSLAM, where evidence grids rather than EKFs are used to represent map information.

An important advantage of particle filters is that they are more robust to data association errors. However, due to the potentially large number of particles, careful memory management is needed for efficient implementation. The consistency and robustness of these algorithms depends on the number k of particles in the filter. In order not to underestimate the uncertainty, this number must grow with the size of the environment that is expected to map.

When the application requires mainly a very accurate localisation of the robot, and a detailed map is of secondary importance, the use of Pose-based SLAM (Eustice et al. 2006; Grisetti et al. 2008; Olson et al. 2006) become interesting. Eustice et al. (2006) proposed an exactly sparse information filter that keeps the entire pose history and marginalises the landmarks. Olson et al. (2006) suggested a gradient descent approach to optimise pose graphs. Grisetti et al. (2009) extended this approach by applying a tree-based parametrisation that increases the speed of convergence. Both approaches assume that the error is uniformly distributed over the pose graph. Konolige et al. (2010b) presented the Sparse Pose Adjustment (SPA), an optimised implementation of the underlying bundle adjustment that solves very large 2D SLAM problems with several thousand poses very quickly. It takes the covariance in the constraints into account. This leads to more a accurate solution, with very fast convergence and is fully non-linear.

In this series of improvements for pose-graphs, g2o was proposed by Kümmerle et al. (2011), a general framework for performing optimisation of non-linear least squares problems that can be represented as a graph. This toolkit exploits the sparse connectivity of the graph and advanced sparse linear solvers to be more efficient. Another pose-based SLAM solution is proposed by Ila et al. (2010), the Information-based Pose SLAM. It maintains efficiency by including only some informative poses from the odometry information, and only a few loops. There is a trade-off between precision and efficiency in the estimation. Although the authors claim an amortised constant cost of updating loop closures until the next one comes up, it is not possible to know in advance when the next informative loop closure will take place.

Pose-based methods do not compute an optimal environment structure, and instead focus on computing the optimal vehicle trajectory. They keep a state vector containing all or some of the poses of the robot, the map must be computed *a posteriori*.

In the vision community, the SLAM problem is known as Structure From Motion (SFM), and it has been classically solved with bundle adjustment (Triggs et al. 2000). In mobile robotics, many SFM ideas from computer vision have been applied with success. Some solution are the proposals by Klein and Murray (2007); Konolige and Agrawal (2008); Mei et al. (2011); Sibley et al. (2009); Strasdat et al. (2010). Klein and Murray (2007) split tracking and map building into parallel threads in their PTAM system, with different timing requirements. While tracking has to be performed in real-time, the map is extended only by selecting keyframes and can be more time consuming. Their approach has set a benchmark with respect to accuracy and speed, although it is still restricted to operation in small desktop environments. Konolige and Agrawal (2008) proposed the FrameSLAM which reduces the number of camera poses and 3D points. They showed that, even with reduced data, the same accuracy could be reached using bundle adjustment. FrameSLAM keeps only some keyframes in a skeleton. It performs a local optimisation in exploration mode, and full optimisation over the skeleton in loop closures. Konolige et al. (2010a) extended this work to the View-based Maps, including place recognition and multisession mapping. Sibley et al. (2009) introduced a new representation of the map structure and camera poses. Map points and camera poses are described by their relative positions. A local-consistency optimiser, an adaptive relative bundle adjustment, updates the state. They show constant-time updates, even in the presence of loop closures, guaranteeing a locally consistent system. The same idea is exploited by Mei et al. (2011) with their RSLAM system. RSLAM is again a locally consistent optimiser rather than an exact solution to the SLAM problem. Very recently, Strasdat et al. (2010) uses a bundle adjustment in sliding a window during exploration mode. In the event of loop closure, the relative similarity transform between all the camera poses is optimized. The scale drift of monocular tracking is also taken into account. Their results in terms of accuracy are comparable to the standard bundle adjustment. In the most recent work from the same authors (Strasdat et al. 2011), they propose a double window to optimise a common cost function. The inner window has the pose-point constraints from the immediate environment to the camera; the outer window has the pose-pose soft constraints of key-poses in the periphery. The constant time claimed by Strasdat et al. (2011) is obtained only for outer window of constant number of key-poses, therefore it is again a locally consistent optimiser rather than a exact solution to the global-metric SLAM problem.

Other interesting approaches to the estimation problem are topological maps (Cummins and Newman 2008; Ranganathan and Dellaert 2011). Topological maps allow one to determine in which place the robot is located, and what the adjacency of the place may be. Cummins and Newman (2008) proposed FAB-MAP, a very efficient visual appearance based system. In FAB-MAP the places of the topology are disjunct images captured by the vehicle. Ranganathan and Dellaert (2011) use a particle filter to infer the topology of the graph of places. The system is independent of the sensor used by the robotic platform. In this thesis we will compare our results with the FAB-MAP system.

1.3 The Data Association problem

Determining a correspondence between the observed data and quantities to be estimated is known as the *data association* problem (Christensen and Hager 2008). It is an essential step for the estimation process, and it is one of the most difficult problems in SLAM (Thrun and Leonard 2008). In the second part of this thesis we discuss the crucial, and sometimes omitted, problem of data association in SLAM. This problem arises in two situations: continuous data association, or feature tracking, and loop closure or the place recognition problem.

1.3.1 Continuous Data Association

Data association has been addressed classically within the EKF paradigm for SLAM by finding the measurement-to-track correspondence (Bar-Shalom and Fortmann 1988) because a prior state and covariance ($\mu_{t-1}, \mathbf{\Sigma}_{t-1}$) are available. This allows one to predict features in the sensor frame, and compare with the current observations. This is done by carrying out statistical tests to find possible matches based on stochastic geometry. When additional information is available, such as texture or appearance in vision sensors, it is possible obtain matchings based not only on location but also on appearance.

The most basic method is the Nearest Neighbour Standard Filter, or simply Nearest Neighbour (NN). The NN rule selects the closest compatible matchings given by the normalised squared innovation test (Bar-Shalom and Fortmann 1988). Although it is a very simple and efficient method and widely used, it is not reliable in cluttered environments or with very noisy sensors because it overlooks the fact that the predicted features are correlated, and therefore, the compatibility should be ensured jointly and not only individually.

The Joint Compatibility Branch and Bound (JCBB) technique of Neira and Tardós

(2001) addresses this issue. It matches features via a deterministic interpretation tree (Grimson 1990) and has been successfully used in different SLAM applications (Clemente et al. 2007; Fenwick et al. 2002; Kaess and Dellaert 2009; Tardós et al. 2002; Williams et al. 2007). JCBB traversal considers a joint Gaussian prior on feature positions and calculates the joint probability that any particular hypothesised set of correspondences is correct. The disadvantage of the JCBB technique is its possible exponential cost in the number of measurements. Paz et al. (2008) proposed the Randomised Joint Compatibility (RJC) to overcome this problem. The RJC randomises the jointly compatible space search in the spirit of random sample consensus RANSAC (Fischler and Bolles 1981). The model is the joint compatibility of a small random set of measurements. The remaining measurements are verified to be jointly compatible with the model. The set with greater support is chosen as the final data association solution.

The RJC was developed for data association between local maps in the D&C SLAM algorithm, due to the growing in the size of the joined maps. But the RJC is also applicable to sequential mapping with a high number of observations. Another efficient algorithm for data association in visual SLAM, the 1-point RANSAC, has been proposed recently by Civera et al. (2009). The 1-point RANSAC is a combination of RANSAC and EKF, that uses the prior probabilistic information from EKF update step in the RANSAC model hypothesis stage. In the visual SLAM context the Active Matching algorithm was developed by Chli and Davison (2008), together with its more efficient version Scalable Active Matching (Handa et al. 2010). This technique searches sequentially for correspondences guided by expected information gain as function of the covariance of the innovation. Both, 1-point RANSAC and Active Matching were conceived to raise the frame rate bound in the sequential matching process in an EKF framework, where the covariance matrices are directly available.

Bibby and Reid (2007) proposed a SLAM solution in dynamic environments (SLAMIDE). The main idea is to carry out the data association, using either NN or JCBB, in sliding windows before to incorporate the information to the whole state. If a data association is wrong it can be detected inside the sliding window, then be rejected before it is incorporated to the global estimate. However, it is not able to incorporate loop closure events.

In terms of local maps, up to now the best way to find the correspondences between submaps is perhaps the RJC. However, for full overlap or high uncertainty in two large submaps finding the correspondences could have a prohibitive computational cost.

1.3.2 Place Recognition

Detecting when a mobile robot is in a place already visited is fundamental to the SLAM context, to recover from failures and to select policies of exploration in active SLAM. Since cameras are easily available and provide rich scene detail, place recognition using visual information has been a problem of great interest in robotics for some time.

Most successful methods consider appearance or geometric information, or a combination of both. Williams et al. (2009) compared three loop closure methods representative of each idea: a map-to-map method that considers mainly geometry, an image-to-image method that considers only appearance, and an image-to-map method that considers both. The best results were obtained for the image-to-image and image-to-map methods, although the image-to-map method does not scale well in large environments.

The image-to-image method considered in the work of Williams et al. (2009) was FAB-MAP, the first successful appearance-only method, proposed by Cummins and Newman (2008). FAB-MAP uses the bag-of-words (BoW) representation (Sivic and Zisserman 2003), supported by a probabilistic framework. This system proved very successful in large scale environments. It can run with full precision (no false positives), although at the expense of low recall (the rate of true positives declines). Avoiding false positives is crucial because they result in failure to obtain correct maps, but avoiding false negatives is also important because they limit the quality of the resulting maps, particularly if large loops are not detected. Geometric information has shown to be important in avoiding false positives while sacrificing less true positives. Angeli et al. (2008) proposed an incremental version of BoW, using a discrete Bayes filter to estimate the probability of loop-closure. Since the Bayes filter can still exhibit false positives in cases where the same features are detected, but in a different geometric configuration, the epipolar constraint was used to verify candidate matchings. Valgren and Lilienthal (2007, 2010) also verify topological localisation candidates using the epipolar constraint. Matching of an image is carried out against the complete image database, which can become inefficient for large environments.

Other methods have shown the importance of incorporating geometric constraints to avoid false positives. Olson (2009) tests the *spatial* consistency of a set of candidate matchings by additionally considering their associated pose estimates. This requires odometry or some other source for the priors on the poses. Cummins and Newman (2010) incorporated a simplified constraint check for an omni-directional camera installed on a car in FAB-MAP 2.0. This system was tested using two extremely large (70km and 1000km) datasets. They obtain recall rates of 48.4% and 3.1%, respectively, at 100% precision. Recently proposed by Paul and Newman (2010), FAB-MAP 3D additionally includes 3D distance between features provided by a laser scanner. This results in higher recall for the same precision in the first urban experiment of FAB-MAP. However, the system can only make inferences about visual features in the laser range.

The place recognition problem has also been addressed using only 3D range data. Steder et al. (2010) extract features from range images obtained by a 3D laser scanner and query a database in order to detect loop closures. This system has high computational requirements compared with systems based on BoWs, but higher recall is attained for the same precision. An important limitation is that this system cannot distinguish between locations with similar shape but different appearance, for example corridors, or with different background beyond sensor's range.

1.4 Contributions

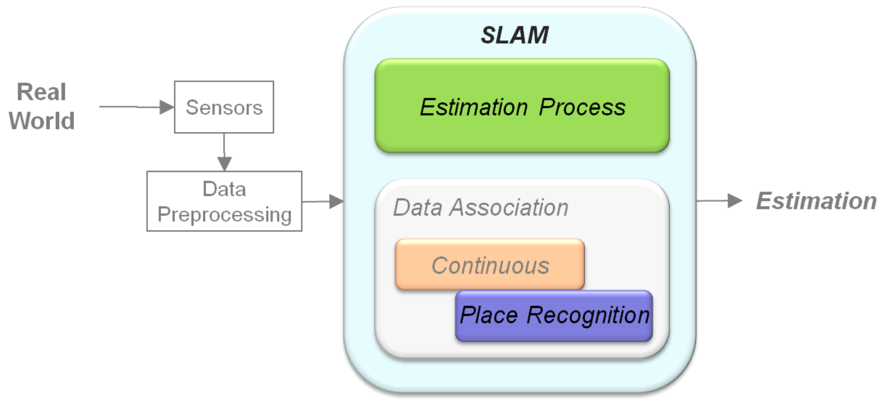

Figure 1.1: Our contributions are focused in the efficiency of the estimation process and in the robustness of the place recognition process.

Our main contributions in this thesis are:

- An **sublinear** algorithm for the state vector estimation, the Combined Filter (CF). The CF SLAM algorithm is a judicious combination of Extended Kalman and Extended Information Filters, using a divide and conquer local mapping strategy. Chapter 2 describes the CF SLAM details with its properties on complexity and consistency and its performance in real environments.

- A **robust** algorithm for loop closing using stereo cameras that considers both appearance and geometric information of points of interest in the images. Chapter

3 is dedicated to describe the place recognition system evaluating it in real and challenging experiments.

Our two main contributions are assembled in a unified featured-based SLAM system, which is tested in different environments with different sensors in chapter 4. We demonstrate how the whole system successfully operates in larger and more complex environments than previous approaches.

Chapter 2

The Combined Filter SLAM

We devote the first part of the thesis to detailing our contribution to the estimation problem, the improvement of the computational efficiency of EKF SLAM. As we have seen in the introduction of the thesis, there are several approaches to the estimation process. In section 2.1 we focus on featured-based SLAM and we describe the filtering and submapping approaches. We include a detailed description of the improvements that have been reported on the use of Kalman and Information filters for SLAM, leading to the algorithm that we propose in this thesis. Then, we describe our contribution to the estimation problem in SLAM, the Combined Filter SLAM (CF SLAM) algorithm, a highly efficient filtering algorithm in section 2.2; the section 2.3 contains a study of its properties relative to computational cost and consistency. We carry out comparisons with state of the art algorithms using benchmark datasets, like the Victoria Park and DLR datasets, in section 2.6. We also propose data association strategies for CF SLAM in section 2.7. Finally, we summarise the results and draw the fundamental conclusions of our contribution.

2.1 Extended Kalman filters, Extended Information filters and Map Joining filters

In this section we summarise the basic concepts of the basic Kalman Filter and the basic Information Filter, as well as Map Joining techniques and the state of art SLAM algorithms that use them.

2.1.1 The Extended Kalman Filter

The Extended Kalman Filter (EKF) is one of the main paradigms in SLAM (Thrun et al. 2005; Thrun and Leonard 2008). In EKF SLAM, a map $(\mu, \mathbf{\Sigma})$ includes the mean of the state distribution μ to be estimated, which contains the current vehicle location and the location of a set of environment features. The covariance of the distribution, represented by $\mathbf{\Sigma}$, gives an idea of the precision in the estimation (0 meaning total precision). EKF SLAM is an iterative prediction-sense-update process whose formulation we believe is widely known and is thus summarised in Table 2.1. During exploratory trajectories, and using a sensor of limited range thus providing a more or less constant number of r features by observation, the size of the map n grows linearly. Given that each EKF update step is $\mathcal{O}(n^2)$, the *total* cost of carrying out EKF SLAM is known to be $\mathcal{O}(n^3)$.

	EKF-SLAM	
Prediction	$\mu_{t\|t-1} = g(u_t, \mu_{t-1})$	$\mathcal{O}(1)$
	$\mathbf{\Sigma}_{t\|t-1} = F_t \mathbf{\Sigma}_{t-1} F_t^T + G_t R_{t-1} G_t^T$	$\mathcal{O}(n)$
Innovation	$\nu_t = z_t - h(\mu_{t\|t-1})$	$\mathcal{O}(r)$
	$S_t = H_t \mathbf{\Sigma}_{t\|t-1} H_t^T + Q_t$	$\mathcal{O}(r^3)$
Test χ^2	$D^2 = \nu_t^T S_t^{-1} \nu_t$	$\mathcal{O}(r^3)$
	$K_t = \mathbf{\Sigma}_{t\|t-1} H_t^T / S_t$	$\mathcal{O}(nr^2)$
Update	$\mathbf{\Sigma}_t = (I - K_t H_t) \mathbf{\Sigma}_{t\|t-1}$	$\mathcal{O}(n^2 r)$
	$\mu_t = \mu_{t\|t-1} + K_t \nu_t$	$\mathcal{O}(n)$
Cost per step	$\mathcal{O}(n^2)$	

Table 2.1: Formulations of the computational cost of each of the operations carried out using the Extended Kalman Filter in the SLAM problem. Variable n is the size of the final state μ_t, and r is the size of the measurement vector z_t, **constant** in EKF-SLAM. The test χ^2 is only required for data association.

Jacobians	
$F_t = \left.\frac{\partial g(u_t, \mu_{t-1})}{\partial \mu_{t-1}}\right\|_{\hat{\mu}_{t-1}}$	$\mathcal{O}(1)$
$G_t = \left.\frac{\partial g(u_t, \mu_{t-1})}{\partial u_t}\right\|_{\hat{u}_t}$	$\mathcal{O}(1)$
$H_t = \left.\frac{\partial h(\mu_{t\|t-1})}{\partial \mu_{t\|t-1}}\right\|_{\hat{\mu}_{t\|t-1}}$	$\mathcal{O}(r)$

Table 2.2: Jacobians required for the EKF and EIF. Variable r is the size of the measurement vector z_t.

2.1.2 The Extended Information Filter

In Extended Information Filter (EIF) SLAM, a map estimated $(\xi, \mathbf{\Omega})$ consists of the information state ξ to be estimated and the information matrix $\mathbf{\Omega}$, which gives an idea of the information known about the estimation (0 meaning no information). EIF SLAM is also an iterative prediction-sense-update process, its formulation is summarised in Table 2.3. The Information filter is an algebraic equivalent to the Kalman filter, because the following equivalences hold (Mutambara 1994):

$$\mathbf{\Omega} = \mathbf{\Sigma}^{-1} \qquad and \qquad \xi = \mathbf{\Sigma}^{-1}\mu \tag{2.1}$$

For this reason, KF and IF are considered dual filters (Mutambara and Al-Haik 1997). Unfortunately, in the nonlinear case the filters are not completely dual, since both the transition function g and the measurement function h require the state as input (Thrun et al. 2005). For this reason, the initial required computation during the prediction step is to derive the state variables μ_{t-1}. In the general case, the EIF is considered computationally more expensive than the EKF: computing the state μ_{t-1} is $\mathcal{O}(n^3)$ because of the inversion of the the information matrix $\mathbf{\Omega}_{t-1}$. In the SLAM context, the information matrix has special structural properties, thus state vector recovery can be carried out by solving an equation system of size n very efficiently through the Cholesky decomposition. An important insight into reducing the computational cost of EIF SLAM was to observe that the information matrix $\mathbf{\Omega}$ is *approximately* sparse (Thrun et al. 2005), and can be easily sparsified. This Sparse Extended Information Filter (SEIF) allows a computational cost of $\mathcal{O}(n)$ (pure exploration) up to $\mathcal{O}(n^2)$ (repeated traversal), although because of sparsification SEIF SLAM is not an exact algorithm. Another important observation regarding EIF SLAM is that if all vehicle locations are incorporated into the information vector, instead of the current one only, the information matrix becomes *exactly* sparse (Eustice et al. 2006). In this Exactly Sparse Delayed-State Filter (ESDF) SLAM, the reduction in the computational cost is the same as in SEIF. Additionally, since no approximations due to sparsification take place, the results are more precise (Eustice et al. 2005). When the state or the information vector contain only the current vehicle location, we have an *online* SLAM problem; if it contains all vehicle locations along the trajectory, we have *full* SLAM.

The total cost of ESDF is known to range from $\mathcal{O}(n^2)$ (pure exploration) to $\mathcal{O}(n^3)$

(repeated traversal), as compared with the always cubic cost of EKF SLAM. Note however that the information vector is ever increasing. Even during revisiting, every new vehicle location is incorporated in the state vector, thus increasing n. The term r in Table 2.3 refers to the field of view of the sensor, we note again that in these cases is constant with respect to n.

	EIF-SLAM	
Prediction	$\mu_{t-1} = \mathbf{\Omega}_{t-1} \backslash \xi_{t-1}$	$\mathcal{O}(nr^2)$-$\mathcal{O}(n^2 r)$
	$\Phi = F_t^{-T} \mathbf{\Omega}_{t-1} F_t^{-1}$	$\mathcal{O}(1)$
	$\mathbf{\Omega}_{t\|t-1} = \Phi - \Phi G_t (R_{t-1} + G_t^T \Phi G_t)^{-1} G_t^T \Phi$	$\mathcal{O}(n)$
	$\xi_{t\|t-1} = \mathbf{\Omega}_{t\|t-1} g(u_t, \mu_{t-1})$	$\mathcal{O}(nr)$
Innovation	$\nu_t = z_t - h(\mu_{t\|t-1})$	$\mathcal{O}(r)$
	$S_t = H_t (\mathbf{\Omega}_{t\|t-1} \backslash H_t^T) + Q_t$	$\mathcal{O}(nr^2)$
Test χ^2	$D^2 = \nu_t^T S_t^{-1} \nu_t$	$\mathcal{O}(r^3)$
Update	$\mathbf{\Omega}_t = \mathbf{\Omega}_{t\|t-1} + H_t^T Q_t^{-1} H_t$	$\mathcal{O}(r)$
	$\xi_t = \xi_{t\|t-1} + H_t^T Q_t^{-1} (\nu_t + H_t \mu_{t\|t-1})$	$\mathcal{O}(r)$
Cost per step	$\mathcal{O}(n)$ to $\mathcal{O}(n^2)$	

Table 2.3: Formulations of the computational cost of each of the operations carried out using the Extended Information Filter in the SLAM problem. Variable n is the size of the final information vector ξ_t, and r is the size of the measurement vector z_t, **constant** in EIF-SLAM. The test χ^2 is only required for data association.

2.1.3 Map Joining SLAM with EKF

Local mapping (or submapping) algorithms were the next contribution to the reduction of the computational cost of SLAM. In these algorithms, local maps of constant size p are sequentially built (in constant time because of the bounded size) and then put together into a global map in different ways.

One of such solutions, Map Joining SLAM (Tardós et al. 2002), works in the following way: given two consecutive local maps $(\mu_1, \mathbf{\Sigma}_1)$ and $(\mu_2, \mathbf{\Sigma}_2)$, the map $(\mu, \mathbf{\Sigma})$ resulting from joining their information together is computed in three initialisation-innovation-update steps, summarised in Table 2.4. A specialised version of the Extended Kalman Filter is used, where the full state vectors and covariance matrices are simply stacked in the predicted map; correspondences can then be established between features from both maps through a prediction function h, equivalent to considering a perfect measurement $z = 0, Q = 0$. Notice that this is possible because EKF allows the consideration of 0 covariance measurements. In this case, h computes the discrepancy of features from both maps in the same reference. The update step includes a computation using the function

g to first delete duplicate features appearing in both maps, and then transform all map features and vehicle locations to a common base reference, usually the starting vehicle location in the first map.

Map Joining SLAM is constant time most of the time, when working with local maps. However, map joining operations are $\mathcal{O}(n^2)$ on the final size of the map, and although it results in great computational savings (it may slash the cost by a large constant), Map Joining SLAM is still $\mathcal{O}(n^2)$ per step, just as EKF SLAM is.

	Join with EKF	
Initialisation	$\mu^- = \begin{bmatrix} \mu_1 \\ \mu_2 \end{bmatrix}$	$\mathcal{O}(n)$
	$\mathbf{\Sigma}^- = \begin{bmatrix} \mathbf{\Sigma}_1 & 0 \\ 0 & \mathbf{\Sigma}_2 \end{bmatrix}$	$\mathcal{O}(n^2)$
Innovation	$\nu = -h(\mu^-)$	$\mathcal{O}(s)$
	$S = H\mathbf{\Sigma}^- H^T$	$\mathcal{O}(s^2)$
Update	$K = \mathbf{\Sigma}^- H^T / S$	$\mathcal{O}(n^2)$
	$\mathbf{\Sigma}^+ = (I - KH)\mathbf{\Sigma}^-$	$\mathcal{O}(n^2 s)$
	$\mu^+ = \mu^- + K\nu$	$\mathcal{O}(ns)$
	$\mu = g(\mu^+)$	$\mathcal{O}(n_2)$
	$\mathbf{\Sigma} = G\mathbf{\Sigma}^+ G^T$	$\mathcal{O}(n_2^2)$
Cost per join	$\mathcal{O}(n^2 s)$	

Table 2.4: Formulations of the computational cost of each of the operations carried out for Map Joining using the Extended Kalman Filter in the best case. Variables n_1, n_2 and n are the size of the first, second and final state vector respectively, s is the size of the overlap between both submaps, and p is the size of the local map, **constant** with respect to the size of the map.

2.1.4 Map Joining SLAM with EIF

The Extended Information filter can also be used to carry out the map joining operations, as reported in the Sparse Local Submap Joining filter (SLSJF) SLAM (Huang et al. 2008a). Its application is not as straightforward as the Map Joining with EKF for two reasons. First, in Map Joining with EKF, correspondences are established by considering a perfect measurement $z = 0, Q = 0$. In the information form, 0 covariance measurements are not allowed since Q^{-1} is required in the formulation. For this reason, in SLSJF SLAM, having two consecutive local maps $(\mu_1, \mathbf{\Sigma}_1)$ and $(\mu_2, \mathbf{\Sigma}_2)$ to join, the resulting map $(\xi, \mathbf{\Omega})$ is predicted in the information form with the information of the first map, and an initial 0 (no information) from the second map. The innovation is computed considering the second map as a set of measurements for the full map ($z_t = \mu_2$, $Q_t = \mathbf{\Omega}_2^{-1}$), and the final update step computes the information state ξ and information matrix $\mathbf{\Omega}$ using the standard EIF equations. Note in Table 2.5 that g has the same functionality as in the previous section except that features are not deleted at this point, and function h transforms the features revisited from the first map to the reference of the second map.

An important observation made in (Huang et al. 2008a) is that the information matrix resulting from the map joining operation using EIF is *exactly* sparse if the vehicle locations coming from each local map are maintained in the final information state. This is a situation very similar to the full SLAM problem, except that not all vehicle locations remain, only a fraction corresponding to the final vehicle locations in each local map. There is an additional final computation of the final state μ, to make it available for potential future map joining operations. This state recovery can be done with a pre-ordering of minimum degree of the information matrix and the sparse Cholesky factorisation to solve the linear system, such as was pointed out by (Huang et al. 2008a). In this thesis we shall see that the cost of this computation can be proportional to n during exploration, and up to $\mathcal{O}(n^2)$ in the worst case.

	Join with EIF	
Initialisation	$\mu^- = g([\mu_1; \mu_2])$	$\mathcal{O}(n_2)$
	$\xi^- = \begin{bmatrix} \xi_1 \\ 0 \end{bmatrix}$	$\mathcal{O}(n)$
	$\mathbf{\Omega}^- = \begin{bmatrix} \mathbf{\Omega}_1 & 0 \\ 0 & 0 \end{bmatrix}$	$\mathcal{O}(np)$
Innovation	$\nu = \mu_2 - h(\mu^-)$	$\mathcal{O}(s)$
	$Q^{-1} = \mathbf{\Omega}_2$	given
Update	$\mathbf{\Omega} = \mathbf{\Omega}^- + H^T \mathbf{\Omega}_2 H$	$\mathcal{O}(n_2 p)$
	$\xi = \xi^- + H^T \mathbf{\Omega}_2 (\nu + H\mu^-)$	$\mathcal{O}(n_2 p)$
	$\mu = \mathbf{\Omega} \backslash \xi$	$\mathcal{O}(np^2)$ to $\mathcal{O}(n^2 p)$
Cost per join	$\mathcal{O}(n)$ to $\mathcal{O}(n^2)$	

Table 2.5: Formulations of the computational cost of each of the operations carried out for Map Joining using the Extended Information Filter in the best case. Variables n_1, n_2 and n are the size of the first, second and final information vector respectively, s is the size of the overlap between both submaps, and p is the size of the local map, **constant** with respect to the size of the map.

Jacobians			
G	$=$	$\left.\frac{\partial g(\mu)}{\partial \mu}\right\|_{\hat{\mu}}$	$\mathcal{O}(n_2)$
H	$=$	$\left.\frac{\partial h(\mu^-)}{\partial \mu^-}\right\|_{\hat{\mu}^-}$	$\mathcal{O}(n_2)$

Table 2.6: Jacobians required for the map joining operations with EKF and EIF. Variable n_2 is the size of the second state or information vector.

2.1.5 Divide and Conquer with EKF

In the Divide and Conquer (D&C) SLAM algorithm (Paz et al. 2008) it was pointed out that SLAM can be carried out in *linear* time per step if map joining operations are carried out in a hierarchical binary tree fashion, instead of a sequential fashion. The leaves of the binary tree represent the sequence of l local maps of constant size p, computed with standard EKF SLAM. These maps are joined pairwise to compute $l/2$ local maps of double their size ($2p$), which will in turn be joined pairwise into $l/4$ local maps of size $4p$, until finally two local maps of size $n/2$ will be joined into one full map of size n, the final map. The $\mathcal{O}(n^2)$ updates are not carried out sequentially, but become more distant as the map grows. An $\mathcal{O}(n^2)$ computation can then be amortised in the next n steps, making the amortised version of the algorithm linear with the size of the map. It can also be shown that the total cost of D&C SLAM is $\mathcal{O}(n^2)$, as compared to the total cost of EKF SLAM, $\mathcal{O}(n^3)$.

In this thesis we aim at further reducing the computational complexity, without any sacrifice in precision or accuracy.

2.2 The Combined Filter SLAM

In the remain of this chapter, we describe our contribution to the estimation problem in SLAM, the Combined Filter SLAM (CF SLAM) algorithm, a highly efficient filtering algorithm.

2.2.1 Method

The algorithm proposed here, Combined Filter SLAM, has three main highlights (see algorithm 1):

1. *Local mapping is carried out using standard online EKF SLAM to build a sequence of maps of constant size p.* Each local map $(\mu_i, \mathbf{\Sigma}_i)$ is computed in $\mathcal{O}(p^3)$, constant with respect to the total map size n. Each local map only keeps the final pose of the robot. EKF SLAM in local maps allows robust data association, e.g. with JCBB (Neira and Tardós 2001), and small local maps remain consistent. Before to close each local map its information form $(\xi_i, \mathbf{\Omega}_i)$ is also computed and stored still in $\mathcal{O}(p^3)$.

2. *Map joining is carried out using EIF, keeping vehicle locations from each local map in the final map.* This allows to exploit the exact sparse structure of the resulting information matrix and the join can be carried out in as low as linear time with the final size of the map. The covariance matrix is not computed after joins at the lower level.

3. *In contrast with the sequential map joining strategy followed by SLSJF, the D&C strategy is followed to decide when map joining takes place.* We will see that this will result in a total computation cost as low as $\mathcal{O}(n \log n)$, as compared with the total cost of SLSJF, $\mathcal{O}(n^2)$. Additionally, the computation per step can be amortised to $\mathcal{O}(\log n)$, as compared with $\mathcal{O}(n)$ for SLSJF. This makes CF SLAM the most efficient SLAM filtering algorithm.

Algorithm 1 The CF SLAM Algorithm

```
$maps \leftarrow \{\}$
while data from sensor do
  $map \leftarrow ekf\_slam$
  if $isempty(maps)$ then
    $maps \leftarrow \{map\}$
  else
    while $size(map) \geq size(maps\{last\})$
    or global map is needed do
      $map \leftarrow eif\_map\_join(maps\{last\}, map)$
      $maps\{last\} \leftarrow \{\}$
    end while
    $maps \leftarrow \{maps, map\}$
  end if
end while
```

2.3 Computational complexity of CF SLAM

We study initially the case of pure exploration, in which the robot is always observing new territory, and thus the sensor measurements have a constant overlap with the map already built. This case is very interesting because is the first situation that any SLAM algorithm will face, and it is also the case where the size of the map increases, and thus also the size of the problem. We discuss several other cases in section 2.5.

In exploratory trajectories, the process of building a map of size n using the proposed CF SLAM follows the divide and conquer strategy: $l = n/p$ maps of size p are produced (not considering overlap), at cost $\mathcal{O}(p^3)$ each, which are joined into $l/2$ maps of size $2p$, at cost $\mathcal{O}(2p)$ each. These in turn are joined into $l/4$ maps of size $4p$, at cost $\mathcal{O}(4p)$ each. This process continues until two local maps of size $n/2$ are joined into one local map of size n, at a cost of $\mathcal{O}(n)$. SLSJF SLAM and our algorithm carry out the same number of map joining operations. The fundamental difference is that in our case the size of the maps involved in map joining increases at a slower rate than in SLSJF SLAM.

The *total* computational complexity of CF SLAM in this case is:

$$\begin{aligned}
C &= \mathcal{O}\left(p^3 l + \sum_{i=1}^{\log_2 l} \frac{l}{2^i}(2^i\, p)\right) \\
&= \mathcal{O}\left(p^3 n/p + \sum_{i=1}^{\log_2 n/p} \frac{n/p}{2^i}(2^i\, p)\right) \\
&= \mathcal{O}\left(p^2 n + \sum_{i=1}^{\log_2 n/p} n\right) \\
&= \mathcal{O}\left(n + n\log n/p\right) \\
&= \mathcal{O}\left(n + n\log n\right) \\
&= \mathcal{O}\left(n\log n\right)
\end{aligned}$$

Therefore, CF SLAM offers a reduction in the total computational cost to $\mathcal{O}\left(n\log n\right)$, as compared with the total cost $O\left(n^3\right)$ for EKF SLAM, and $\mathcal{O}\left(n^2\right)$ for D&C SLAM and SLSJF SLAM. Furthermore, as in D&C SLAM, the map to be generated at step t will not be required for joining until step $2\,t$. This allows us to amortise the cost $\mathcal{O}(t)$ at this step by dividing it up between steps $t+1$ to $2\,t$ in equal $\mathcal{O}(1)$ computations for each step. In this way, our amortised algorithm becomes $\mathcal{O}(\log n)$ *per step*. In the worst cases the cost can grow up to $\mathcal{O}(n)$, but the cost of D&C SLAM and SLSJF SLAM will also grow, see section 2.5.

2.4 CF SLAM vs. other filtering algorithms

2.4.1 Computational cost

To illustrate the computational cost of the algorithm proposed, we conducted a simulated experiment using a simple MATLAB implementation of CF SLAM, D&C SLAM (Paz

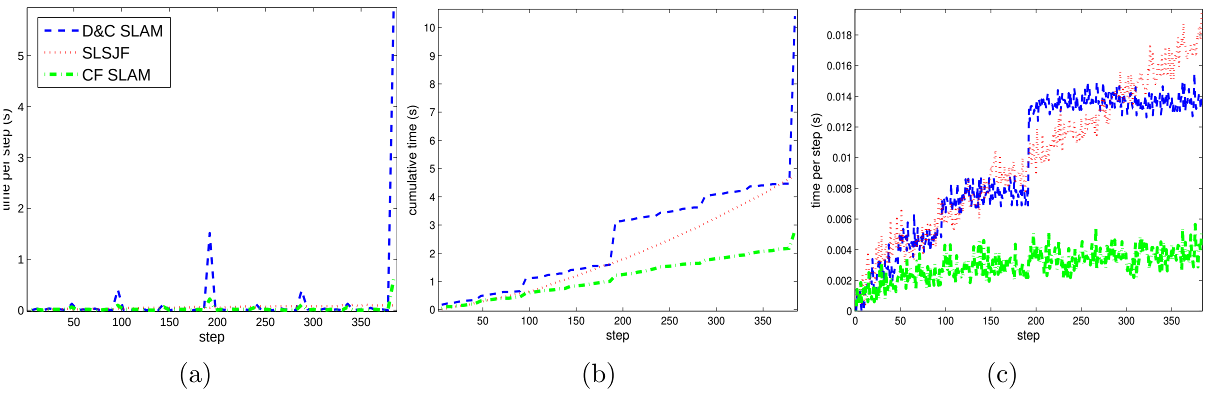

Figure 2.1: Computational time in the simulated execution for D&C SLAM (blue), SLSJF SLAM (red) and our algorithm, CF SLAM (green): Time per step 2.1(a); Total time of execution 2.1(b); Time per step for SLSJF vs. amortised time per step for D&C SLAM and our algorithm, CF SLAM 2.1(c). The final map contains 1093 features from 64 local maps.

et al. 2008), and SLSJF (Huang et al. 2008a) (with reordering using *symmmd* instead of the heuristic criteria proposed there). The simulated environment contains equally spaced point features $1.33m$ apart, and a robot equipped with a range and bearing sensor with a field of view of 180 degrees and a range of $2m$ in a pure exploratory trajectory. Local maps are built containing $p = 30$ features each. All tests are done over 100 MonteCarlo runs. Fig. 2.1 shows the resulting execution costs of the three algorithms. We can see that the total costs of D&C SLAM and the SLSJF tend to be equal, Fig. 2.1(b). This is expected, since both have a total cost of $\mathcal{O}(n^2)$. We can also see that the total cost of our algorithm increases more slowly, it is expected to be $\mathcal{O}(n \log n)$. Finally, we can see that the amortised cost of our algorithm exhibits an $\mathcal{O}(\log n)$ behaviour, always smaller than the cost of the other two algorithms, Fig. 2.1(c).

We also simulated a robot moving in a 4-leaf clover trajectory, Fig. 2.2(a). The robot is equipped with a range and bearing sensor. The features are uniformly distributed with a separation between them of $6m$. There are 1660 features and 9150 steps. 477 submaps were obtained. The cost for each EKF step in mean was $1.6ms$ with a total of $14s$, equal for all the algorithms tested. Fig. 2.2(b) shows the computation cost per step of Map Joining SLAM and SLSJF vs. the amortised cost for the D&C SLAM and CF SLAM. We can see the sublinear cost of CF SLAM in the map updates as expected. Fig. 2.2(c) shows the cumulative costs of map updates. The algorithms based on EKFs did not solve the problem completely because they exceeded the available memory before the end of the experiment.

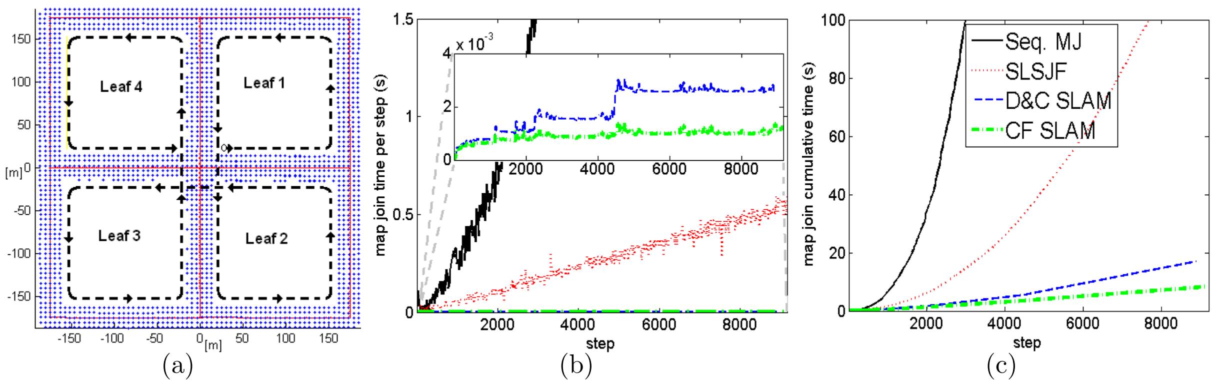

Figure 2.2: Simulated experiment of a 4-leaf clover trajectory (a). In (b) map update time per step, and map update cumulative times for all algorithms in (c).

2.4.2 Consistency

When the ground truth is available as in this simulated experiment, we can carry out a statistical test on the estimation $(\mu, \mathbf{\Sigma})$ for filter consistency. We define the consistency index, CI, as:

$$CI = \frac{D^2}{\chi^2_{n,1-\alpha}} \tag{2.2}$$

where D^2 is the Mahalanobis distance or Normalised Estimation Error Squared (NEES) (Bar-Shalom et al. 2001), $n = dim(\mu)$ and $(1 - \alpha)$ is the confidence level (95% typically). When $CI < 1$, the estimation is consistent with the ground truth, otherwise the estimation is optimistic, or inconsistent.

It is known that local map-based strategies, e.g. SLSJF and D&C SLAM, improve the consistency of SLAM by including fewer linearisation errors than strategies based on one global map, e.g. Treemap (Huang and Dissanayake 2007). We tested the consistency of SLSJF, D&C SLAM and CF SLAM on the simulated experiments with 100 MonteCarlo runs. Fig. 2.3 shows the evolution of the mean consistency index of the vehicle position in x (left) and y (center), and orientation ϕ (right), during the steps of the trajectory. We can see that the performance of the indexes for D&C SLAM and for our proposal are very similar and clearly better than for SLSJF. This is due to the fact that both D&C SLAM and our proposal follow a tree structure to carry out the map joining process. In contrast, in SLSJF map joining is sequential, thus errors increase faster in the global map. Recently, a more consistent filter based on SLSJF, I-SLSJF, was proposed by Huang et al. (2008b). This filter, in addition to being more computationally expensive than the original SLSJF, requires setting a threshold empirically to decide when it is necessary to

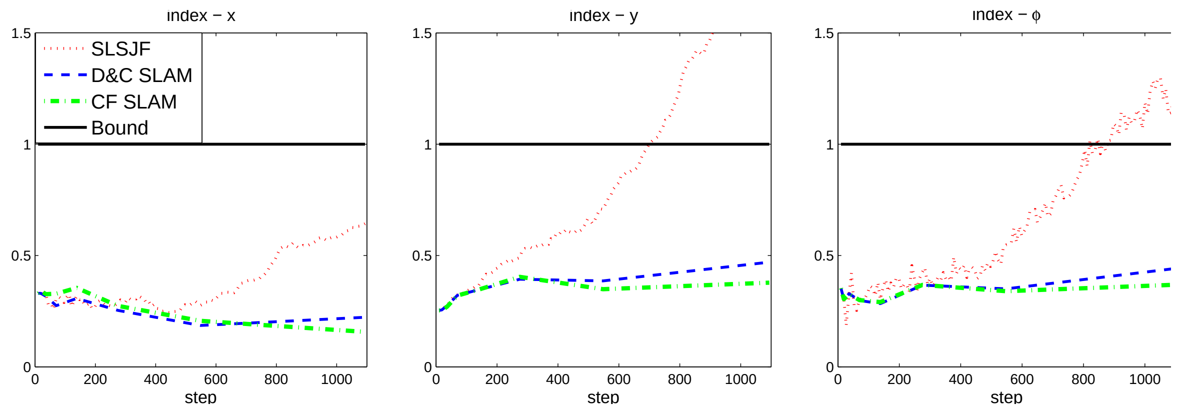

Figure 2.3: Mean consistency index CI in x, y, and ϕ for SLSJF, D&C SLAM and our CF SLAM.

solve the least squares problem and recompute the state vector from all the local maps stored.

2.5 Factors that have influence in the computational cost

2.5.1 Vehicle trajectory

Given that local mapping is a constant time operation, we concentrate on the computational cost of map joining in CF SLAM. The state recovery is the most computationally expensive operation in this case. State recovery is carried out using the Cholesky factorisation, with a previous minimum degree ordering of the information matrix. The cost of this operation depends on the sparsity pattern of the information matrix and the density of non-zero elements (Gilbert et al. 1992; Huang et al. 2008a). This in turn depends on the environment, on the sensor used and more importantly, on the trajectory of the robot.

We have used the simulated experiments to study the effect of the trajectory of the vehicle in the computational cost of the map joining operation. Fig. 2.4 shows the trajectory studied (left), the sparsification pattern of the information matrix of the final map (middle), and the mean cost (for the 100 Monte Carlo runs) of state recovery and joining between maps versus the dimension of the state vector after joining (right).

To determine the order of the computational cost, we compute a fit to equation $y = ax^b$ for the state recovery and for map joining costs. The independent variable is the dimension of the state vector resulting from each map joining. The dependent variable is the cost of the operation: `sr` for the state recovery $\mu = \mathbf{\Omega}\backslash\xi$, and `jEIF` is the cost of all operations involved in map joining with EIF, including `sr`. The results of the fit can be seen in Table 2.7. The sum of squared errors (SSE), the coefficient of determination (R^2) and root mean squared errors (RMSE) are reported.

The most important results are:

- In pure *exploratory trajectories*, Fig. 2.4 (top), the fit suggests that the exponent b can be considered equal to 1 in both state recovery and map joining operations, see Table 2.7 (top). Thus, as we said in the previous section, in the case of exploration, the cost of map joining has a linear behaviour with respect to the dimension of the state vector, and can be amortised in CF SLAM to attain $\mathcal{O}(\log n)$.

- We have also studied *lawn mowing*, Fig. 2.4 (upper middle). This type of trajectory is frequent in underwater mosaicing applications (Eustice et al. 2006). In this case, the cost can increase to $\mathcal{O}(n^{1.3})$ (see the exponent from the fit, Table 2.7).

- In another type of trajectory, *outward spiral*, Fig. 2.4 (lower middle), the cost can increase to $\mathcal{O}(n^2)$. Outward spirals are frequent in airborne mapping applications (Bryson and Sukkarieh 2008).

- In the worst case, *repeated traversal* (in this case a loop), Fig. 2.4 (bottom), the cost of map joining is linear most of the time, except in the full overlap, when the operation is quadratic with the dimension of the state vector.

Three things are important to note:

1. Whatever the cost of the map joining operation, it can be amortised in CF SLAM. This means that in the worst case, when map joining is $\mathcal{O}(n^2)$, CF SLAM is $\mathcal{O}(n)$ per step.

2. In these cases, the computational cost of D&C SLAM and SLSJF also increase in the same manner: in the worst case, both will be $\mathcal{O}(n^2)$ per step, so CF SLAM will *always* be better.

3. Worst case situations will probably not very frequent, once a map of the environment of interest is available, the robot can switch to localisation using an *a priori* map, a much less expensive task computationally.

Table 2.8 summarises the computational costs of all algorithms in the best and worst cases.

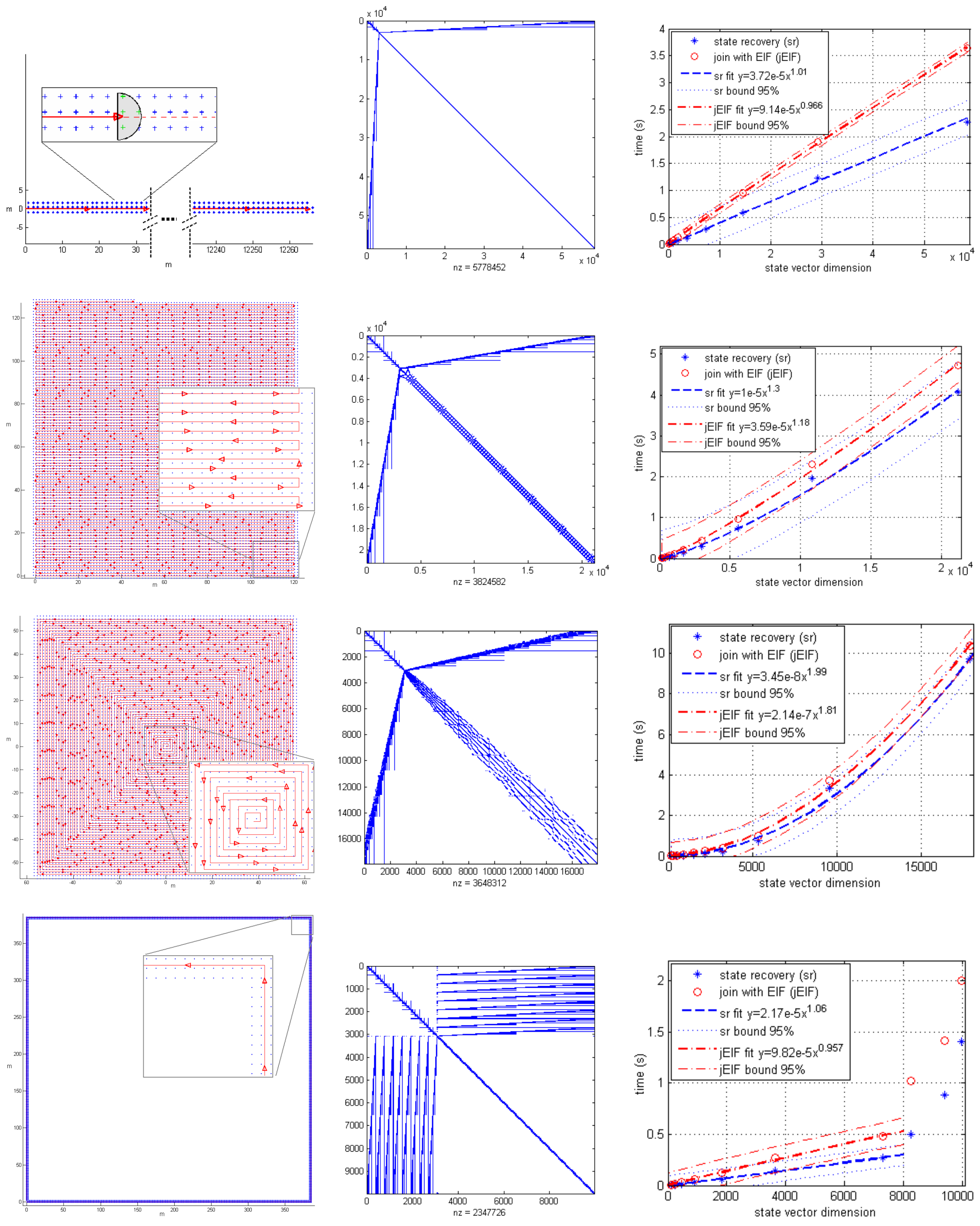

Figure 2.4: Computational cost of state recovery in four cases: exploration with 27651 features (top), lawn mowing with 9056 features (upper middle), out-ward spiral with 7423 features (lower middle), several loops with 3456 features (bottom), all from 1024 local maps. From left to right: ground truth environment and trajectory, sparse information matrix obtained by our algorithm and execution time to do joining and recovery state versus the state vector's dimension with their fit functions. In order to concentrate in studying computational costs these simulations were carried out with noise equal to zero.

Trajectory		b	(95%)	SSE	R^2	RMSE
Exploration	sr	1.01	(0.956,1.058)	0.1385	0.9976	0.1316
	jEIF	0.97	(0.955,0.977)	0.0094	0.9999	0.0342
Lawn mowing	sr	1.30	(1.21,1.39)	0.6849	0.9976	0.2926
	jEIF	1.18	(1.13,1.237)	0.2900	0.9991	0.1904
Out-ward spiral	sr	1.99	(1.816,2.157)	0.9726	0.9993	0.3497
	jEIF	1.81	(1.695,1.92)	0.6629	0.9995	0.2880
Inside the loops	sr	1.06	(0.982,1.139)	0.0072	0.9985	0.0379
	jEIF	0.96	(0.884,1.03)	0.0119	0.9976	0.0487
Exploration with smallest local maps	sr	1.14	(1.097,1.174)	0.1151	0.9990	0.1023
	jEIF	1.08	(1.032,1.123)	0.1958	0.9980	0.1334

Table 2.7: Results of the fit to $y = ax^b$, both the cost of state recovery (`sr`) and the joining with EIF (`jEIF`). We can see the value of the exponent b with 95% confidence bounds, the sum of squared errors (SSE), the coefficient of determination (R^2) and root mean squared errors (RMSE) for the simulations of Fig. 2.4 and Fig. 2.5(right).

	Cost per step		Total cost	
	Best	Worst	Best	Worst
SLSJF	$\mathcal{O}(n)$	$\mathcal{O}(n^2)$	$\mathcal{O}(n^2)$	$\mathcal{O}(n^3)$
D&C SLAM	$\mathcal{O}(n)$ amort.	$\mathcal{O}(n^2)$ amort.	$\mathcal{O}(n^2)$	$\mathcal{O}(n^3)$
CF SLAM	$\mathcal{O}(\log n)$ amort.	$\mathcal{O}(n)$ amort.	$\mathcal{O}(n \log n)$	$\mathcal{O}(n^2)$

Table 2.8: Computational costs for all filtering algorithms in the best case (pure exploration) and in the worst case (repeated traversal). Note that the CF SLAM is the most efficient always.

2.5.2 Local map size

The selection of the local map size p can also influence the computational cost of CF SLAM. Local maps of a large size p (for example $p = 350$) cannot be computed in real time, and also increase the density of non-zero elements in the information matrix (see Fig. 2.5, top left). If on the contrary the local map size is too small ($p = 4$), a large number of robot poses will appear in the state vector (Fig. 2.5, top right). Both situations may result in the cost of map joining not being linear any more (Fig. 2.5, bottom).

In the first case, the density of non-zero elements in $\mathbf{\Omega}$ is 1 in every 12, and thus map joining in the lower levels of the tree (the most frequent) are very expensive, more than $4s$ in the simulation. In the case of small local maps, the exponent from the fit increases to 1.14, see Table 2.7. The density is much lower, 1 in 1070, but the state vector is much larger because we have many more poses. In Fig. 2.5 the number of features is different because the memory requirements of the scenario on the left overflowing the capacity of MATLAB. In our experience, a good rule of thumb is that we should select p to keep the feature variable vs. pose variable ratio between 5 and 20.

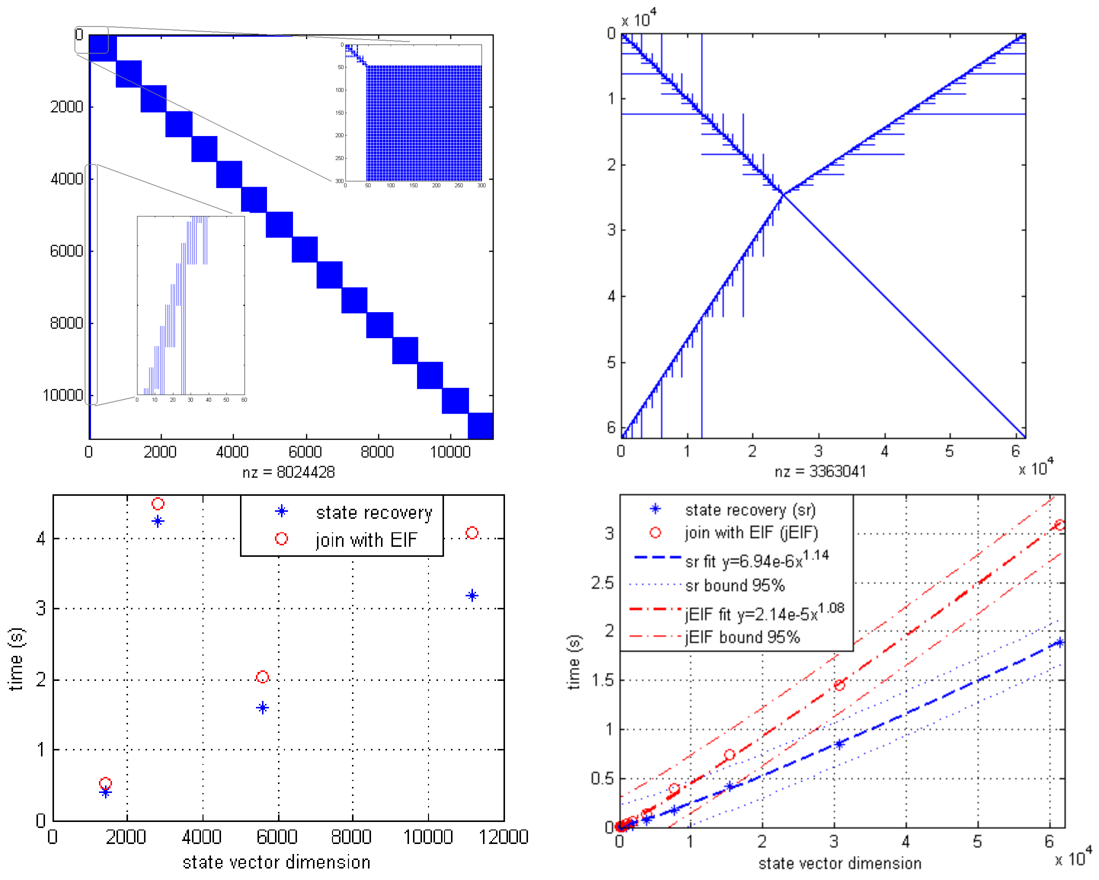

Figure 2.5: Results of different sizes of local maps. The sparse information matrix pattern (top) and execution time of state recovery and map joining (bottom), both in exploration trajectory. On the left the local map size is 350 features, note the time needed for a final map of 5564 features from 16 local maps. On the right the local map size is 4 features (field of view of the sensor) and the final map has 18431 features from 8192 local maps.

2.6 Experiments

To compare the performance of the Combined Filter with other popular EKF and EIF based algorithms we use publicly available datasets. All algorithms were implemented in MATLAB and executed on 2.4GHz Intel Core 2 CPU 6600 and 3GB of RAM.

2.6.1 The Victoria Park dataset: Comparison with iSAM, iSAM2, TSAM2 and CI Graph

The Fig. 2.6(left) shows the resulting map obtained by CF SLAM on the Victoria Park dataset. The trajectory of the vehicle explores and revisits frequently. We can see in Fig. 2.6 (center and right) that CF SLAM is the most efficient for map updates.

Different setups of Victoria Park are used in the literature, considering a different

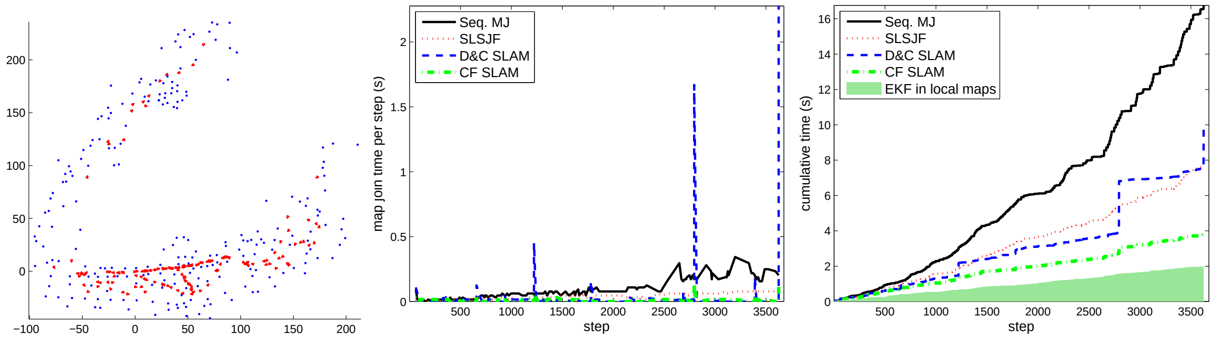

Figure 2.6: Results using the Victoria Park dataset. On the left, the final map with CF SLAM. Computational time per step for map updates (center), and cumulative total cost including each EKF step inside of the local maps (right).

number of odometry steps and also different noise models for the sensor data. We sample one in every two odometry steps, processing a total of 3625. The iSAM algorithm has also used this dataset for its tests, sampling at every odometry step. Kaess et al. (2008) implemented it in OCaml on a 2GHz Pentium M laptop computer. The authors report a cumulative time of 159s with known data association. Kaess et al. (2011) reported 31.3s for a more recent implementation of iSAM (iSAM1) and 27.2s for iSAM2 (an graph-based version of iSAM1 much more efficient), both on laptop with Intel Core 2 Duo 2.4GHz processor. Comparatively, CF SLAM takes 4.15s for solving all the dataset: 2.1s for building local maps, 2.05s for map joins. Although our sampling frequency is one half, this only affects the speed of computation of the local maps, potentially doubling 2.1s of the 4.15s for a total of 6.25s, still much lower. The work of Ni and Dellaert (2010) recently reports results of Tectonic SAM (TSAM2), a batch algorithm of smoothing and mapping with submapping, using also Victoria Park. They report a total time for optimising 200 submaps of 4.5s on an Macbook Pro with 2.8GHz CPU, without reporting the time for building the 200 submaps. The particle filter approach used over this dataset, the FastSLAM 2.0 (Montemerlo et al. 2003), implemented on 1GHz pentium PC, reported a total time of 54s using 1 particle, and 315s with 50 particles. The very recent CI-Graph algorithm of Pinies et al. (2009) solved the Victoria Park dataset in a total time greater than 50s implemented in MATLAB on a Pentium IV at 2.8GHz.

2.6.2 The DLR dataset: Comparison with Treemap

In the DLR dataset, the robot is equipped with a camera, and carries out a trajectory almost all indoors. Features are white cardboard circles placed on the ground. This

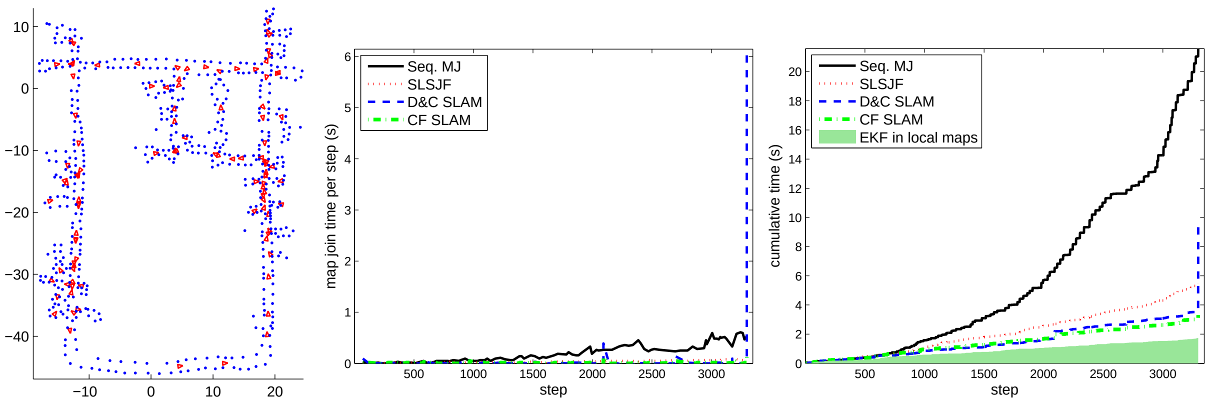

Figure 2.7: Results using the DLR-Spatial-Cognition dataset. Computational cost per step for map updates (center), and cumulative total cost including each EKF step inside of the local maps(right).

dataset has 560 features and 3297 odometry steps. The path consists of a large loop with several smaller loops in the way. The cumulative computational costs are show in Fig. 2.7(right). In this mostly exploratory dataset, both D&C SLAM algorithms are clearly superior than both sequential algorithms.

Frese (2006) reported a total execution time of 2.95s with the Treemap for this dataset, with known data association, implemented in C++ on an Intel Xeon, 2.67GHz. Our algorithm implemented in MATLAB spent 3.4s. We believe that the CF SLAM algorithm is much more simple to implement and use. Furthermore, Treemap is expected to be less consistent in general, it being an absolute map algorithm (Huang and Dissanayake 2007).

2.7 CF SLAM with unknown correspondences

The problem of data association is often ignored when evaluating the efficiency and effectiveness of a SLAM algorithm. In CF SLAM the state covariance is only available in local mapping. When the covariance matrix is not directly available, data association can be usually solved in two ways: (1) recovering the covariance necessary sub-matrices and carrying out statistical tests to find possible matches based on stochastic geometry; (2) if additional information is available, such as texture or appearance in vision sensors, we can obtain matchings based not on location but on appearance. In the following we describe two data association algorithms, one belonging to each category, that can be used in combination with CF SLAM.

2.7.1 Data association using geometrical information

In some situations, only geometrical information, the uncertain location of features relative to the sensor location, is available for data association. Such is the case of 2D points or straight walls obtained with a laser sensor.

As already has been noted by different authors (Huang et al. 2008a; Kaess and Dellaert 2009) recovering the covariance, or parts, is sometimes vital for reliable data association solutions. Kaess and Dellaert (2009) recovered the marginal covariances with dynamic programming in their iSAM framework, and then applied successfully the JCBB technique. Huang et al. (2008a) recovered columns of the covariance matrix by solving a sparse linear equation efficiently.

In CF SLAM, data association inside a local map is carried out using RJC because the corresponding covariance matrix is available. The data association that remains to be solved is the identification of features that appear in two consecutive maps, call them $M_1 = \{\mu_1, \xi_1, \mathbf{\Omega}_1\}$ and $M_2 = \{\mu_2, \xi_2, \mathbf{\Omega}_2\}$, either local maps at the lower level, or maps resulting from previous joins in the D&C map joining process. When the two maps to be joined are local maps, their corresponding covariances are available and data association can be done with the RJC also. If not, we first determine the overlap between the two maps, features that can potentially have pairings, and then we recover the covariance matrix for those features only. We proceed as follows:

1. *Identify the overlap, a set of potential matches*

   This is referred to as individual compatibility, IC. Individually compatible features are obtained by tessellating the environment space, as was proposed by Paz et al. (2008), but in our case we represent the grid in polar coordinates, see Fig. 2.8. For each feature in the second local map M_2, we assign an angular window of constant width in angle and height proportional to its distance from the origin, so that more distant features will have a larger region of uncertainty. The features in the first local map M_1 are referenced on M_2 through the last vehicle pose in M_1, μ_{x1}, which is the origin of map M_2. The uncertainty of μ_{x1} is recovered using equation 2.3 (below) and propagated on the these features, transformed to polar coordinates and embedded to angular windows. Features that intersect are considered individually compatible, giving IC.

$$\mathbf{\Omega\Sigma}_{x1} = e_{x1} \tag{2.3}$$

e_{x1} is a column vector with ones in the correspondent components to the pose x_1 and zeros for the rest.

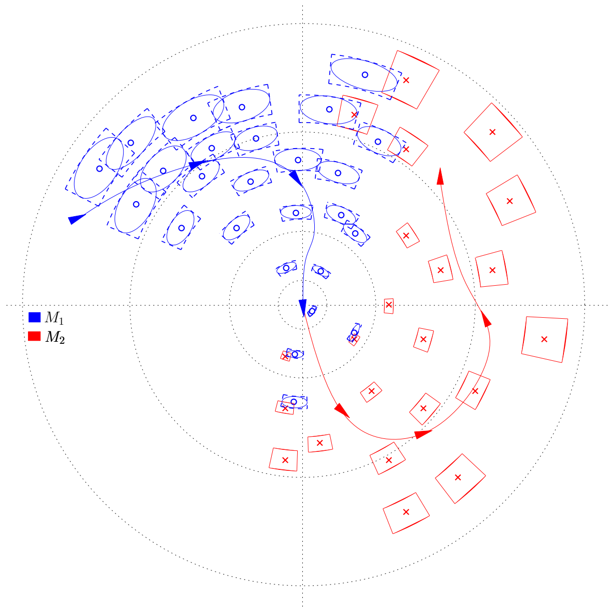

Figure 2.8: Computing the individual compatibility matrix for two local maps using polar coordinates. The angular windows for the features in the M_2 have constant width in angle and height proportional to the distance to the origin. Blue ellipses represent the uncertainties of the predicted features of the first local map with respect to the base reference of the second. The ellipses are approximated by bounding windows.

2. *Partial recovery of covariances*

   For intermediate maps that are not at the lower local level CF SLAM does not compute covariances. As shown by Huang et al. (2008a), we can recover some columns of the covariance matrix by solving the sparse linear equation 2.4. The columns that we require are given by IC. We form a column selection matrix E_{IC} to obtain the columns that are given by IC. If column i of the covariance matrix is required, we include this column vector in E_{IC}:

$$e_i = [\overbrace{0, \cdots, 0, 1}^{i}, 0, \cdots, 0]^T$$

   The sparse linear system to be solved is as follows:

$$\mathbf{\Omega\Sigma}_{IC} = E_{IC} \tag{2.4}$$

This partial recovery of the covariance matrix allows one to use robust joint compatibility tests for data association. The efficiency of solving equation 2.4 is the same as for the recovery of the state vector: in the best case, in exploration trajectories, the order is $\mathcal{O}(n)$, amortised $\mathcal{O}(\log n)$. In the worst case, repeated traversal, the overlap will be the full map, and the cost will be $\mathcal{O}(n^3)$, amortised $\mathcal{O}(n^2)$. Here we reuse the Cholesky decomposition used for the state vector recovery.

3. *Prediction and Observation*

   At this point the features of M_1 that have potential matches according to IC, and their covariances, are transformed to be referenced on M_2.

4. *Randomised Joint Compatibility*

   We use the RJC algorithm of Paz et al. (2008), a combination of JCBB and RANSAC that allows robust data association to be carried out very efficiently, without traversing the whole solution space.

Algorithm 2 Data association for the Combined Filter using geometrical information only

```
**Input:** Two maps: $\langle M_1 = \{\mu_1, \xi_1, \mathbf{\Omega}_1\}, M_2 = \{\mu_2, \xi_2, \mathbf{\Omega}_2\}\rangle$
**Output:** Hypothesis $\mathcal{H}$
  Find the set of potential matches $IC \leftarrow (\mu_1, \mu_2)$
  **if** covariance matrices are available **then**
    extract covariances
    $(\mathbf{\Sigma}_{1i}, \mathbf{\Sigma}_{2j}) \leftarrow select(\mathbf{\Sigma}_1, \mathbf{\Sigma}_2, IC)$
  **else**
    recover partial covariances
    $(\mathbf{\Sigma}_{1i}, \mathbf{\Sigma}_{2j}) \leftarrow recoveryP(\mathbf{\Omega}_1, \mathbf{\Omega}_2, IC)$ eq: 2.4
  **end if**
  $predictions = (h, H\mathbf{\Sigma}H) \leftarrow predict\_map(\mu_{1i}, \mathbf{\Sigma}_{1i})$
  $observations = (z, R) \leftarrow (\mu_{2j}, \mathbf{\Sigma}_{2j})$
  $\mathcal{H} \leftarrow RJC(predictions, observations, IC)$
```

In the following, we will show that using this algorithm, CF SLAM is computationally as efficient as D&C SLAM but requires less memory because the full covariance matrix is not computed. We use the same experiments that in the previous sections.

The 4-leaf clover simulated experiment

Data association was determined based only on geometric information using algorithm 2. Fig. 2.9 shows the maps obtained with each algorithm on the first row. On the second

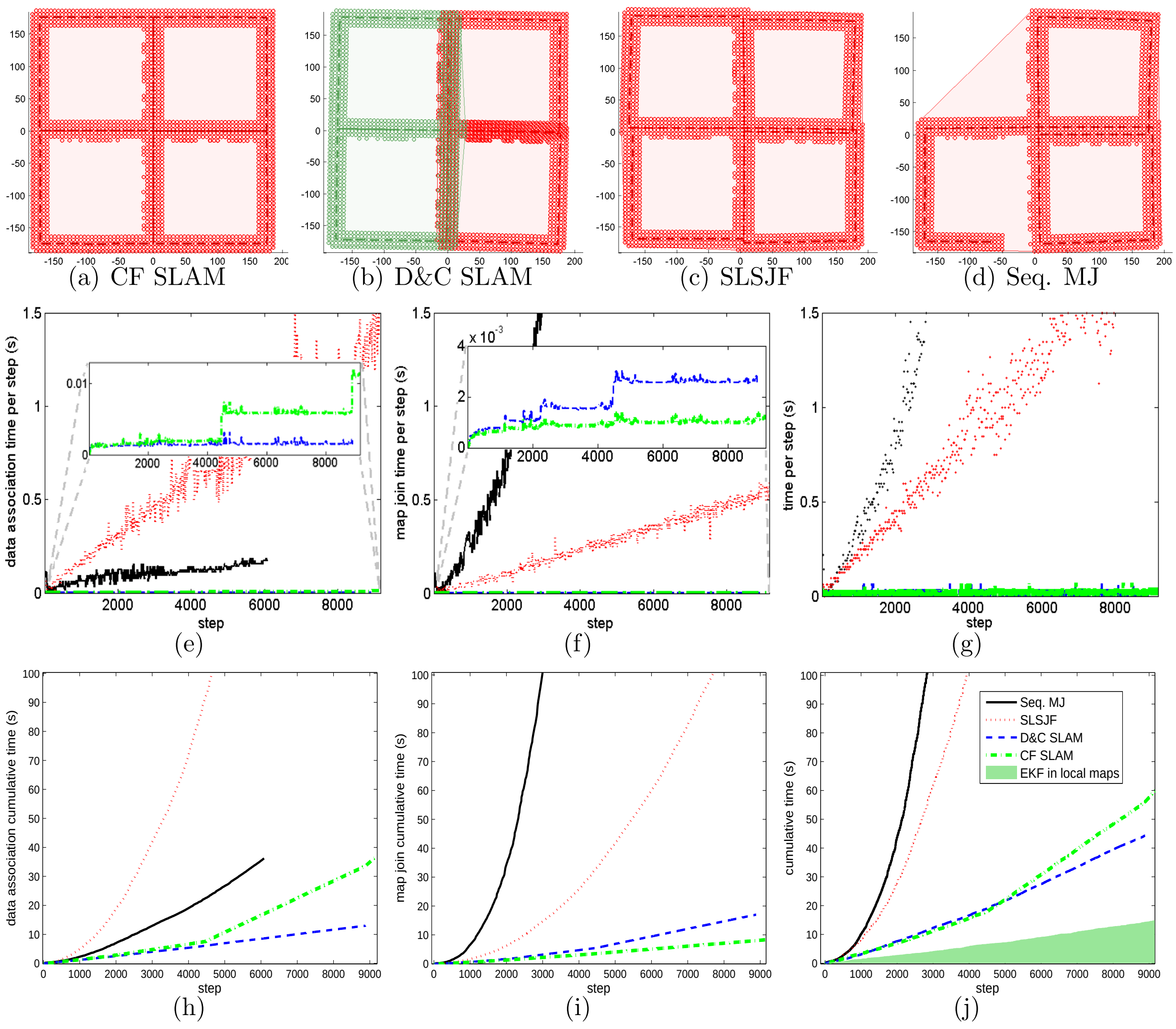

Figure 2.9: Simulated experiment of a 4-leaf clover trajectory. First row, the maps resulting for each algorithm (only CF SLAM and SLSJF are able to compute the final map). In the second row the computational times per step, and the cumulatives on the last row. In (e,h) the computational costs for solving data association, in (f,i) for map updates, and the total cost including each EKF step inside of the local maps for all algorithms in (g,j). Note that D&C SLAM cannot finish and thus its apparent lower cost.

row, it shows the computation cost per step of Map Joining SLAM and SLSJF vs. the amortised cost for the D&C SLAM and CF SLAM: left, cost of data association, center: cost of map updates, right: total cost including local map building. On the third, it shows the cumulative costs in same order than before. The algorithms based on EKFs did not solve the problem completely because they exceeded the available memory before the end of the experiment.

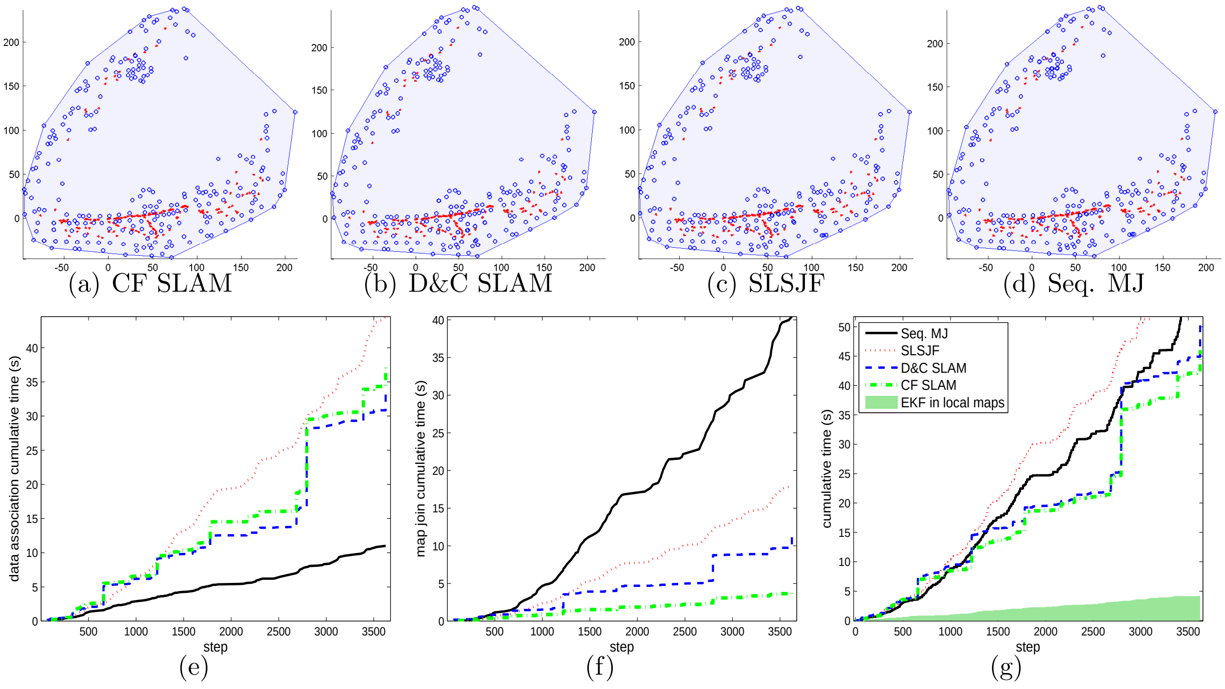

Figure 2.10: Victoria Park experiment. Top, the maps resulting for each algorithm. Bottom, in 2.10(e) the cumulative computational costs for solving data association, in 2.10(f) for the map updates, and the total cost for all algorithms in 2.10(g).

The Victoria Park dataset

The figure 2.6 shows the resulting map obtained by CF SLAM on the Victoria Park dataset. All algorithms solve this dataset correctly. The trajectory of the vehicle explores and revisits frequently, so the uncertainty does not grow much and errors are kept small. The data association was determined with algorithm 2. This dataset is interesting to compare CF SLAM and SLSJF. Both algorithms require the recovery of the covariance sub-matrix for the overlap between the maps to be joined. There are some areas where the overlap is almost complete, thus requiring the recovery of almost the full covariance matrix. The cumulative computational costs are in Fig. 2.10(g). We can see that CF SLAM is the most efficient for map updates, but Map Joining SLAM is most efficient for data association. In total, both algorithms that use the D&C strategy tend to be most efficient.

The DLR dataset

The path consists of a large loop with several smaller loops in the way. Position errors grow enough so that sequential algorithms, Map Joining SLAM and SLSJF, become weak and fail in the data association to close the loop, see Fig. 2.11(c,d). The D&C algorithms, D&C SLAM and CF SLAM have better consistency properties, and both solve the data

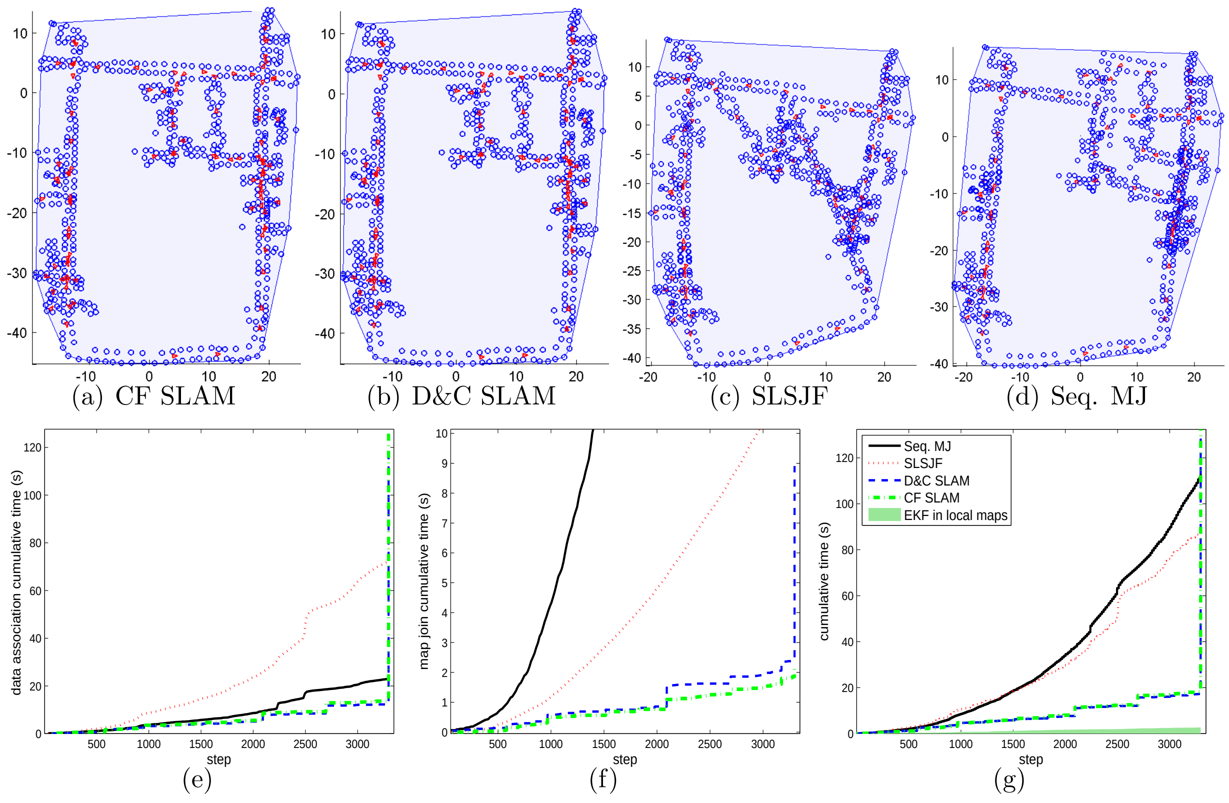

Figure 2.11: Results using the DLR-Spatial-Cognition dataset. Top, the maps resulting for each algorithm. Bottom, in 2.11(e) the computational costs for solving data association. In 2.11(f) the map update time per step, and the cumulative time for all algorithms in 2.11(g).

association for the loop closing in this dataset, see Fig. 2.11(a,b). The cumulative computational costs are shown in Fig. 2.11(e-i). In this mostly exploratory dataset, both D&C SLAM algorithms are clearly superior than both sequential algorithms. During loop closing, the costs of data association for both D&C algorithms are higher than that of both sequential algorithms, for the good reason that data association is computed correctly and the loop can be closed.

Olson (2009) reported a total time of 199s for solving data association using spectrally clustered local matches, implemented on a 2.46GHz Intel proccesor. Our algorithm implemented in MATLAB spent 128s in data association between local maps.

2.7.2 Data association using appearance information

In some cases, features in local maps can have associated appearance information, such as texture coming from vision. In these cases, appearance can be coded using descriptor vectors d from for example SIFT (Lowe 2004) or SURF (Bay et al. 2006), then the map is represented by $M = \{\mu, \xi, \mathbf{\Omega}, d\}$. In these cases, we can proceed as follows in CF SLAM:

1. *Obtain a set of potential matches*

   We find the best possible matches between the descriptors in M_1 and M_2 by searching for the nearest neighbour in the descriptor space. In this way we obtain the individual compatibility matrix, IC.

2. *Obtain a pairwise hypothesis using RANSAC*

   For each pair of minimum local maps, map i belonging to M_1 and map j belonging to M_2, that have a minimum number of matches (5 in our case) in IC, we use RANSAC (Fischler and Bolles 1981) to find the subset $\mathcal{H}_{ij}$ of matches that corresponds to the best rigid-body transform between the two local maps. In Fig. 2.12, the transformations between the pairs $(i = 1, j = 3)$, $(i = 2, j = 3)$ and $(i = 3, j = 2)$ are not evaluated because they do not have sufficient matches.

3. *Obtain the final hypothesis*

   In most cases, the final hypothesis $\mathcal{H}$ is simply the result of joining all $\mathcal{H}_{ij}$. When there is ambiguity (one local map matched with two or more other local maps), we prefer the hypothesis for pairs of maps that have a smallest relative distance, because they have smaller relative errors. In Fig. 2.12 there is ambiguity between $\mathcal{H}_{41}$ and $\mathcal{H}_{42}$. In this case we accept hypothesis $\mathcal{H}_{41}$.

Algorithm 3 Data association using appearance information

```
Input: Two maps: $\langle M_1 = \{\mu_1, \xi_1, \mathbf{\Omega}_1, d_1\}, M_2 = \{\mu_2, \xi_2, \mathbf{\Omega}_2, d_2\}\rangle$
Output: Hypothesis $\mathcal{H}$
  Find set of potential matches $IC \leftarrow (d_1, d_2)$
  for each pair minimum local maps $i, j$ in $IC$ do
    $\mathcal{H}_{ij} \leftarrow RANSAC(\mu_{1i}, \mu_{2j})$
  end for
  $\mathcal{H} \leftarrow select(\mathcal{H}_{ij})$
```

The visual stereo SLAM experiment

Finally, we test CF SLAM in a 3D environment with high feature density. The sensor is a Triclops camera carried in hand. The path consists of a loop inside the Rose Building at the University of Sydney. We obtain the 3D position of points from the computation of the dense stereo point cloud that corresponds to each SIFT feature. The experiment consists of 132 frames, with a total of 6064 features. Fig. 2.13(a) shows the map obtained

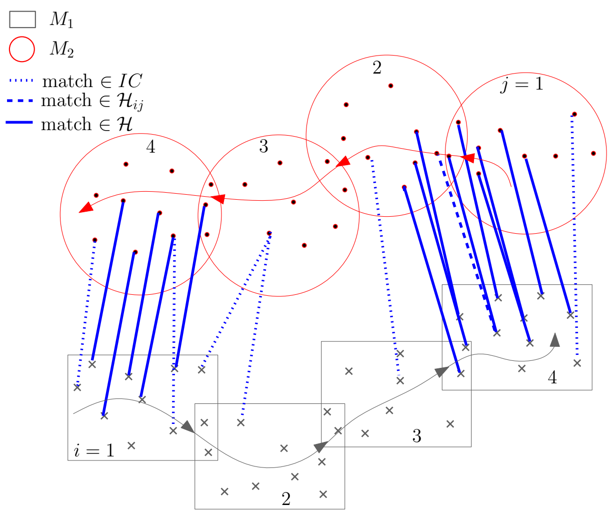

Figure 2.12: Computing the data association hypothesis from two local maps. The rectangles and circles show the minimum local maps of M_1 and M_2 respectively. All lines are potential matches, and form IC. The lines that are not dotted belong to a hypothesis between a pair of the minimum local maps, $\mathcal{H}_{ij}$. The solid lines represent the final hypothesis $\mathcal{H}$.

with CF SLAM. SLSJF obtains an incorrect map, Fig. 2.13(b). SLSJF is a sequential map joining algorithm, thus it is expected to provide less consistent results than D&C algorithms. In these experiments, this results in incorrect loop closure.

Both Map Joining SLAM and the D&C SLAM exceeded available memory in MATLAB. The data association is obtained with algorithm 3. Cumulative computational costs are shown in Fig. 2.13: for data association (c), for map updates (d) and total cumulative cost (e). CF SLAM clearly outperforms all the other algorithms.

2.8 Discussion

In this chapter we have described the Combined Filter SLAM algorithm, which is always more efficient than any other filtering algorithm for SLAM. It can execute in as low as $\mathcal{O}(\log n)$ per step. CF SLAM brings together the advantages of different methods that have been proposed to optimise EKF and EIF SLAM. There is no loss of information, because the solution is computed without approximations, except for linearisations. It is conceptually simple and easy to implement. There are no restrictions on the topology of the environment and trajectory, although, as it is the case in many SLAM algorithms, the computational efficiency will depend on this.

An important property of a SLAM algorithm is whether it is *on-line*, or provides the full vehicle and map estimation in every step, *delayed*, or providing a suboptimal estima-

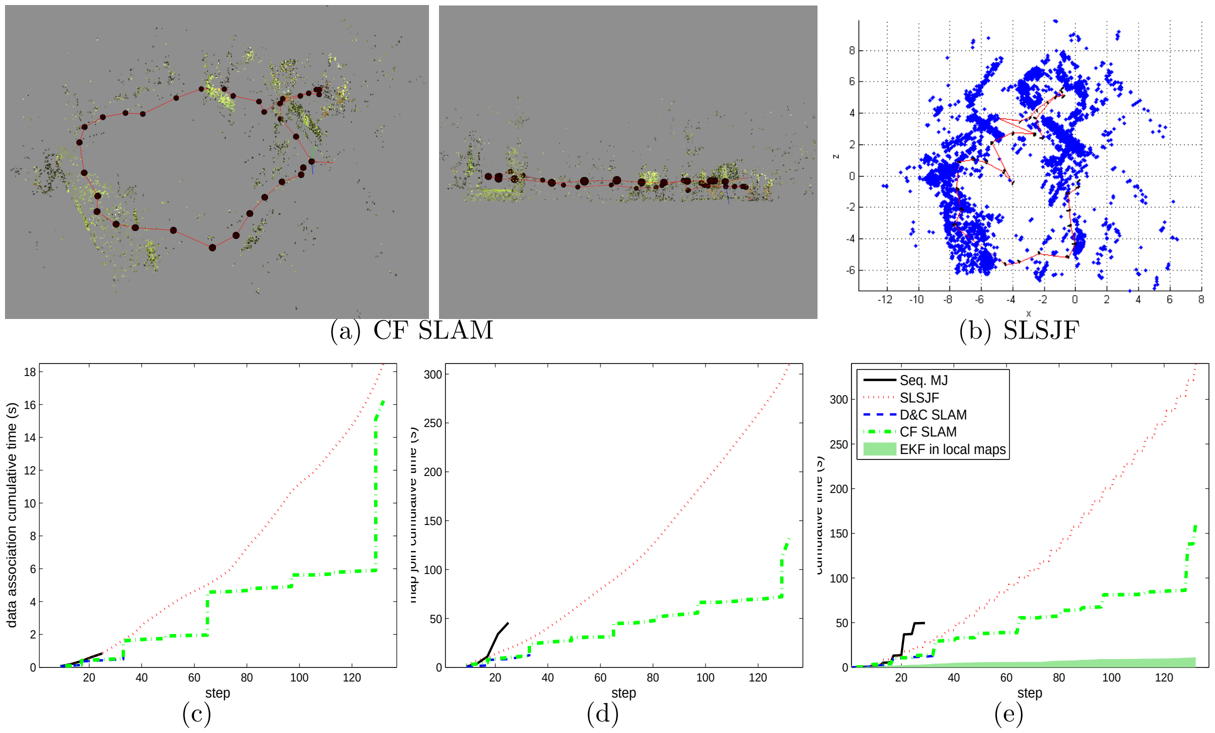

Figure 2.13: Final 3D map using 132 shoots of dense stereo data from a Triclops Pointgrey camera with the CF SLAM (a). We show the cumulative cost for data association (c), map joining (d) and total cost including build local maps, map joining and data association (e). Map Joining SLAM and D&C SLAM exceed available memory capacity in shoots 24 and 32, respectively. The incorrect final map with SLSJF (b).

tion of the map and vehicle states at every step, but requiring additional computation in case the mission requires to have the best estimation, and finally *off-line*, or batch, carrying out the full computation only in case the vehicle and map states are required at a certain step. EKF and EIF SLAM, Map Joining, SLSJF, Treemap, CI-Graph, and iSAM are on-line; D&C SLAM and CF SLAM are delayed, and finally algorithms like Tectonic SAM are off-line. The selection of an appropriate algorithm for a specific mission must take this into account. It can be an overkill to use an on-line algorithm in applications where the map is only required at the end of the mission or very infrequently during the mission.

CF SLAM provides the robot with a local map with all the information needed for local navigation tasks for a very low computational cost. This allows using processor time for other important tasks, such as image processing and data association. This can be essential in situations of limited computational power such as space exploratory rovers. If at a certain moment the robot needs all the environment information with respect to a global reference, for instance to make decisions on global navigation like returning home, CF SLAM can provide the full map carrying out a single additional computation step for a cost as low as $\mathcal{O}(n)$. In these situations, the robot will have a precise map to switch from SLAM to navigation using an *a priori* map. We think that such orders are usually less frequent during a mission in many applications, specially in large scale. For applications requiring global knowledge of the map and vehicle position at every step CF SLAM may be less adequate than sequential algorithms like Map Joining SLAM, SLSJF, CI-Graph or iSAM, given the accumulated delay in computing the global map that CF SLAM incurs in. Finally, in applications where off-line processing is acceptable, we have shown that CF SLAM provides a solution in less time than any other filtering algorithm. Being a local mapping algorithm, the solution provided will have good consistency properties. Algorithms like Tectonic SAM that re-linearise the full problem might provide even more consistent solutions. This is an interesting issue to be investigated.

The estimation problem in SLAM is crucial and nowadays is well understood in the robotic community. CF SLAM is the most efficient filtering algorithm to date. CF SLAM is in the same order, or better, of efficiency than other algorithms with different approaches (graphical models and particle filters) in the state of the art. Nevertheless, any estimation algorithm for SLAM will be not able to work in real applications without a front-end algorithm in order to establish the correct data association. In the next chapter of this thesis we will address that issue, the importance and the effect of the data association over computational efficiency and precision.

Also, we have proposed two basic algorithms for data association, one using covariance based statistical tests and other appearance information. Here we have seen that the CF SLAM algorithm remains in the worst case as computationally effective as D&C SLAM, the fastest to our knowledge that maintains the full covariance matrix and thus allows data association based on stochastic geometry, see Table 2.9. In the order of thousands of features, CF SLAM will outperform D&C SLAM because of reduced memory requirements. If appearance information is available for data association, CF SLAM outperforms all filtering algorithms discussed.

From our experiments it is clear that the greatest computational weight can lie in data association when the robot is revisiting a place after a large exploration period, closing a loop. Sequential SLAM algorithms are weak at solving the data association in those revisited places, see Figs. 2.11(c-d) and 2.13(b). CF SLAM is able to successfully handle those cases, see Fig. 2.14. Although, we obtain a good performance of the continuous data association in the CF SLAM and D&C SLAM, it demands high computational resources,

	Cost per step		Total cost	
	Best	Worst	Best	Worst
seq. MJ	$\mathcal{O}(n^2)$	$\mathcal{O}(n^2)$	$\mathcal{O}(n^3)$	$\mathcal{O}(n^3)$
SLSJF	$\mathcal{O}(n)$	$\mathcal{O}(\cancelto{n^3}{n^2})$	$\mathcal{O}(n^2)$	$\mathcal{O}(\cancelto{n^4}{n^3})$
D&C SLAM	$\mathcal{O}(n)$ amort.	$\mathcal{O}(n^2)$ amort.	$\mathcal{O}(n^2)$	$\mathcal{O}(n^3)$
CF SLAM	$\mathcal{O}(\log n)$ amort.	$\mathcal{O}(\cancelto{n^2}{n})$ amort.	$\mathcal{O}(n \log n)$	$\mathcal{O}(\cancelto{n^3}{n^2})$

Table 2.9: Computational costs for all filtering algorithms recovering columns of the covariance matrix, in the best case (pure exploration) and in the worst case (repeated traversal). Note that the CF SLAM is the most efficient in the best case and it is one of the best in the worst case.

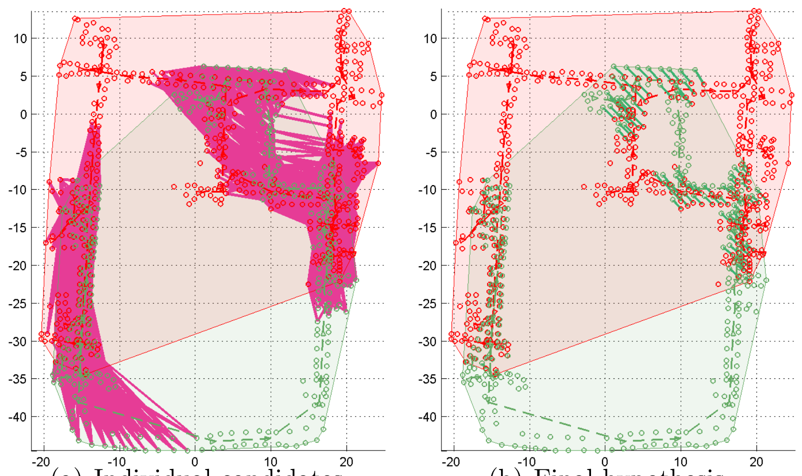

(a) Individual candidates (b) Final hypothesis

Figure 2.14: Data association when there is a loop closure after an exploration for the DLR dataset. In (a) we show all de individual possible associations (magenta links) and in (b) the final association (green links) using algorithm 2.

see high step in Fig. 2.11(e).

However, loops can be large enough so that estimates of vehicle location are not precise enough for these data association algorithms to be useful, or computationally too demanding. In the next chapter we investigate data association algorithms that do not make use of vehicle estimates and are applicable in very large environments.

Chapter 3

Robust Place Recognition

In this chapter we describe our contribution to one of the data association problems in SLAM known as place recognition. The approach proposed here attempts to detect previously visited places based on a process of inference using probabilistic graphical models. In section 3.1 we explain the technical and intuitive bases of probabilistic graphical models, in section 3.2 we detail how the conditional random fields are incorporated in the place recognition system. We describe the detailed method in section 3.2.1. In section 3.3 we compare the results from our system with the state of the art in visual place recognition using benchmark datasets. Finally, we summarise the results and draw the fundamental conclusions of our contribution.

3.1 Preliminaries

Probabilistic graphical models have been used in the machine learning field to solve problems of classification or labelling. The problem of classification is closely related to the data association problem. In the classification process, the goal is to find the correspondences between a set of observed data and a set possible classes or states. In data association, we wish to find the correspondences between two sets of features observed at different times. This idea was first explored by Ramos et al. (2007) using as the probabilistic graphical model the conditional random field (CRF) of Lafferty et al. (2001). The work of Ramos et al. (2007) inspired us to pursue in this path.

Probabilistic graphical models use a graph-based representation to model a joint probability distribution over a multi-dimensional space (of random variables) and a graph that is a compact representation of a set of independences that hold in the distribution. In our

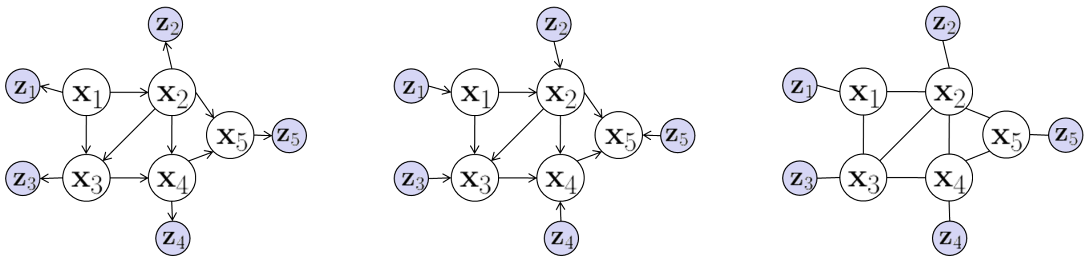

(a) HMM: $p(\mathbf{x}, \mathbf{z})$ (b) MEMM: $p(\mathbf{x}|\mathbf{z})$ (c) CRF: $p(\mathbf{x}|\mathbf{z})$

Figure 3.1: Different probabilistic graphical models.

case, each node represents a random variable and each edge represents the probabilistic relationship between the connected variables.

Graphical models can be directed or undirected. In the *directed graph*, also named Bayesian Network, the edges have a particular direction and therefore impose a one-way causality. The *undirected graph*, also named Markov Random Field (MRF), does not have a preferred direction allowing causality both ways.

Graphical models can also classified in generative models and discriminative models. *Generative models* represent the join distribution over the states and the observations. *Discriminative models* describe a conditional distribution over the states given some observations.

In these categories we can find (see Fig. 3.1), Hidden Markov Models (HMMs): a generative model with directed graph, Maximum Entropy Markov Models (MEMMs): a discriminative model with directed graph, and Conditional Random Fields (CRFs): a discriminative model with undirected graph. Both MEMMs and CRFs allow conditional probabilities to be computed, HMMs allow joint probabilities to computed.

These different probabilistic graphical models have their pros and cons (Koller and Friedman 2009). For instance, in terms of computational cost for learning, HMMs and MEMMs are better than CRFs. In the richness of the features, MEMMs and CRFs are better than HMM. HMMs and MEMMs suffer from the label bias problem because of one-way causality, unlike CRF. In the computer vision community, CRFs have been broadly used with success in different tasks: denoising images (Tappen et al. 2007), segmentation (He et al. 2004), object and gesture recognition (Quattoni et al. 2007), and stereo vision (Scharstein and Pal 2007). On the other hand, the robotic community has seen the advantages of this tool and it has been used in tasks like segmentation of 2D and 3D laser scans for mapping (Douillard et al. 2011; Lim and Suter 2007), clustering of dynamic objects (Tipaldi and Ramos 2009), and extracting places and activities from GPS traces

(Liao et al. 2007).

3.1.1 Conditional Random Fields

Conditional random fields are probabilistic undirected graphical models first developed by Lafferty et al. (2001) for labelling sequence data. CRFs are a case of Markov Random Fields, and thus satisfy the Markov properties, where there is no need to model the distribution over the observations (Bishop 2006; Koller and Friedman 2009). If the neighbourhood of a node A (i.e. all nodes with edges to A) in the graph is known, the assignment to A is independent of the assignment to another node B outside the neighbourhood of A.

Instead of relying on Bayes' rule to estimate the distribution over hidden states $\mathbf{x}$ from observations $\mathbf{z}$, CRFs directly model $p(\mathbf{x}|\mathbf{z})$, the *conditional* distribution over the hidden variables given observations. Due to this structure, CRFs can handle arbitrary dependencies between the observations. This makes them substantially flexible when using complex and overlapped attributes or observations.

The nodes in a CRF represent hidden states, denoted $\mathbf{x} = \langle \mathbf{x}_1, \mathbf{x}_2, \cdots, \mathbf{x}_n \rangle$, observations are denoted $\mathbf{z}$. The nodes $\mathbf{x}_i$, along with the connectivity structure represented by the undirected graph, define the conditional distribution $p(\mathbf{x}|\mathbf{z})$ over the hidden states $\mathbf{x}$. Let $\mathcal{C}$ be the set of cliques (fully connected subsets) in the graph of a CRF. A CRF factorises the conditional distribution into a product of *clique potentials* $\phi_c(\mathbf{z}, \mathbf{x}_c)$, where every $c \in \mathcal{C}$ is a clique in the graph, and $\mathbf{z}$ and $\mathbf{x}_c$ are the observed data and the hidden nodes in such clique. Clique potentials are functions that map variable configurations to non-negative numbers. Intuitively, a potential captures the "compatibility" among the variables in the clique: the larger a potential value, the more likely the configuration. Using the clique potential, the conditional distribution over hidden states is written as:

$$p(\mathbf{x}|\mathbf{z}) = \frac{1}{Z(\mathbf{z})} \prod_{c \in \mathcal{C}} \phi_c(\mathbf{z}, \mathbf{x}_c) \tag{3.1}$$

where $Z(\mathbf{z}) = \sum_{\mathbf{x}} \prod_{c \in \mathcal{C}} \phi_c(\mathbf{z}, \mathbf{x}_c)$ is the normalising partition function. The computation of this function can be exponential in the size of $\mathbf{x}$. Hence, exact inference is possible for a limited class of CRF models only, e.g. in tree-structured graphs.

Potentials $\phi_c(\mathbf{z}, \mathbf{x}_c)$ are described by log-linear combinations of *feature functions* $\mathbf{f}_c$, i.e., the conditional distribution (3.1) can be rewritten as:

$$p(\mathbf{x}|\mathbf{z}) = \frac{1}{Z(\mathbf{z})} \exp \left\{ \sum_{c \in \mathcal{C}} \mathbf{w}_c^T \cdot \mathbf{f}_c(\mathbf{z}, \mathbf{x}_c) \right\} \tag{3.2}$$

where $\mathbf{w}_c$ a weight vector, which represents the importance of different features for correctly identifying the hidden states. Weights can be learned from labelled training data.

Inference

The process of *inference* allows answering queries using the graphical model as our model of the problem, and it is required for training (learning) and decoding (Cohn 2007; Koller and Friedman 2009). Inference in a CRF estimates the marginal distribution of each hidden variable $\mathbf{x}_i$, and can thus determine the most likely configuration of the hidden variables $\mathbf{x}$ (i.e., the maximum a posteriori, or MAP, estimation). Both tasks can be solved using *belief propagation* (BP) (Pearl 1988), which works by transmitting messages containing beliefs through the graph structure of the model. Each node sends messages to its neighbours based on messages it receives and the clique potentials. BP generates exact results in graphs with no loops, such as trees or polytrees. For cyclic graphs, approximate inference methods like loopy belief propagation can be used (Murphy et al. 1999).

Parameter learning

The goal of parameter learning is to determine the weights of the feature functions used in the conditional likelihood (3.2) for fitting the model to training data. CRFs learn these weights discriminatively by maximising the conditional likelihood of labelled training data. We resort to maximising the *pseudo-likelihood* of the training data, which is given by the product of all local likelihoods $p(\mathbf{x}_i|\text{MB}(\mathbf{x}_i))$; where $\text{MB}(\mathbf{x}_i)$ is the Markov Blanket of variable $\mathbf{x}_i$, which contains the immediate neighbours of $\mathbf{x}_i$ in the CRF graph. Optimisation of this pseudo-likelihood is performed by minimising the negative of its log, resulting in the following objective function:

$$L(\mathbf{w}) = -\sum_{i=1}^{n} \log p(\mathbf{x}_i|\text{MB}(\mathbf{x}_i), \mathbf{w}) + \frac{\mathbf{w}^T\mathbf{w}}{2\sigma_{\mathbf{w}}^2} \tag{3.3}$$

The rightmost term in (3.3) serves as a zero-mean Gaussian prior, with variance $\sigma_{\mathbf{w}}^2$, on each component of the weight vector, and is used to avoid overfitting.

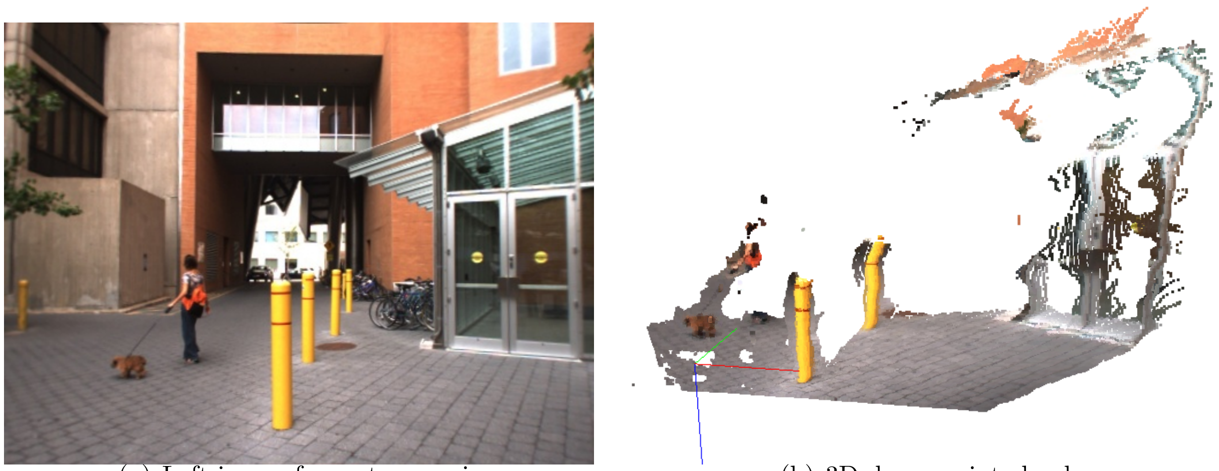
(a) Left image from stereo pair (b) 3D dense point cloud

Figure 3.2: Scene from an outdoor environment. We use only an image from the stereo pair for the appearance information 3.2(a), and the 3D dense point cloud 3.2(b).

3.1.2 Data Association with CRFs

In the problem that we are interested in, data association in mobile robots, perhaps the first application of CRFs was introduced by Ramos et al. (2007), called CRF-Matching, for matching 2D laser scans. The idea of CRF-Matching is take two sets of points, from different times of acquisition, and find their point-to-point correspondences. Ramos et al. (2007) show that CRF-Matching is much more robust to high rotational and translational movements of the robot than the classical Iterative Closest Point algorithm. Later, Ramos et al. (2008) extended the idea to associate image features, using a 2D Delaunay triangulation as graph structure, and then a loopy belief propagation method for inference.

From now on, we focus our interest in stereo cameras. The use of a stereo camera allows us to combine appearance information with 3D metric information when available, see Fig. 3.2.

Our contribution here is the extension of CRF-Matching to 3D point clouds. It includes two keys ideas:

1. Include only characteristic points as nodes in the graph and not the thousands provided by the stereo. Lim and Suter (2007) use CRFs and sub-sample the 3D laser data with an adaptive data reduction based on spatial properties in order to reduce both learning and inference times. We take advantage of texture in visual information to sub-sample the 3D dense information and consider only salient visual features and their coverage areas. We use the extractor SURF (Bay et al. 2006) on

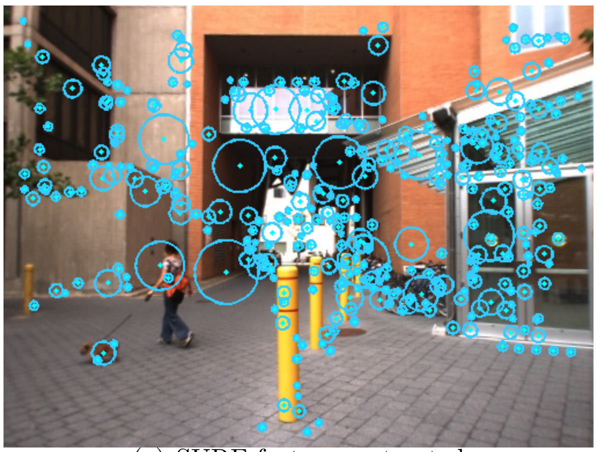

(a) SURF features extracted

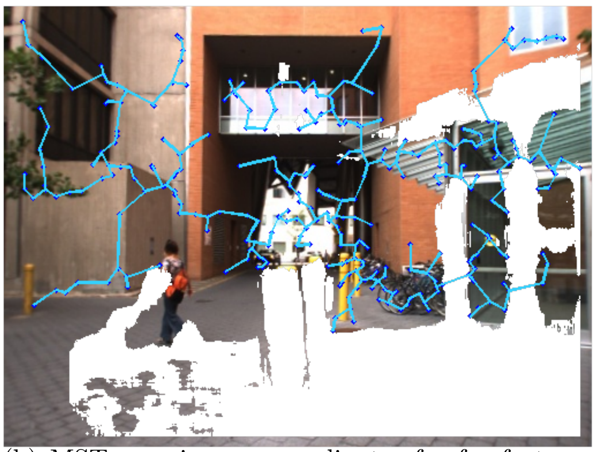

(b) MST over images coordinates for far features ($\mathcal{G}_{Im}$)

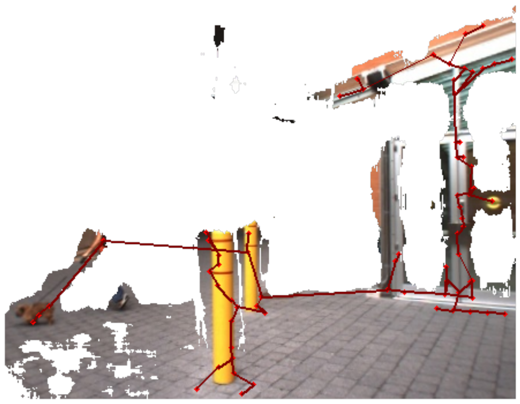

(c) MST over 3D metric coordinates for near features ($\mathcal{G}_{3D}$)

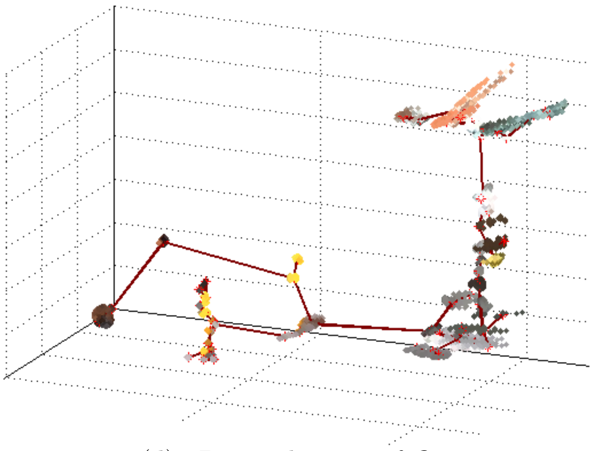

(d) 3D visualitation of $\mathcal{G}_{3D}$

Figure 3.3: In each scene we get the SURF features over one image of the stereo pair 3.3(a), and compute the two minimum spanning trees: one for features with 3D information (near features), and the other for the remaining ones (far features). On 3.3(b), we show the graph for far features ($\mathcal{G}_{Im}$) in blue, in dark red the graph for near features ($\mathcal{G}_{3D}$) on 3.3(c). We apply the CRF-Matching over both graphs. The minimum spanning tree of $\mathcal{G}_{3D}$ is computed according to the metric coordinates, here projected over the images only for visualisation. On 3.3(d), we show $\mathcal{G}_{3D}$ in metric coordinates with the 3D point cloud (textured) of each vertex in the tree. The MST gives us an idea of the dependencies between features in a scene, and enforce the consistency of the features association between scenes.

one of the images for that purpose, see Fig. 3.3(a).

2. Use a Minimum Spanning Tree as graph structure for our CRF model, instead of the dense Delaunay triangulation. This idea was previously used by Quattoni et al. (2007) in the context of object classification in images. In that work, equivalent classification performance was shown for MSTs in comparison with more densely connected graphs. By definition, the minimum spanning tree connects points that are close in the measurement space, highlighting intrinsic localities in the scene.

> This implies: first, the associations are jointly compatible within neighbourhoods, and second, the compatibility is enforced and propagated from neighbourhood to neighbourhood by the edges between them. In addition, trees allow exact inference algorithms, as compared, for instance, with loopy belief propagation for cyclic graphs, which is approximate and more expensive. As Quattoni et al. (2007), our results show that MSTs properly encode connections between the hidden variables and ensures global consistency in both image and 3D space.

In our framework of data association, the hidden states correspond to all the possible associations between the n features in scene A and the m features in scene B, i.e. $\mathbf{x}_i \in \{0, 1, 2, \ldots, m\}$, where the additional state 0 is the outlier state. Observations are provided by the sensors, e.g. 3D point clouds, appearance descriptors, or any combination of them.

The data association process is done by inferring over the matches between SURF-points of the scenes. Here we refer to SURF-point as the pixel in the image where the SURF-feature was detected.

We model the scene as two graphs: the first graph ($\mathcal{G}_{3D}$) models the near objects, i.e. those pixels with sufficient disparity from the stereo, and hence with 3D information, see Fig. 3.3(c) and 3.3(d). And the second graph ($\mathcal{G}_{Im}$) models the far objects from pixels without disparity information, see Fig. 3.3(b). The nodes of the graphs are the SURF-points extracted before, and the edges of the graphs result from computing the minimum spanning tree (MST), according to the Euclidean distances between the pixel coordinates in the case of $\mathcal{G}_{Im}$, and between the 3D metric coordinates in the case of $\mathcal{G}_{3D}$.

Feature description

With the graph structure defined for our CRF models, we have to define $\mathbf{f}_c(\mathbf{z}, \mathbf{x}_c)$ in eq. 3.2. The CRF matcher can employ arbitrary local features to describe shape, image properties, or any particular aspect of the data. Our features describe *differences* between shape (only for $\mathcal{G}_{3D}$) and appearance (for both graphs) of the features. The local features we use are the following:

Shape difference: These features capture how much the local shape of dense stereo data differs for each possible association. We use the geodesic, PCA and curvature distance.

The *geodesic distance*, defined as the sum of Euclidean distances between points in the minimum spanning tree, provides information about the density of the neighbourhood of

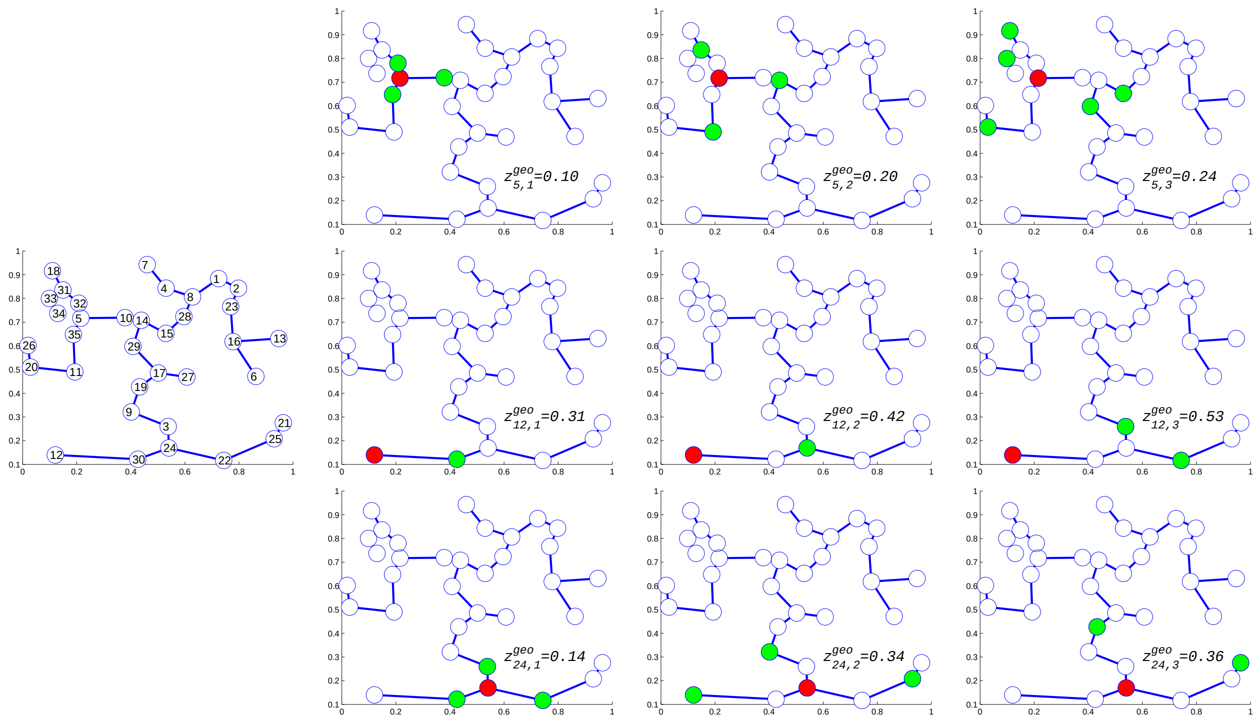

Figure 3.4: Geodesic distances in a randomly generated minimum spanning tree. Columns correspond to neighbourhoods of order 1, 2 and 3, respectively, for three different nodes (rows).

each node of the graph. It can be calculated for different neighbourhoods representing local or long-term shape information. Given points $z_{A,i}$, $z_{B,j}$ and a neighbourhood k, the geodesic distance feature is computed as:

$$\begin{aligned}\mathbf{f}_{geo}(i,j,k,z_A,z_B) &= \left\| z^{geo}_{A,i,k} - z^{geo}_{B,j,k} \right\| \\ &= \left\| \sum_{l=i}^{i+k-1} \|z_{A,l+1} - z_{A,l}\| - \sum_{l=j}^{j+k-1} \|z_{B,l+1} - z_{B,l}\| \right\| \end{aligned} \tag{3.4}$$

where i and j correspond to the hidden state $\mathbf{x}_i$ that associate the feature i of the scene A with the feature j of the scene B. The neighbourhood k of $\mathbf{x}_i$ in the graph corresponds to all the nodes separated k nodes from $\mathbf{x}_i$. In our implementation, this feature is computed for $k \in \{1, 2, 3\}$. A similar feature is used to match 3D laser scans by Anguelov et al. (2005).

We also use *Principal Component Analysis* over the dense 3D point cloud that is contained within a radius given by the scale obtained by the SURF extractor for each node in the graph, textured points in Fig. 3.3(d). The *PCA distance* is computed as the absolute difference between the variances of the principal components of a dense point cloud $z^{pca}_{A,i}$ in scene A and $z^{pca}_{B,j}$ in scene B:

$$\mathbf{f}_{PCA}(i, j, z^{pca}_{A}, z^{pca}_{B}) = \left| z^{pca}_{A,i} - z^{pca}_{B,j} \right| \tag{3.5}$$

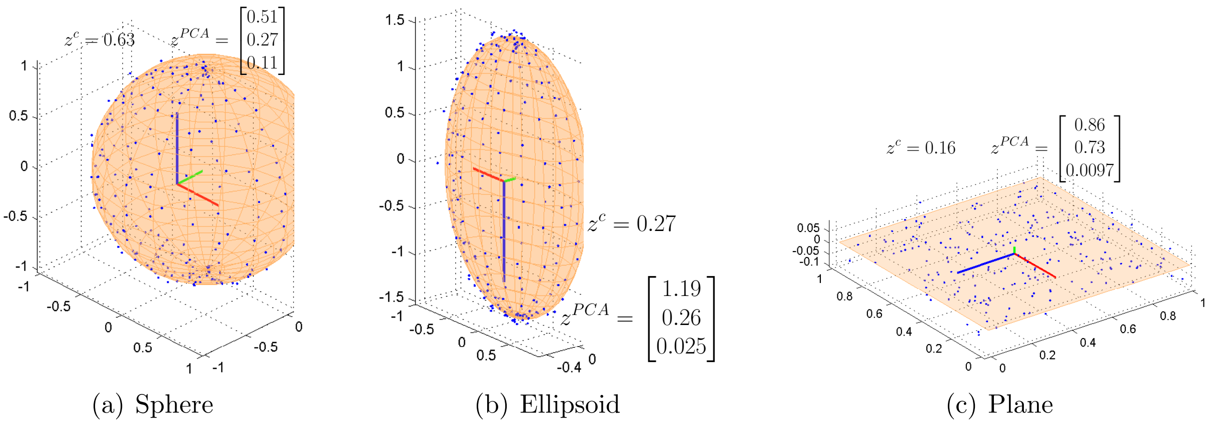

Figure 3.5: Synthetic examples of point clouds in a node of the graph. These point clouds are used in the PCA and curvature distances. The synthetic shapes are with additive gaussian noise.

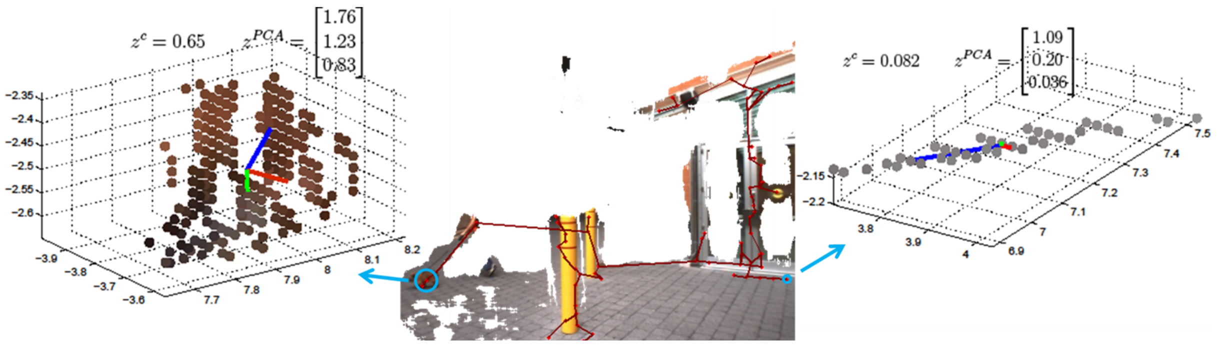

Figure 3.6: Real examples of point clouds in nodes of the graph from the scene in Fig. 3.2.

As proposed by Pauly et al. (2002), another way to consider local shape is computing the curvature of a surface through a point cloud (Klasing 2010). Then we use the *difference between the curvatures* of the dense point clouds. This feature is computed as:

$$\mathbf{f}_{curv}(i, j, z^{c}_{A}, z^{c}_{B}) = \left\| z^{c}_{A,i} - z^{c}_{B,j} \right\| \tag{3.6}$$

where $z^c = \frac{3s_3}{s_1+s_2+s_3}$, and $s_1 \geq s_2 \geq s_3$ are the *singular values* of the point cloud of each node.

Klasing (2010) describe many more shape features for laser returns. Exploring those features in the CRF-matching proposed by us is one of our pending tasks.

Visual appearance: These features capture how much the local appearance from the points in the image differs for each possible association. We use the *SURF distance.* This feature calculates the Euclidean distance between the descriptor vectors for each possible association:

$$\mathbf{f}_{SURF}(i, j, z_A^{descr}, z_B^{descr}) = \left\| z_{A,i}^{descr} - z_{B,j}^{descr} \right\| \tag{3.7}$$

Ramos et al. (2008) also include as features the distances between the individual dimensions of the descriptor space. In our training and validations data we do not find a significant improvement in the accuracy of the labelling, and this greatly increases the size of the weight vector.

All previous features described are unary, in that they only depend on a single hidden state i in scene A (indices j and k in the features denote nodes in scene B and neighbourhood size). In order to generate mutually *consistent* associations it is necessary to define features, over the cliques, that relate the hidden states in the CRF with each other.

Pairwise distance: This feature measures the consistency between the associations of *two* hidden states $\mathbf{x}_i$ and $\mathbf{x}_j$ and observations $z_{A,i}$, $z_{A,j}$ from scene A and observations $z_{B,k}$ and $z_{B,l}$ in scene B:

$$\mathbf{f}_{pair}(i, j, k, l, z_A, z_B) = \| \| z_{A,i} - z_{A,j} \| - \| z_{B,k} - z_{B,l} \| \| \tag{3.8}$$

The z_A and z_B are in metric coordinates for $\mathcal{G}_{3D}$, and in pixels for $\mathcal{G}_{Im}$.

In addition to the features described, we define two more binary features for the outlier state, just as Ramos et al. (2007), in order to handle features from scene A that do not have a correspondence in scene B, then their hidden sate must be set to "outlier". One feature function is local and one for pairwise. Whenever the outlier feature is true, the value of all corresponding features are set to zero. In the learning process the algorithm learns weights for the binary outlier features.

Learning weights

The learning phase of our CRF-Matching is as follows:

1. Capture a sequence of stereo images.

2. Randomly choose a subset stereo images, in 200 frames k, uniformly distributed over the experiment.

3. Label each frame k using the scene in the frame $k-1$ with data associations based on RANSAC over the best body rigid transformation for the SURF-points with 3D information, and over the fundamental matrix for the remaining SURF-points in the image.
4. Build in each scene k the graph structures with the MST: one over the euclidean distances in metric space for $\mathcal{G}_{3D}$, and another over pixel coordinates for $\mathcal{G}_{Im}$.
5. Compute the features defined in the previous section for each graph.
6. Learn the weights of the CRF models using the pseudo-likelihood over a percentage of the subset chosen (training set).
7. Validate the learning process with the remaining scenes (validation set).

We show the performance of the data association with two different datasets. The first is taken from the RAWSEEDS (2009) Project. This project contains stereo sequences from two different campuses, the campus Bicocca of the University of Milano and the campus Bovisa of the Politecnico di Milano, taken with a Videre stereo camera. The scenes correspond to indoors and outdoors, and a mix of them, in both static and dynamic environments. We choose for the learning and validation process the experiment *Bovisa_2008-09-01_Static* taken on the September first of 2008 in the campus Bovisa with mix of indoors and outdoors in a static environment. In Fig. 3.7 we can see some sample images of the subset for learning. We have used the data corresponding to the Stereo Vision System with an 18cm baseline. Images (640x480 px) are taken at 15 fps.

Delaunay vs. MST:
We carry out a a 10-fold cross-validation procedure in order to verify that the accuracy of the data association using the CRFs as proposed for us is not affected by using MST instead of Delaunay triangulation. For this, the pairs of scenes used for learning the weights, both in 3D and image, are randomly permuted and equally divided into ten groups. We use nine groups for training, and the 10th for validation (training and validation data are mutually exclusive). This process is repeated 10 times and the evaluation metrics are computed across folds for all the validation trials.

We perform the 10-fold cross validation for $\mathcal{G}_{3D}$ and $\mathcal{G}_{IM}$, both with the Delaunay triangulation and the minimum spanning tree graph structures. We show the results of the statistic test in the accuracy of the matching with respect to the labelling in Table 3.1.

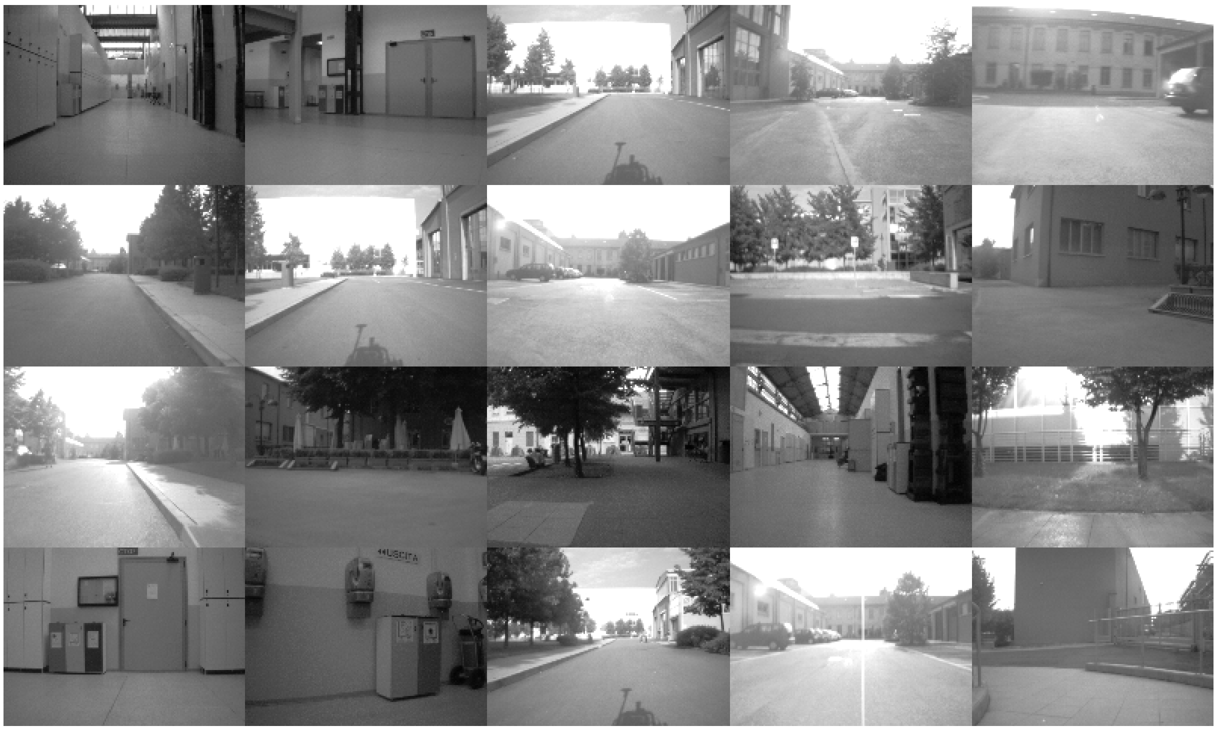

Figure 3.7: Sample of right images from stereo pair of the RAWSEEDS dataset used for learning.

The results in the validation data suggest that there is no statistic evidence to prefer the Delaunay triangulation instead of the MST as graph structure for our CRF matching processes. These results agree with the conclusion drawn by Quattoni et al. Quattoni et al. (2007).

Relative importance of features:
We study the influence of each feature proposed in the CRF-Matching in the learning stage. Now we randomly divide the set used for learning into two 60-40% groups; 60% for training and 40% for validation. Then, we carry out learning with all the features but one at a time. We show the accuracy in data association in Table 3.2 for both graphs.

The accuracy that we obtain in each case shows that $\mathbf{f}_{SURF}$ and $\mathbf{f}_{pair}$ are the most relevant features in the inference process. This result is expected. However, in the validation set for $\mathcal{G}_{3D}$ we lose about 2% in the mean accuracy of data association when we remove any other feature. This is a short analysis about the influence of each feature in the inference process that could be extended. For instance, we could analyse many more combinations by adding or removing features. That kind of analysis remains as future work for us.

In Table 3.3 we can see the weights as result of the learning process in the mixed

Table 3.1: Mean and standard deviation of the accuracy in a 10-fold cross validation test with both graph structures: Delaunay triangulation and MST

	$\mathcal{G}_{3D}$		$\mathcal{G}_{IM}$	
	Delaunay	MST	Delaunay	MST
Training set				
Mean	76.65%	88.01%	81.38%	79.53%
Std. dev.	1.70%	0.67%	0.16%	0.17%
Validation set				
Mean	75.05%	87.34%	81.36%	79.53%
Std. dev.	8.30%	5.10%	1.32%	0.99%

Table 3.2: Accuracy in training and validation sets for the data association for both graphs, removing one feature at a time in the learning stage

	$\mathcal{G}_{3D}$		$\mathcal{G}_{IM}$	
	Training	Validation	Training	Validation
no $\mathbf{f}_{geo}$	86.65%	84.48%		
no $\mathbf{f}_{SURF}$	65.87%	60.92%	19.55%	19.28%
no $\mathbf{f}_{PCA}$	87.63%	84.99%		
no $\mathbf{f}_{curv}$	87.86%	84.68%		
no $\mathbf{f}_{pair}$	85.10%	83.27%	77.84%	77.83%
All features	87.70%	86.45%	78.92%	78.99%

static dataset, corresponding to the last row in Table 3.2. The weights are learned for both graphs.

We remark here that the process of labelling with RANSAC is not perfect, sometimes you can obtain mistakes in the labels. But the learning process has shown be robust against that error, mainly due to the a majority of good labels.

We can see that the model is not over-fit to the training set in the different tests carried out above.

		SURF	*geo*			*PCA*			*curv*	*pair*	*outlier*	
			k=1	k=2	k=3	1st	2nd	3rd			*local*	*pair*
$\mathcal{G}_{3D}$	**w**	-8.55	0.15	0.80	1.09	0.16	-1.34	0.06	-1.68	-4.60	-1.24	-0.83
$\mathcal{G}_{Im}$	**w**	-15.82								-18.69	-2.27	-0.57

Table 3.3: Weights obtained in the learning process in the RAWSEEDS dataset. A higher value in magnitude has more importance in eq. 3.2

The second dataset used was taken in the MIT campus in multiple sessions around of the Stata Center building, with indoor and outdoor routes taken on July of 2010. The stereo images were collected with a BumbleBee2, from PointGrey, with an 8cm baseline. The environment is dynamic, with people and cars in motion. For the learning and validation process, we chose 200 images (512x384 px) uniformly distributed in time from an indoor session taken on April 8th of 2010. In Fig. 3.8 we can see some sample images of the chosen subset.

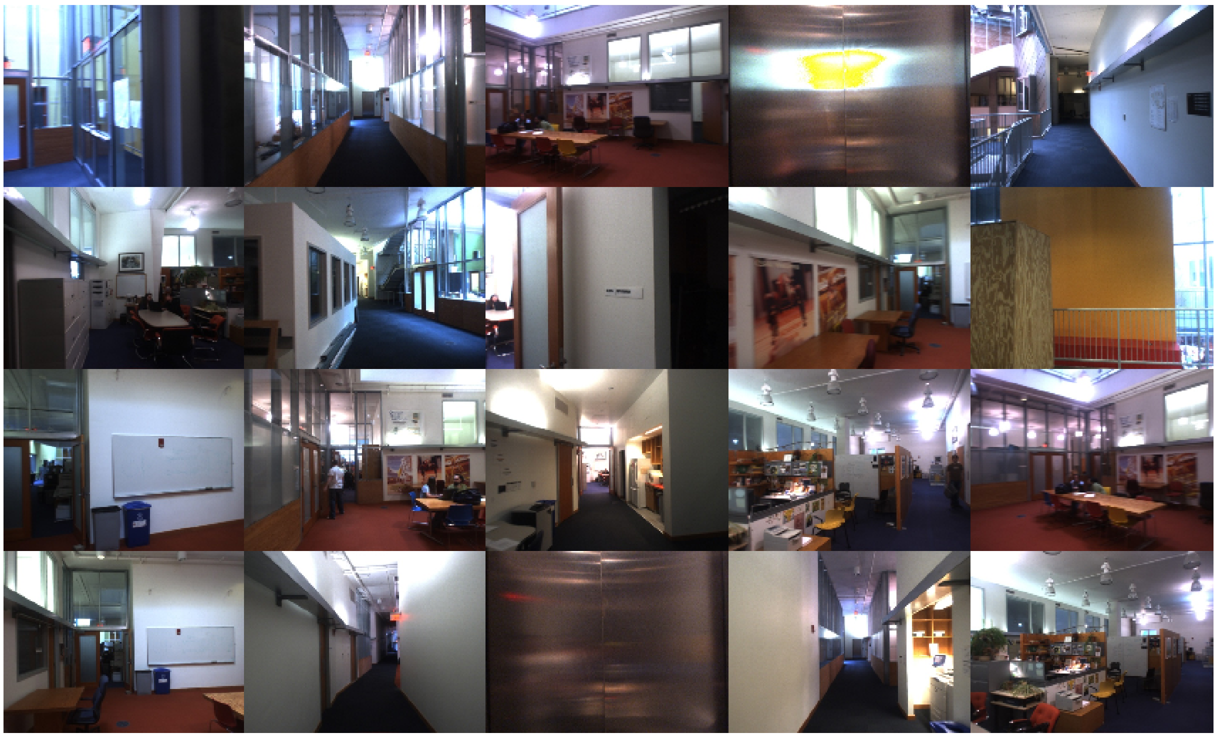

Figure 3.8: Sample of left images from stereo pair of a Stata Center indoors session used for learning.

Table 3.4 shows the weights as result of the learning process with the indoor dataset in the Stata Center building. The weights are learned for both graphs.

From the Table. 3.5 we can see that the model is not over-fit to the subset of training.

		SURF	*geo*			*PCA*			*curv*	*pair*	*outlier*	
			k=1	k=2	k=3	1^{st}	2^{nd}	3^{rd}			*local*	*pair*
$\mathcal{G}_{3D}$	**w**	-15.45	-1.10	-0.53	-0.83	-0.41	-3.40	-0.22	0.54	-17.46	-2.09	-1.10
$\mathcal{G}_{Im}$	**w**	-19.56								-12.63	-1.77	-0.74

Table 3.4: Weights obtained in the learning process in the Stata Center indoors session.

	$\mathcal{G}_{3D}$		$\mathcal{G}_{Im}$	
	Training set	Validation set	Training set	Validation set
Accuracy	85.61%	81.44%	72.17%	74.37%

Table 3.5: Statistics of the learning process in the Stata Center indoors session.

In the Fig. 3.9 we show a typical result of the data association between sequential scenes with the parameter previously learned over a Stata Center outdoors session taken on July 19th of 2010. The process take $\approx 0.3s$ in average for both graphs (including the SURF extraction).

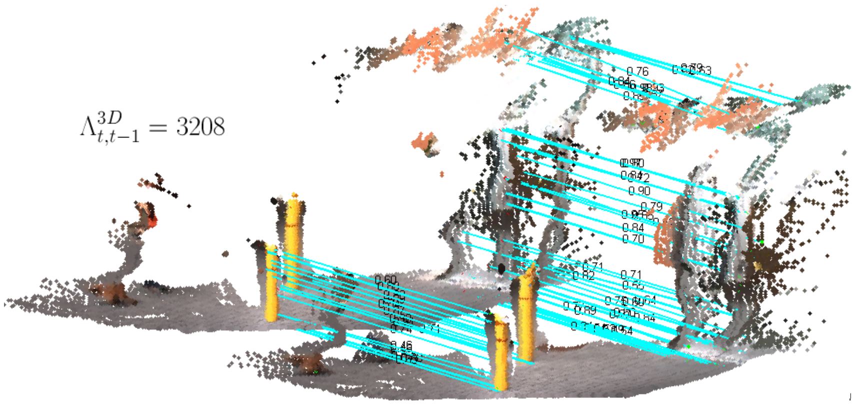

(a) CRF-Matching over 3D information

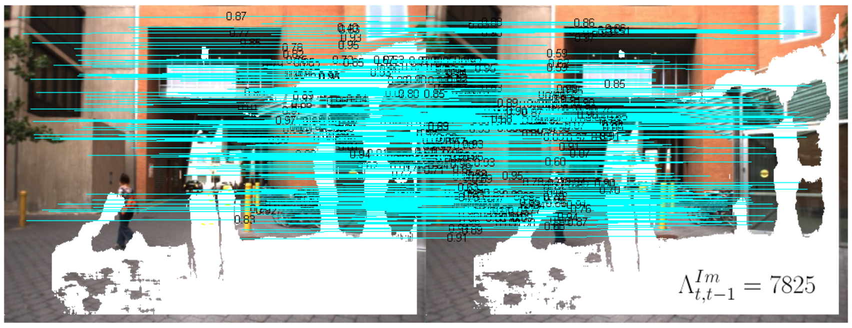

(b) CRF-Matching over image information

Figure 3.9: Data association results with CRF-Matching for each graph, $\mathcal{G}_{3D}$ in (a) and $\mathcal{G}_{Im}$ in (b). The scenes have one second of separation. In both we show the individual probabilities of associations and the negative log-likelihood for the maximum-a-posteriori Λ.

3.2 Using CRFs for Place Recognition

Up to now, we have seen how to find the correspondences between two scenes, in both 3D and image space, with CRF-Matching. This very powerful tool has its advantages and limitations. The main advantage is that it allows us carry out robust similarity comparisons only using the information provided by the sensor. The limitation is the computational cost: two scenes can be compared in constant time, thus the cost of finding similar scenes in a sequence with n scenes will be $\mathcal{O}(n)$.

With this issue in mind, we propose to solve the place recognition problem by using two complementary techniques. The *first* one is based on the bag-of-words method (BoW) of Sivic and Zisserman (2003), which reduces images to sparse numerical vectors by quantising their local features. This enables quick comparisons among a set of images to find those which are similar. We rely on the efficient technique of detection of *candidates* to loop closing developed and implemented by Dorian Gálvez-López[1]. Here, we only give a

[1]Available at http://webdiis.unizar.es/˜dorian

short description of his implementation and its novelties.

After candidates generation, only the unclear loop closure candidates are *verified* by matching the scenes with CRFs. We also propose accepting the loop closure candidates based on a normalised similarity score in terms of the likelihoods of the matched scenes with respect to recent images. Ramos et al. (2007) proposed the possibility of detecting loop closures with CRF by taking the maximum log-likelihood of the match between the current and all previous scans. Comparing the current location against all the previous ones is impractical in real applications. Furthermore, their metric does not provide a way to decide between true and false loop closures.

Our basic idea is to exploit the efficiency of BoW for detecting candidate revisited places in real-time, and in unclear cases use the robustness of CRF-Matching to verify that candidate matches are correct.

3.2.1 Method

Our place recognition system can be summarised in algorithm 4.

Algorithm 4 Place recognition system

```
Input: Scene at time $t$, Database $\langle 1, \dots, t-1 \rangle$
Output: Time $t'$ of the revisited place, or null
  $Output = Null$
  Search the bag-of-words database for the best matching scene at $t'$ with score $\eta_c(t,t')$
  if $[t-1, t'_1], ..., [t-\tau_l, t'_{\tau_l}]$ matched and $|t'_i - t'_j| \leq \tau_d$ then
    {Loop candidate detected}
    if $\eta_c(t,t') \geq \alpha^+$ then
      $Output = t'$    {Accepted}
    else
      if $\eta_c(t,t') \geq \alpha^-$ then
        {Loop candidate verification}
        Build $\mathcal{G}_{3D}$ and $\mathcal{G}_{Im}$
        Infer with CRFs and compute the scores $\eta_{\mathcal{G}}$
        if $\eta_{3D}(t,t') \leq \beta_{3D} \wedge \eta_{Im}(t,t') \leq \beta_{Im}$ then
          $Output = t'$    {Accepted}
        end if
      end if
    end if
  end if
  Add current scene to the Database
```

Loop Closing Detection

The first component is based on the bag-of-words method (BoW) of Sivic and Zisserman (2003) which is implemented in a hierarchical way, thus improving efficiency (Nister and Stewenius 2006). In this implementation we use 64-SURF-features, see Fig. 3.3(a) with the novelties proposed by Gálvez-López in (Cadena et al. 2011a):

Normalised similarity score Representing images as numerical vectors is very convenient since it allows performing really quick comparisons between images. Given two vectors v and w, their similarity is measured as the score $s(v, w)$:

$$s(v, w) = 1 - \frac{1}{2}\left\| \frac{v}{||v||} - \frac{w}{||w||} \right\| \tag{3.9}$$

where $||.||$ stands for the L_1-norm. Note that this score is 0 when there is no similarity at all, and 1 when both vectors are the same.

In the special case where the acquired data are sequential the vectors v and w are associated to instants of time t and t'. It is expected to have lots of very similar images in our problem, since they are collected close in time. This may make the matched vector with highest score s be incorrect in many cases. It is desirable to distinguish those cases, but the range over which the score s varies is very dependent on the query image. For these reasons, a metric of similarity is defined, the *normalised similarity score*, as:

$$\eta_c(t, t') = \frac{s(v_t, w_{t'})}{s(v_t, v_{t-\gamma})} \tag{3.10}$$

The score obtained is normalised from a match between v_t and $w_{t'}$ with the expected score for the query vector v_t. The expected value for v_t is the score obtained when comparing it against a very similar vector. Here, the vector obtained $\gamma = 1s$ ago. The higher η_c is, the more similar two images are. Unlike score s, values of the normalised score η_c from different images can be directly compared. Note that the normalised similarity score can be defined for any similarity score.

Temporal consistency To detect loops, a temporal constraint is imposed. A loop candidate between images at time t and t_0 is detected if there are matches $< v_t, w_{t_0} >$, $< v_{t-1}, w_{t_1} >$, ..., for a short time interval $\tau_l = 4$ seconds, and the timestamps t_0, t_1, ..., are close (i.e. their difference is within $\tau_d = 2$ seconds). These temporal values were selected according to the frequency of image sequences, and the expected reliability of the method.

Double threshold Finally, the match $< v_t, w_{t_0} >$, with normalised score $\eta_c(t, t_0)$, is checked by a *double threshold* (α^-, α^+) in order to be accepted as a loop closure. There are three possibilities:

1. if $\eta_c(t, t_0) \geq \alpha^+$ the match is considered highly reliable and accepted;

2. if $\alpha^- < \eta_c(t, t_0) < \alpha^+$ the match is checked by CRF-Matching in the next step of verification.

3. if $\eta_c(t, t_0) \leq \alpha^-$ the match is ignored.

Loop Closing Verification

We use the CRF matcher stage over the loop closing candidates provided by the BoW stage. We compute the negative log-likelihood (Λ) from the MAP associations between the scene in time t, against the loop closing candidate in time t', $\Lambda_{t,t'}$, and the scene in $t - \gamma$, $\Lambda_{t,t-\gamma}$, $\gamma = 1s$.

The negative log-likelihood Λ^{3D} of the MAP association for $\mathcal{G}_{3D}$ provides a measure of how similar two scenes are in terms of close range, and Λ^{Im} for $\mathcal{G}_{Im}$ in terms of far range. Thus, in order to compare how similar the current scene is with the scene in t', $\Lambda_{t,t'}$, with respect to how similar the current scene is with the scene in $t - \gamma$, $\Lambda_{t,t-\gamma}$, we use again a normalised similarity score as:

$$\eta_{\mathcal{G}} = \frac{\Lambda^{\mathcal{G}}_{t,t'}}{\Lambda^{\mathcal{G}}_{t,t-\gamma}} \tag{3.11}$$

where $\mathcal{G}$ indicates the graph.

Score $\eta_{\mathcal{G}}$ is compared to $\beta_{\mathcal{G}}$, a control parameter of the level of similarity we demand for $(t, t-\gamma)$, where a smaller β means a higher demand. By choosing different parameters for near and far information we can balance the weights of each in our acceptance.

3.3 Experiments

3.3.1 Front-facing cameras

We tested the place recognition system in three datasets from the RAWSEEDS Project: static indoors, static outdoors and dynamic mixed. These three and the training datasets were collected on different dates and in two different campuses. Please refer to the RAWSEEDS (2009) Project for more details. We use the weights learned from the training dataset, see table 3.3.

For the first bag-of-words stage, we have to set the minimum confidence expected for a loop closure candidate, α^-, and the minimum confidence for a trusted loop closure, α^+. In Fig. 3.10 we can see the precision-recall performance of the detection by varying the minimum confidence value expected for a loop closure candidate of BoW, α^- (with fixed minimum confidence level for a trusted loop closure, $\alpha^+ = 0.6$). We selected the working values $\alpha^- = 0.15$. We have set these parameters by observing their effect on the precision-recall curves achieved by the BoW algorithm on its own in the indoor and outdoor datasets tested (see Fig. 3.10). Since these datasets are fairly heterogeneous, we think these values can work well in many situations. It might depend on the vocabulary size, though.

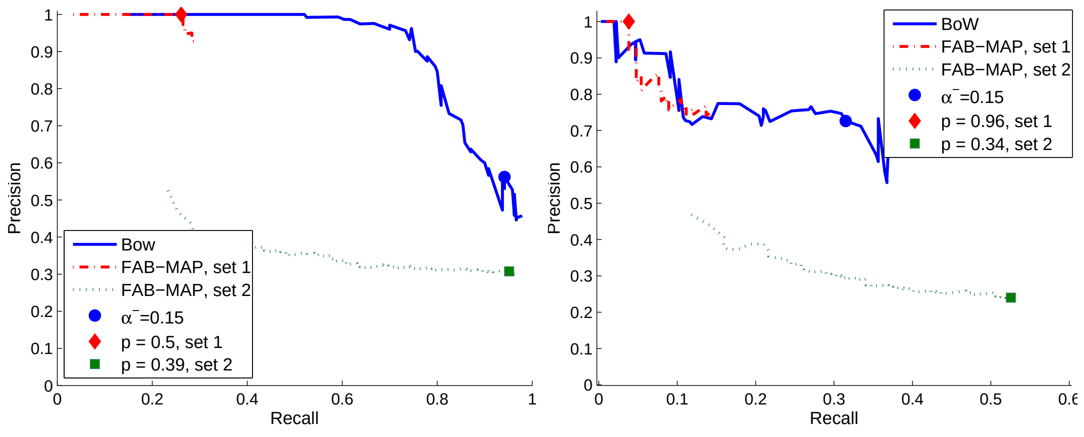

(a) Indoor (b) Outdoor

Figure 3.10: Precision and Recall in the (a) indoor dataset and (b) outdoor dataset, without CRF verification or epipolar constraint.

For the second CRF matcher stage, we work on the set-point given by the α parameters selected. Then, by varying the β parameters we obtain the precision-recall curves of the Fig. 3.11. Note the scale and the improvements with respect to the BoW precision-recall curve. We set the β parameters in order to obtain 100% precision, see below. We do this to compare recall. We use the parameters obtained for the outdoor dataset also in the mixed dataset. All the parameters used are shown in Table 3.6.

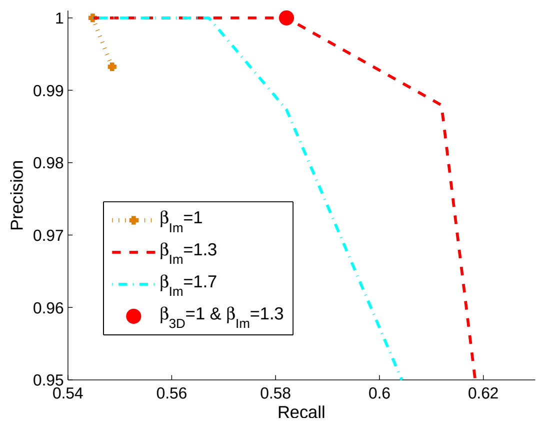

(a) Indoor

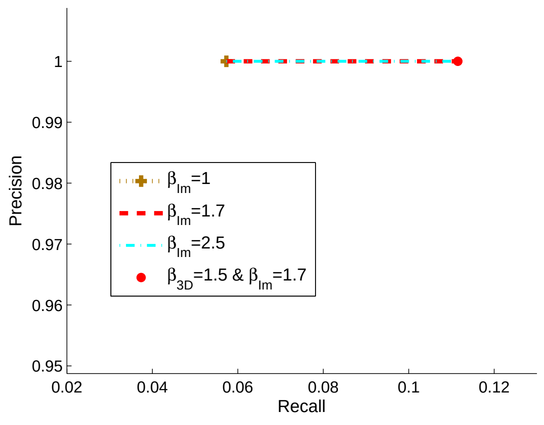

(b) Outdoor

Figure 3.11: Precision and Recall in (a) the indoors dataset and (b) outdoors dataset with CRF verification. Each curve is computed for a constant value of β_{Im} and sweeping of β_{3D} parameter between $[0, 3]$.

We have compared the results from our system against the state-of-the-art technique FAB-MAP 2.0 of Cummins and Newman (2010). The FAB-MAP software[2] provides some predefined vocabularies. We have used the FAB-MAP indoor vocabulary for our indoor dataset and the FAB-MAP outdoor vocabulary for our mixed and outdoor datasets. This technique has a set of parameters to tune in order to obtain the best performance in each experiment. The parameters that we have modified are the following ones (for further details please see Cummins and Newman (2008, 2010)):

- p: Probability threshold. The minimum matching probability required to accept that two images were generated at the same place.
- $P(\text{obs}|\text{exist})$: True positive rate of the sensor. Prior probability of detecting a feature given that it exists in the location.
- $P(\text{obs}|\neg\text{exist})$: False positive rate of the sensor. Prior probability of detecting a feature given that it does not exist in the location.
- $P(\text{newplace})$: Probability for new place. Prior probability that the last image is a new place.

[2]The software and vocabularies were downloaded from `http://www.robots.ox.ac.uk/~mobile/`

- σ: Likelihood smoothing factor. Factor for smoothing the likelihood values through consecutive places.
- *Motion Model*: Model Motion Prior. This biases the matching probabilities according to the expected motion of the robot. A value of 1.0 means that all the probability mass goes forward, and 0.5, means that probability goes equally forward and backward.
- *Dis. Local*: Disallow N local matches. Set the prior to be zero on the last N places. We use the same parameter in our system during the BoW stage for not producing matches against the last N scenes.

The final values used by us are shown in table 3.6. Figs. 3.10(a,b) show the precision-recall curves varying the probability of acceptance p. We have chosen two parameter sets in order to obtain different results. The first one is tuned to obtain the maximum possible recall at one hundred percent precision. The second set is tuned to obtain the maximum possible recall, to improve the precision in a second step with geometrical checking. Since the last available version of the FAB-MAP software does not implement the geometrical checking described by Cummins and Newman (2010), we implemented the geometrical checking based on epipolar geometry. This epipolar constraint consists in computing the fundamental matrix (by using RANSAC and the 8-point algorithm (Hartley 1997)) between the two matched scenes by FAB-MAP. This test is passed if a well conditioned fundamental matrix can be obtained.

The results of FAB-MAP over the datasets are shown in Figs. 3.12(a), 3.14(a) and 3.15(a) for the first set of parameters and in Figs. 3.12(b), 3.14(b) and 3.15(b) for the second set of parameters plus the geometrical checking with the epipolar constraint.

In order to show the improvements of our stage of loop closure verification, we have checked the same candidates with the epipolar constraint. The results are shown in

Table 3.6: Parameters for the experiments

	FAB-MAP 2.0							Our System		
	Indoor		Outdoor		Mixed			Indoor	Outdoor	Mixed
	set 1	set 2	set 1	set 2	set 1	set 2				
p	0.50	0.39	0.96	0.53	0.62	0.29	α^+	0.6	0.6	0.6
$P(\text{obs}\|\text{exist})$	0.31	0.31	0.39	0.31	0.37	0.31	α^-	0.15	0.15	0.15
$P(\text{obs}\|\neg\text{exist})$	0.05	0.01	0.05	0	0.05	0	β_{3D}	1	1.5	1.5
$P(\text{newplace})$	0.9	0.9	0.9	0.9	0.9	0.9	β_{Im}	1.3	1.7	1.7
σ	1	0.99	1	1	1	1	τ_l	4s		
Motion Model	0.8	0.8	0.8	0.6	0.6	0.6	τ_d	2s		
Dis. Local	20s						Dis. Local	20s		

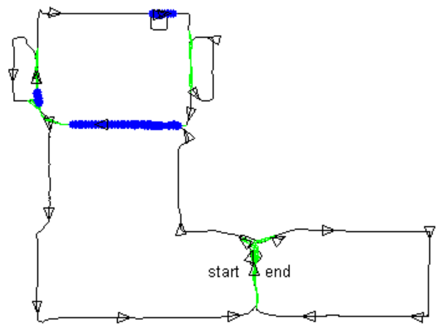

(a) FAB-MAP (set 1)

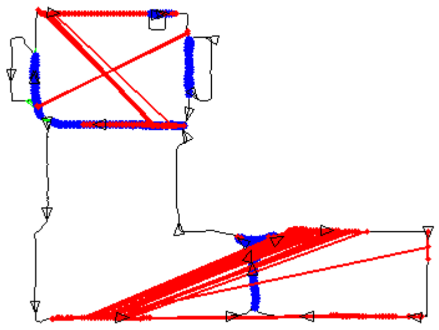

(b) FAB-MAP (set 2) + Epipolar Constraint

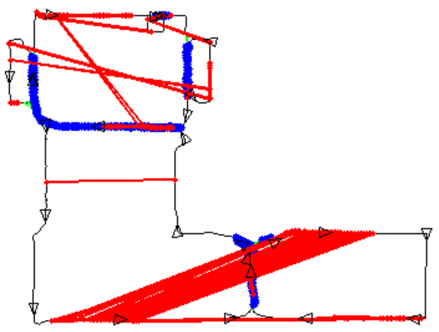

(c) BoW + Epipolar Constraint

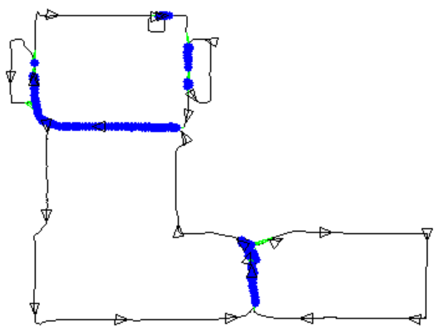

(d) Our System

Figure 3.12: Loops detected by each of the methods in the Indoor dataset. First row: FAB-MAP with the set 1 of parameters (left), FAB-MAP with the set 2 of parameters plus the epipolar constraint (right). Second row: BoW + epipolar constraint (left), and our system (right). Black lines and triangles denote the trajectory of the robot; light green lines, actual loops, deep blue lines denote true loops detected, and light red lines denote false loops detected.

Figs. 3.12(c),. 3.14(c) and 3.15(c). In all the cases the precision was less than 100%. The results of our system over the datasets are shown in Figs. 3.12(d), 3.14(d) and 3.15(d), and the comparative statistics of all experiments made in the Table 3.8.

The indoor experiment is shown in Fig. 3.12. Some loop closures are not detected (Fig. 3.12(a)), including the big area on the beginning of the map, especially important in the experiment because if no loop is detected in that area, a SLAM algorithm can hardly build a correct map after having traversed such a long path (around 300 metres). In Fig. 3.12(b) and 3.12(c) all the loop closures are detected but with too many false positives due to perceptual aliasing, see Fig. 3.13; this is disastrous for any SLAM algorithm. The result from our system is shown in Fig. 3.12(d). At 100% precision we can detect all the loop closure areas.

In the outdoor dataset, FAB-MAP does not detect all the loop closures either, as shown in Fig. 3.14(a). In Fig. 3.14(b) almost all the loop closures are detected at 100% precision, and the recall is close to the one obtained by our system (see second block,

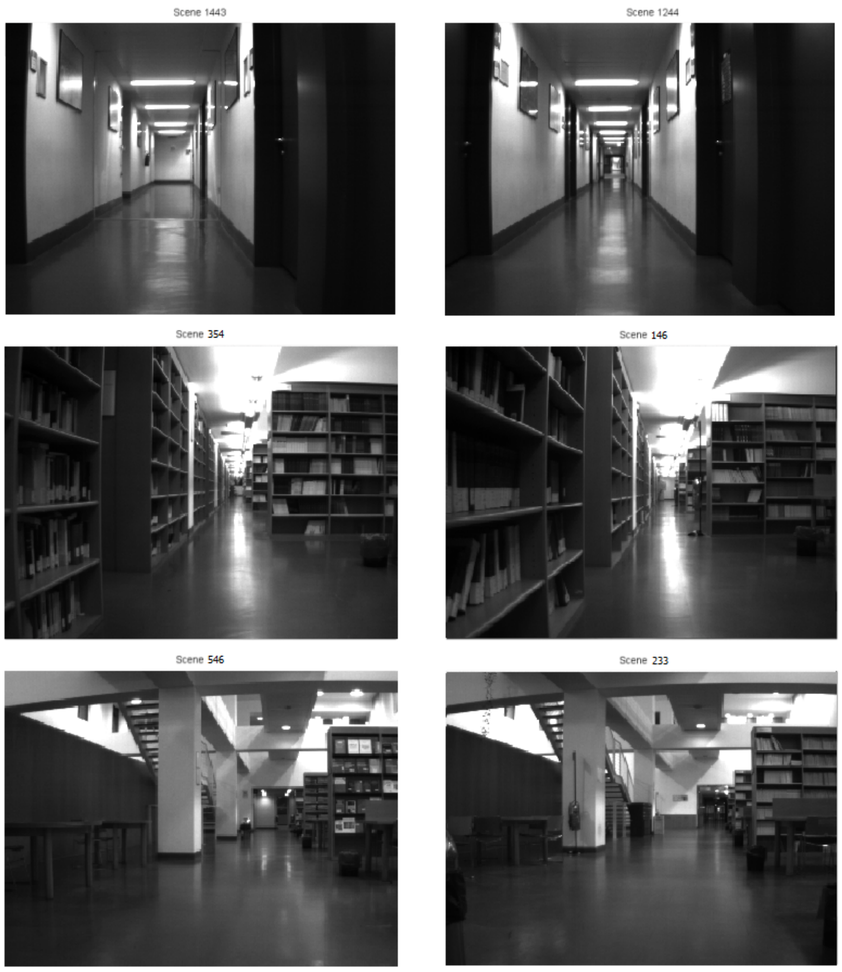

Figure 3.13: Three of the false positive cases that the FAB-MAP and BoW plus epipolar constraint obtain in the indoor dataset.

second and fourth row, of Table 3.8), but the biggest loop is missed at the starting and final point of the experiment, in the top-right area of the map. An example of a false negative in this area is shown in Fig. 3.16(a). The verification with the epipolar constraint over the candidates of our first stage results in some false positives, see Fig. 3.14(c). The result of our system is shown in Fig. 3.14(d). At 100% of precision we can detect all the loop closure areas.

For the experiment in the dynamic mixed environment, both FAB-MAP and our system obtain 100% precision, though our system results in a higher recall level (Table 3.8, third block). Furthermore, FAB-MAP does not detect all the loop closure zones in the map (see figures 3.15(a) and 3.15(b)). Examples of false negative cases are shown in Fig. 3.16(b). This cases are correctly matched by our system (see 3.15(d)). In this experiment, the verification with epipolar constraint over the candidates of our first stage result again in some false positives, see Fig. 3.15(c).

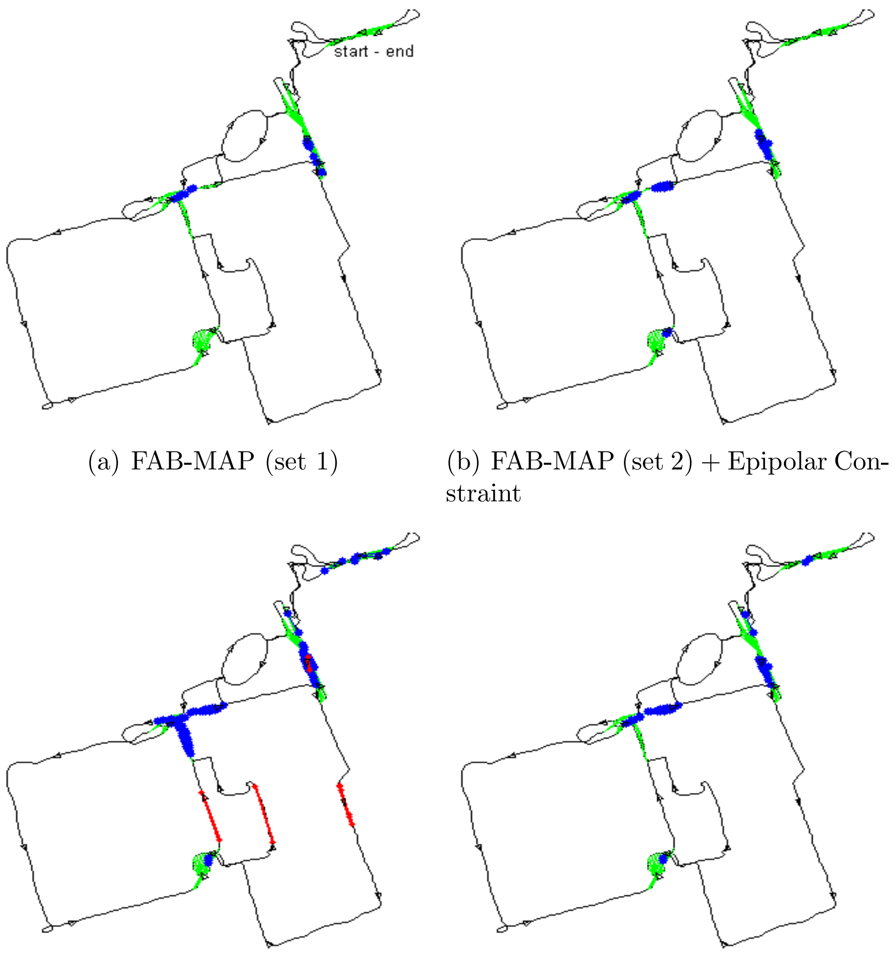

(a) FAB-MAP (set 1)

(b) FAB-MAP (set 2) + Epipolar Constraint

(c) BoW + Epipolar Constraint

(d) Our System

Figure 3.14: Loops detected by each of the methods in the Outdoor dataset. First row: FAB-MAP with the set 1 of parameters (left), FAB-MAP with the set 2 of parameters plus the epipolar constraint (right). Second row: BoW + epipolar constraint (left), and our system (right). Black lines and triangles denote the trajectory of the robot; light green lines, actual loops, deep blue lines denote true loops detected, and light red lines denote false loops detected.

The system also was evaluated using a dataset taken at the MIT campus. In the Fig. 3.17 we sketch the trajectories (using Google Maps) and results. Both our system and FAB-MAP obtain similar results in precision and recall. The weights used for CRF matcher are from Table 3.4. The parameters for both, FAB-MAP 2.0 and our system are shown in Table 3.7. In this dataset it was not necessary to use the geometrical checking over the FAB-MAP results, but we have to lower the probability threshold to obtain the better recall possible at full precision. FAB-MAP with the same parameters but with $p = 0.9$ obtains a recall of 17.7% and only detects 3 of the 5 loops.

The on-line system runs at 1 fps in all the experiments executed. We have a research implementation in C++ using the OpenCV library. In Table 3.9 we show the average

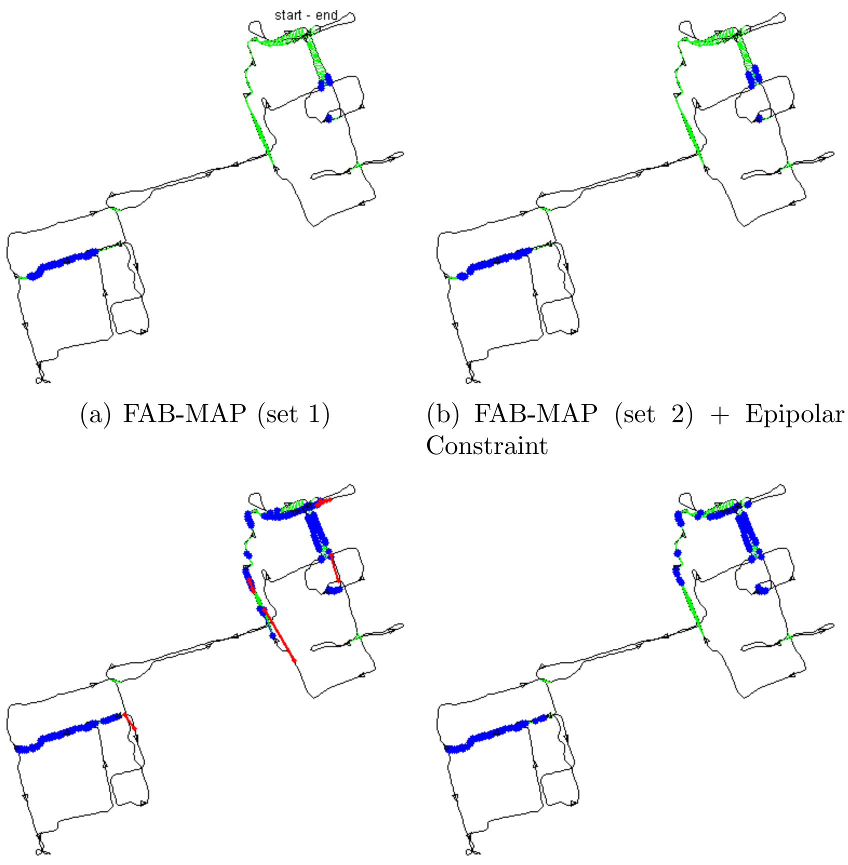

(a) FAB-MAP (set 1)

(b) FAB-MAP (set 2) + Epipolar Constraint

(c) BoW + Epipolar Constraint

(d) Our System

Figure 3.15: Loops detected by each of the methods in the Mixed dataset. First row: FAB-MAP with the set 1 of parameters (left), FAB-MAP with the set 2 of parameters plus the epipolar constraint(right). Second row: BoW + epipolar constraint (left), and our system (right). Black lines and triangles denote the trajectory of the robot; light green lines, actual loops, deep blue lines denote true loops detected, and light red lines denote false loops detected.

Table 3.7: Parameters for MIT Campus experiments

FAB-MAP 2.0	p	$P(\text{obs}\|\text{exist})$	$P(\text{obs}\|!\text{exist})$	Motion Model
	0.33	0.39	0.05	0.6
Our system	α^+	α^-	β_{3D}	β_{Im}
	0.6	0.15	1.5	1.7

and maximum times for each stage of the system on a 2.3 GHz IntelCore i3 CPU M350 and 4GB of RAM. For the whole system, the average and the maximum times were computed only when all the stages were executed. Note that the maxima for each stage happen in different scenes. That is more evident in the inference process for $\mathcal{G}_{3D}$ and $\mathcal{G}_{Im}$: when a scene provides us with more 3D points, it leaves us with less background information. For a scene, the number of nodes and hidden states between $\mathcal{G}_{3D}$ and $\mathcal{G}_{Im}$ are complementary. The times reported for the CRFs in the graphs include computing the MSTs, the corresponding features and the inference for each one. The times for the

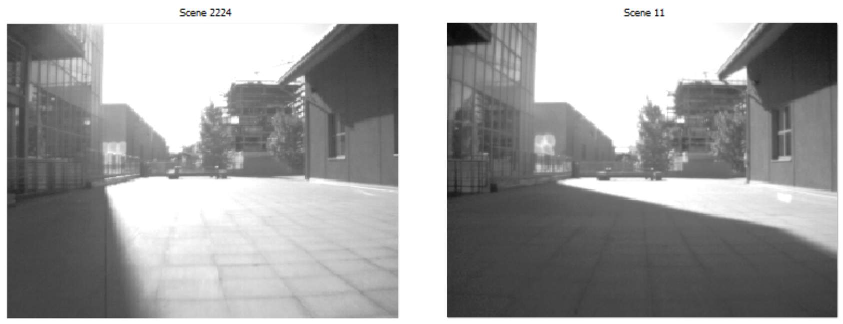

(a) Outdoor (start-final)

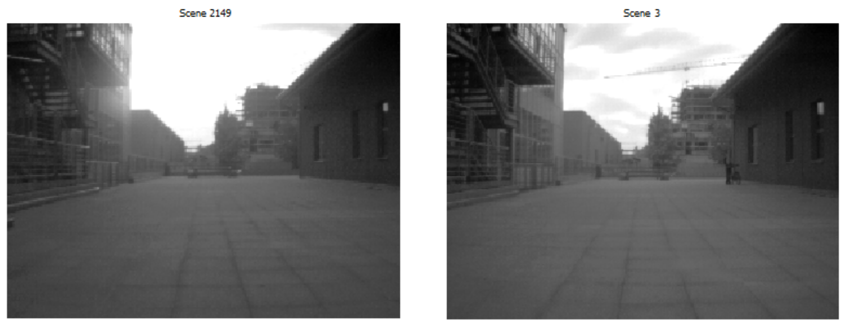

(b) Mixed (start-final)

Figure 3.16: False negatives of FAB-MAP with geometrical checking, both with parameter sets 1 and 2, in the outdoor and mixed datasets. These scenes correspond to the biggest loops in the trajectories.

Table 3.8: Results for all datasets

	Precision	Recall	loop zones found/actual
RAWSEEDS Indoor			
FAB-MAP set 1	100%	26.12%	2 / 6
FAB-MAP set 2 + EC	52.37%	82.46%	6 / 6
BoW + EC	58.54%	80.6%	6 / 6
Our System	**100%**	**58.21%**	**6 / 6**
RAWSEEDS Outdoor			
FAB-MAP set 1	100%	3.82%	2 / 9
FAB-MAP set 2 + EC	100%	10.83%	3 / 9
BoW + EC	92.63%	28.03%	6 / 9
Our System	**100%**	**11.15%**	**6 / 9**
RAWSEEDS Mixed			
FAB-MAP set 1	100%	13.47%	3 / 8
FAB-MAP set 2 + EC	100%	15.27%	3 / 8
BoW + EC	92.9%	47.01%	6 / 8
Our System	**100%**	**35.63%**	**5 / 8**
Multisession MIT			
FAB-MAP	100%	38.89%	5 / 6
Our System	**100%**	**38.27%**	**5 / 6**

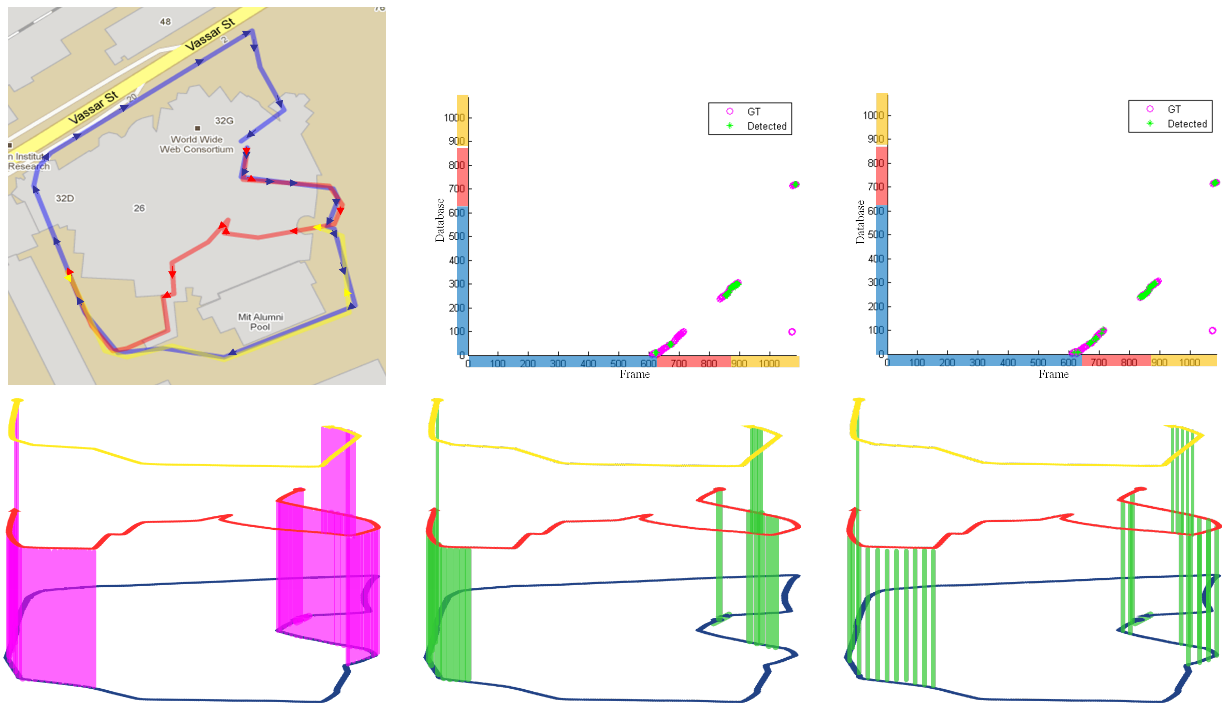

Figure 3.17: Multisession experiment in the MIT campus. Loops closure(green lines and stars) detected in the Stata Center multi-session dataset with FAB-MAP (top-middle and bottom-middle) and our system (top and bottom right). Different colours correspond to different sessions (blue, red and yellow). On the top, the Google map (left) and we show the query of the current frame vs. the database with the frames already added (middle and right). Ground truth (GT) is showed on bottom-left with magenta lines, on top with magenta circles.

whole system include computing the 3D point cloud from the disparity map and writing and reading the SURF descriptors and point clouds on disk.

Table 3.9: Computational times for our system (in s)

	SURF extraction	BoW	CRF Matcher		Whole System
			$\mathcal{G}_{3D}$	$\mathcal{G}_{Im}$	
Average	0.15	0.01	0.15	0.15	0.47
Maximum	0.30	0.04	0.36	0.65	1.04

3.3.2 Inclined cameras

In the above tests, the stereo camera system has an inclination with respect to the horizontal of zero degrees. Therefore, the overlap between scenes in a straight trajectory is considerable even with long displacements because the far information in the images. It is even more significant between successive scenes at 1 fps as we sample. The normalised similarity scores $(\eta_c, \eta_{3D}, \eta_{Im})$ that we use in our place recognition system take advantage of this issue to better discriminate revisited places. The next question is how the α and β parameters should change if we know the configuration is different?

In order to answer this question we use the New College dataset (Smith et al. 2009). This was gathered while traversing 2.2km through a college's grounds and adjoining parks in the University of Oxford. In this dataset the stereo camera has an inclination with respect to the horizontal of -13 degrees. Then, the most of the scene is cover by the ground. Although this configuration is more suitable to obstacle avoidance than to place recognition tasks, it serves us to evaluate the changes in parameters of our system.

Again, we take the stereo images at 1 fps and execute our place recognition system. Here, we use the previous learning with the static mixed dataset form RAWSEEDS, the vocabulary for the detection stage as well as CRFs' weights for the verification stage.

In the loop detection stage, the first thing that we find is the high perceptual aliasing that affects the appearance based methods. The first parameter that we have to change is the minimum confidence level for a trusted loop closure, α^+, we rise it up to 1. Otherwise, cases as that we show in Fig. 3.18 are accepted without going through the verification stage. Because, η_c is not as discriminative as with front facing cameras; the appearance of the scene k with respect to $k-1$ changes a lot but it keeps similar words.

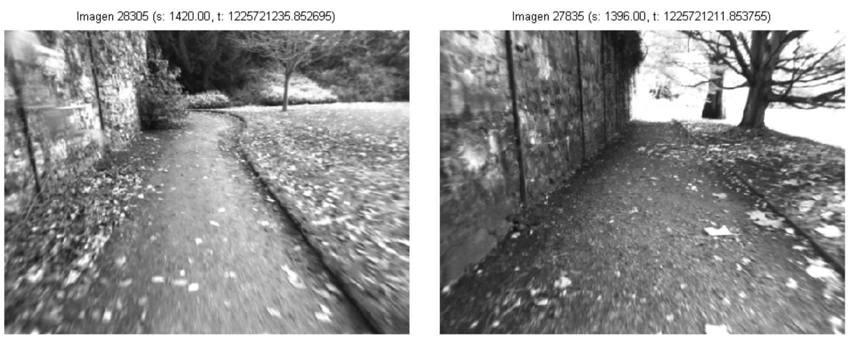
Imagen 28305 (s: 1420.00, t: 1225721235.852695)
Imagen 27835 (s: 1396.00, t: 1225721211.853755)

Figure 3.18: False positive for our system with $\alpha^+ = 0.6$.

In the loop verification stage, we initially maintain the β parameters for outdoors, 1.5 for $3D$ and 1.7 for Im. With the stereo looking down, we have less far information to infer, but the normalised score η_{Im} will discriminate as before. Then we do not need change β_{Im}. A different case is the discriminative ability of η_{3D}. Since in this environment the appearance and shape features used in $\mathcal{G}_{3D}$ are very repetitive, we need to be more strict with the value of β_{3D}. We select the same as before for indoors, 1.0. Otherwise, cases like the one that we show in the Fig. 3.19 would be false positives. We show the final result of our system in Fig. 3.21(b).

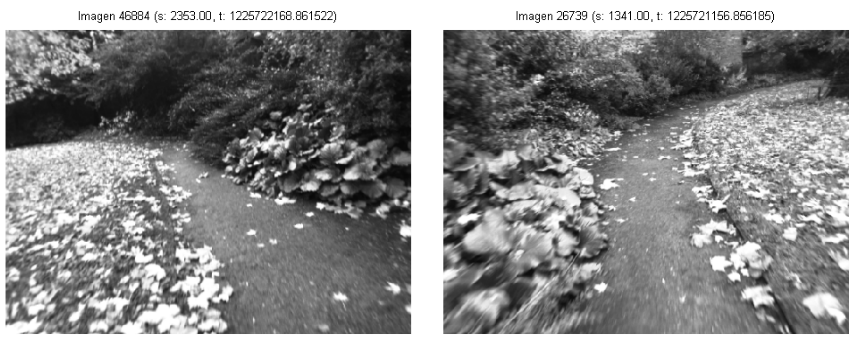
Imagen 46884 (s: 2353.00, t: 1225722168.861522)
Imagen 26739 (s: 1341.00, t: 1225721156.856185)

Figure 3.19: False positive for our system with $\beta_{3D} = 1.5$ in the New College dataset.

Again, we compare our final results in the New College dataset against FAB-MAP 2.0. Newman et al. (2009) already use FAB-MAP in this dataset but using the Ladybug panoramic camera with $p = 0.99$ and a verification stage using either the stereo images or the 3D laser returns in the geometrical check. We proceed in the same way as the previous experiments but with the parameters by default in the downloaded software. With the same probability threshold than Newman et al. (2009) $p = 0.99$, the FAB-MAP obtains false positives like the one we show in Fig. 3.20. This is removed by the epipolar constraint. We show the final result in Fig. 3.21(a). See the next section for a discussion of these results.

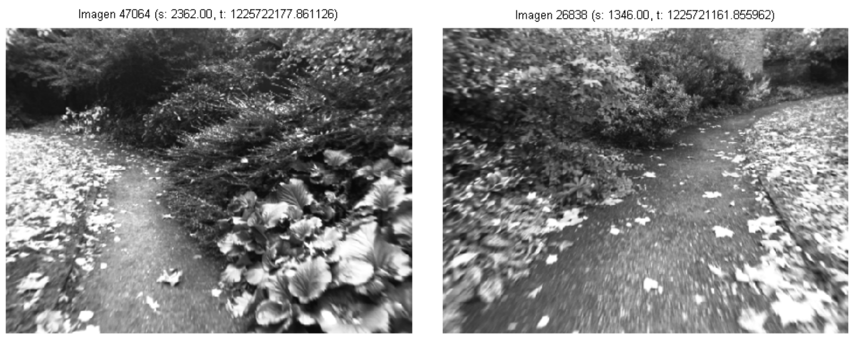
Imagen 47064 (s: 2362.00, t: 1225722177.861126)
Imagen 26838 (s: 1346.00, t: 1225721161.855962)

Figure 3.20: False positive for FAB-MAP without epipolar constraint with $p = 0.99$ in the New College dataset

The final parameters used for both, FAB-MAP 2.0 and our system are showed in Table 3.10 and the corresponding results in Table 3.11.

Please note that the cases in Figs. 3.19 and 3.20 correspond to the same area in the parkland part of the experiment, very close in global position. But, they come from paths in opposite directions.

Table 3.10: Parameters for New College dataset

FAB-MAP 2.0	p	$P(\text{obs}\|\text{exist})$	$P(\text{obs}\|!\text{exist})$	Motion Model
	0.99	0.39	0.05	0.9
Our system	α^+	α^-	β_{3D}	β_{Im}
	1.0	0.15	1.0	1.7

Table 3.11: Results for New College dataset

	Precision	Recall
FAB-MAP + EC	100%	26.7%
Our System	100%	25.2%

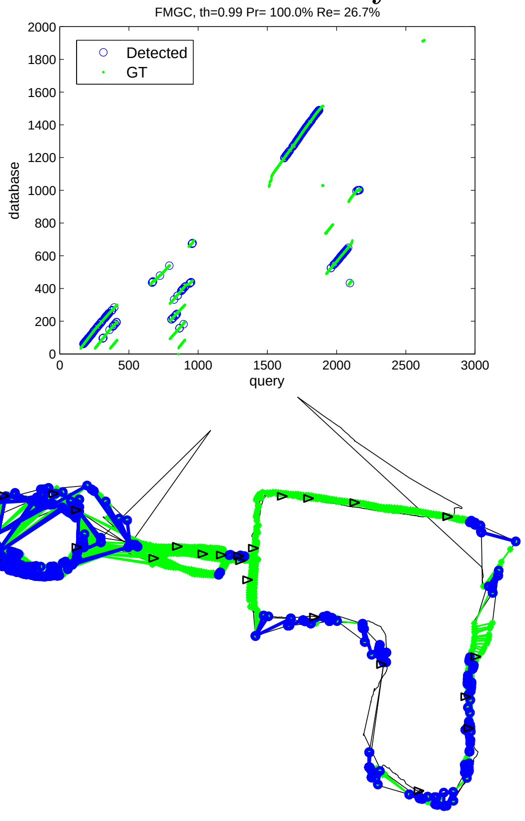

(a) FAB-MAP 2.0 + Epipolar Constraint

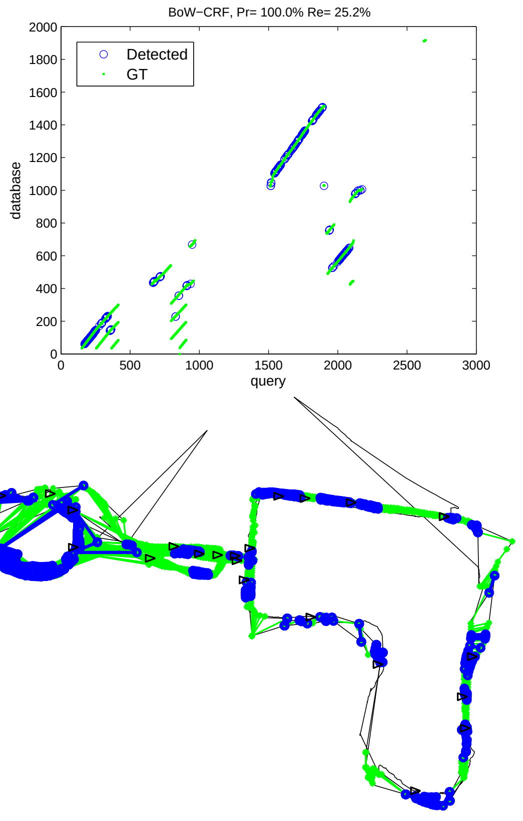

(b) Our System

Figure 3.21: Loops detected in the New College dataset. Black lines and triangles denote the trajectory (GPS) of the robot; light green lines, actual loops, deep blue lines denote true loops detected.

3.4 Discussion

In this chapter we have presented a place recognition system that combines two powerful matching algorithms, bag-of-words and conditional random fields, to robustly solve the place recognition problem with stereo cameras. We have evaluated our place recognition system in public datasets and in different environments (indoor, outdoor and mixed). In all cases the system can attain 100% precision (no false positives) with higher recall than the state of the art (less false negatives) in the front-facing configuration, and detecting all (especially important) loop closure zones. No false positives means that the environment model will not be corrupted, and less false negatives means that it will be more precise. Our system also is more robust in situations of perceptual aliasing.

As mentioned by Piniés et al. (2010), the effectiveness of FAB-MAP decreases when the camera looks forward, because FAB-MAP models the environment as "a collection of discrete and disjoint locations" (Cummins and Newman 2008). However, in our experiments the stereo camera system faces forward and distant objects (e.g., buildings in outdoor scenes) persist for many frames, thus making scenes overlap and be less discriminative. This causes the matching probability mass of FAB-MAP to be flattened over the scenes. It is easier for our system to overcome those situations because our normalised similarity scores (η_c, η_{3D}, η_{Im}) for matching acceptance are computed at each frame and take into account the similarity between consecutive frames.

As expected, when the FAB-MAP's assumption of disjoint locations is satisfied, e.g. the camera looks down, we obtain satisfactory results with no changes in its parameters. Our place recognition system was initially developed for a stereo camera looking forward. With some adjustment for a different configuration, we can obtain the same recall at full precision as FAB-MAP, and also detect more loops closure zones. In the case studied, the only change in our system was to be stricter in two parameters. We increase α^+, trusting pure appearance based acceptance less. We also decrease β_{3D} given that less 3D overlapping with the previous scene implies less discriminative power of the normalised similarity score η_{3D}.

By using jointly the CRF-Matching algorithm over visual near 3D information (here provided by stereo vision, but also possible with range scanners, etc.) and far information, we have demonstrated that challenging false loop closures can be rejected. Furthermore, CRF-Matching is also able to fuse any other kind of information, such as image colour, with ease.

Our place recognition system is able to run in real time, processing scenes at one frame per second. In most cases, after extracting the SURF features (max. $300ms$), our system only takes $11ms$ to detect if there are possible loop closures, and $300ms$ to check them when it is necessary.

In our experiments with front-facing cameras, the β thresholds for acceptance of the CRF matching turned out to be clearly different for indoor and for outdoors scenarios. These parameters will also depend on the velocity of motion, mainly due to the fact that we use scenes from the previous second as reference in the comparisons. Incorporating the computation of these thresholds as part of the learning stage would also make the system more flexible.

An important line of future work is addressing the place recognition problem over time. Our system performs well in multi-day sessions using parameters learned in different months, and this is also true of alternative systems such as FAB-MAP. The environment can also change during the operation in the same session, see Fig. 3.16. Our algorithm is also able to detect places revisited at different times of day, while alternative systems sometimes reject them in order to maintain high precision.

Several extensions are possible for operation in longer periods of time. The vocabulary for the BoW has shown to be useful in different environments, which suggests that a rich vocabulary does not require frequent updates. The learned parameters in the CRF stage can be re-learned in sliding window mode depending on the duration of the mission. The system would then be able to adjust to changing conditions. In cases of periodical changes, such as times of day or seasons, we will need to maintain several environment models and select the most appropriate for a given moment of operation.

Chapter 4

Experiments Using the Combined Filter and BoW-CRF Place Recognition

In this chapter our two main contributions are assembled into a unified featured-based SLAM system, which is tested in diverse environments with different sensors. Our purpose is to show that these two components can be very valuable to build robust and efficient SLAM systems.

Several successful SLAM systems have been have proposed by different robotic groups around the world. In our opinion, two of the most impressive and complete experimental results are Konolige et al. (2010a) in indoor environments and Newman et al. (2009) in outdoor environments.

View-based Maps proposed by Konolige et al. (2010a) are topological maps that use geometric feature matching in stereo views and maintain a vocabulary tree to check loop-closure candidates. The system structure is shown in Fig. 4.1(c). Odometry is computed from the stereo vision. The system has the advantage of scalability: using incremental techniques, new views can be added and the skeleton is optimised online. Skeletons are similar to the pose graphs familiar from laser SLAM work although the latter typical have just 2D implementations. Also, skeletons retain the images that are captured at each node, for future matching via place recognition with a simple bag-of-words approach with a strong geometrical checking. The skeleton is optimised by bundle adjustment and can handle multi-sessions. Recently, McDonald et al. (2011) propose a 6DoF multisession visual SLAM system using also a stereo camera based on the iSAM with anchor nodes

(Kim et al. 2010) and our place recognition system.

Newman et al. (2009) present an impressive integrated system with laser, stereo and omni vision, using visual odometry for front-end tracking from stereo cameras, and FAB-MAP for on-line loop closure using an omnidirectional camera system. When FAB-MAP gives a loop closure, a metric constraint is computed using either the dense point cloud from the stereo or ICP with the laser data. The constraints are used in a batch optimisation. Maps can be stitched together over non-contiguous runs using batch-mode processing.

Using topological maps, Cummins and Newman (2010) have shown the largest experiment with their FABMAP 2.0, Fig. 4.1(b). Using an omni-directional camera installed on a car and a soft geometrical constraint check, their system was tested using two extremely large (70km and 1000km) datasets.

A complete feature-based SLAM system is proposed by Piniés et al. (2010). They implemented CI-Graph (Pinies et al. 2009) as the core algorithm for the estimation and bag-of-words with geometrical checking for loop closures. This system was evaluated using two datasets from the RAWSEEDS Project, one indoors and one outdoors. The sensors used for estimation were the trinocular camera system on board the robot and the odometry when it is available. The map contains 3D point features in both cartesian and in inverse depth parametrisation (Montiel et al. 2008). Place recognition works over one of the images of the trinocular system.

Systems based on visual odometry are very convenient for exploration tasks (Maimone et al. 2007), Fig. 4.1(a). These systems have the important advantage of constant time execution. In only exploratory trajectories which an environment feature is seen for a certain window of time and never more, visual odometry can obtain the same precision in the estimation of the sensor location as a SLAM system. On the Mars Exploration Rovers (Maimone et al. 2007), the visual odometry algorithm uses image feature tracking between stereo image pairs to estimate the translation and rotation between image captures. Unfortunately, visual odometry does not cope with loop closings, and thus, eventual drift in these cases is inevitable.

These systems require very careful engineering in each stage, from the selection and management of the features to track, to the use of weak links for multisession SLAM in (Konolige et al. 2010a), or the semantic labeling of the point clouds in (Newman et al. 2009). The intention of the system implemented here, Fig. 4.1(d), is to show the good performance in efficiency and robustness of our two contributions working together.

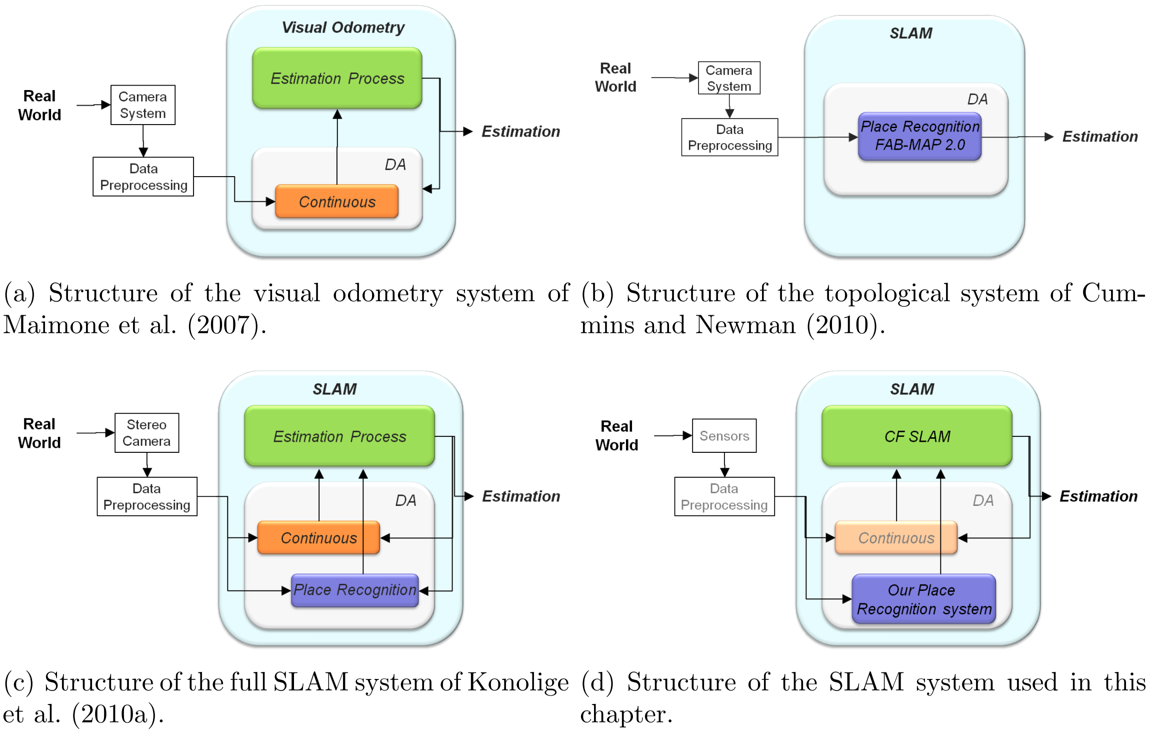

(a) Structure of the visual odometry system of Maimone et al. (2007).

(b) Structure of the topological system of Cummins and Newman (2010).

(c) Structure of the full SLAM system of Konolige et al. (2010a).

(d) Structure of the SLAM system used in this chapter.

Figure 4.1: System structure of some outstanding SLAM systems.

Analysis related to the type of features to track, parametrisation, or the kind of odometry to use (if at all) is out of the scope of this chapter.

4.1 System Overview

Our feature based SLAM system architecture is shown in Fig. 4.2(a).

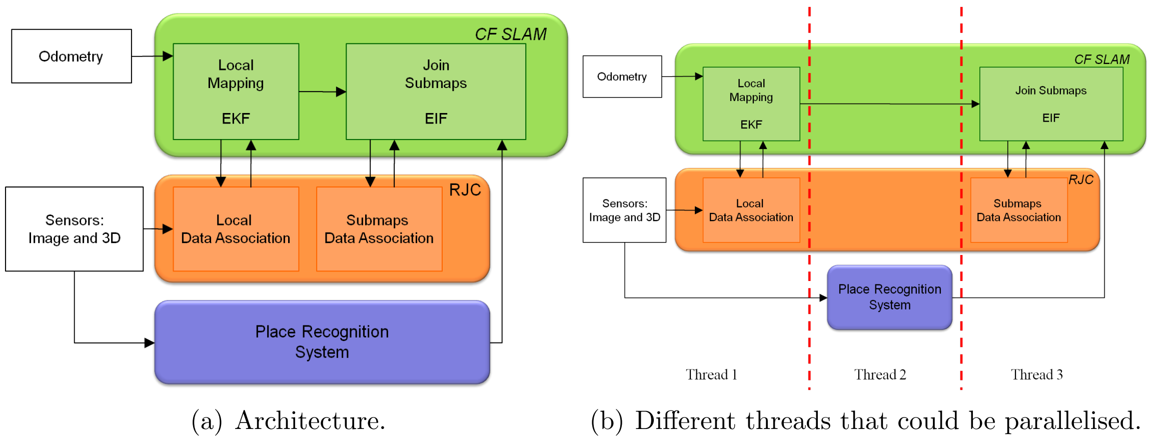

(a) Architecture.

(b) Different threads that could be parallelised.

Figure 4.2: Our feature based SLAM system.

The estimation process is carried out with the CF SLAM algorithm (Cadena and Neira 2009, 2010) detailed in this thesis in Chapter 2. Data association inside local maps is carried out with randomised joint compatibility (RJC) of Paz et al. (2007). We also use RJC as data association algorithm between local maps in the limits of the submaps. To detect revisited places, we use our place recognition system first proposed by Cadena et al. (2010, 2011b) and explained in this thesis in Chapter 3. When map joining CF SLAM queries the place recognition system to see if there is a loop closing between the two sub-maps.

In the following we detail the system components organised by threads, see Fig. 4.2(b).

4.1.1 Local Mapping - Thread 1

Information coming from the sensors is processed to carry out local mapping with a basic EKF SLAM. Since we have available the state covariance, RJC is used for data association. The modules in this thread work as follows:

1. *Odometry*: if available, vehicle odometry is obtained to be used in the EKF prediction step. We keep a pose in the state vector with six components $[x, y, z, \phi, \theta, \psi]$, three Euclidean coordinates and the roll-pitch-yaw angles. In the experiments where the odometry is not available, we use a constant velocity model in which we represent the pose with twelve components in the state vector: three Euclidean coordinates, three angles and six parameters for linear and angular velocities.

2. *Sensors*: these provide the images and the 3D information either from 3D lidar or computed from the stereo cameras. We extract SURF-points in the images and send them to local data association. If the SURF-points have related 3D information, we also use it.

3. *Local Mapping - EKF*: Runs a basic EKF SLAM. Besides the state vector and covariance, we also save the timestamps and descriptors at the first time that each feature was added to the map.

4. *Local Data Association*: This module finds the correspondences between the features already in the map with the observations in the current step. Individual compatibility is computed in the descriptor space and the RJC is carried out with the covariance matrix in order to get reliable correspondences.

When a local map reaches a minimum of features f_{min} and a minimum of steps s_{min} we compute its information form and send it to the map joining process. A new local map is initialised. We enforce a minimum of steps here to guarantee that the map joining process can be amortised in a known number of steps.

4.1.2 Place Recognition - Thread 2

The place recognition system can process images and 3D information from the sensors at 1 fps with their respective timestamps. As explained in section 3.2, SURF points are used for the loop candidates detection stage. With the 3D information, we compute the features and the graphs for the inference in the CRF stage of loop closure validation. We use the SURF and 3D extraction already computed by the sensors module.

The revisited places are sent to the map joining process along with their timestamps.

4.1.3 Joining Submaps - Thread 3

We join the local maps with a divide and conquer strategy, see Fig. 4.3. The modules in this process are:

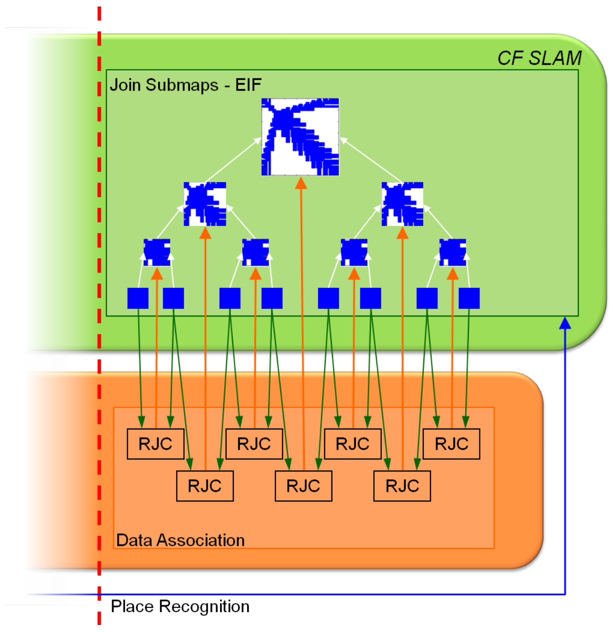

Figure 4.3: A more detailed view of the submap joining process.

1. *Data Association*: Taking advantage of the fact that the local maps have the state covariance available, we execute the RJC algorithm over each consecutive pair of local maps. In this way, correspondences between two sequential submaps can be solved in constant time, independent of the size of the submaps to join in EIF form.

When the local maps are not necessary any more, they are eliminated from memory. Timestamps and descriptors are kept in the computed submaps.

2. *Join submaps - EIF*: This module joins two submaps with EIF. Each join uses the correspondences between submaps from the data association module. In case the two submaps contain timestamps corresponding to revisited places according to the place recognition system, the features in those timestamps are paired in the descriptor space and also used in the joining process.

   Although this joining process can be amortised as we explained in chapter 2, in our prototype, amortisation is not yet implemented.

In our prototype, the CF SLAM and the data association processes are implemented in MATLAB. The place recognition process is implemented in C++ using the OpenCV library. The system runs on a 2.3 GHz IntelCore i3 CPU M350 and 4GB of RAM.

4.2 Evaluation

In this section we evaluate the system using publicly available datasets over two different sensors and robotic platforms, using the RAWSEEDS (2009) Project and the Ford Campus Vision and Lidar Dataset of Pandey et al. (2011).

Here we show four experiments, in three different locations: a building of the Bicocca-campus belonging to the Università di Milano-Bicocca in Milan (Italy), another in the Bovisa-campus of the Politecnico di Milano, located in via Durando, Milan (Italy), and in the Ford Research campus located in Dearborn, Michigan (USA), see Fig. 4.4.

The datasets were obtained in a variety of urban environments and situations: indoors, outdoors, mixed (indoor-outdoor), static, dynamic, and with natural and artificial illumination.

4.2.1 With Stereo Cameras

First we evaluate our SLAM system on a robotic platform with a stereo camera. We use three datasets from the RAWSEEDS project.

We process the data at 5 frames per second in our local mapping and at 1 fps in our place recognition system. In local mapping, we select $f_{min} = 50$ and $s_{min} = 50$ steps

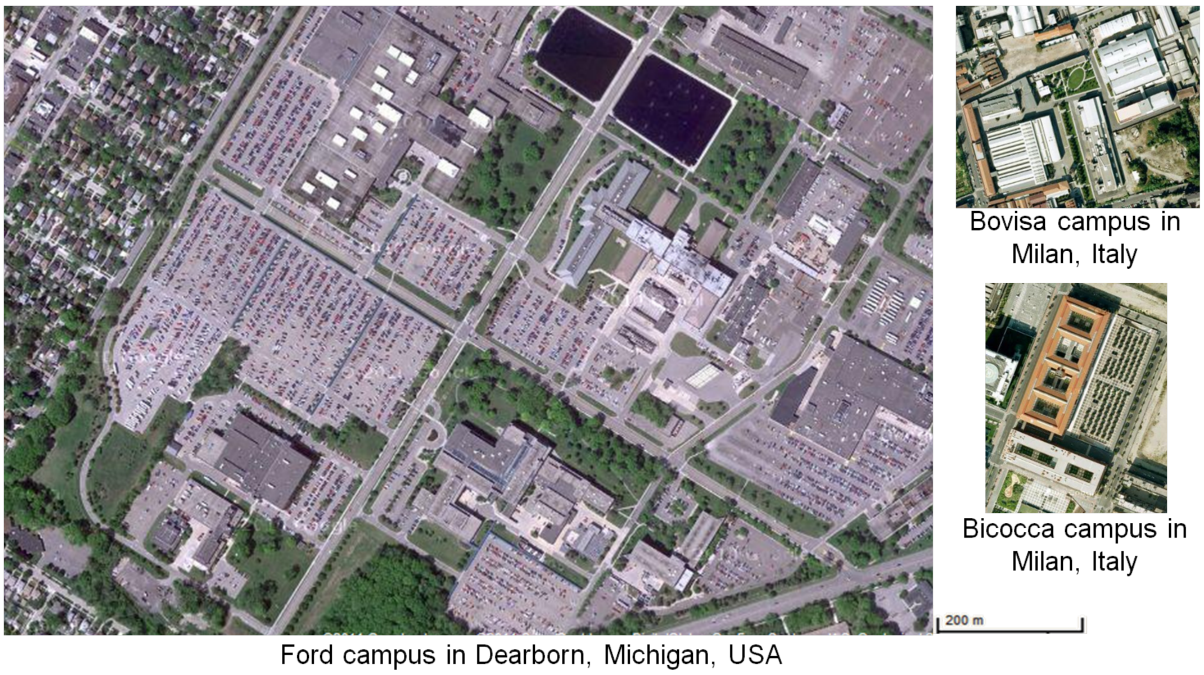
Bovisa campus in Milan, Italy
Bicocca campus in Milan, Italy
200 m
Ford campus in Dearborn, Michigan, USA

Figure 4.4: Locations used for the experimental evaluation of our system. The satellite images are courtesy of Google Maps.

resulting in at least 10s per local map.

For local mapping we use features parametrised in 3D Euclidean coordinates when the SURF points have 3D information from the dense stereo. For the remaining SURF-points, we use the inverse depth parametrisation of Montiel et al. (2008). When the local map is closed and another must be initialised, the inverse depth features with enough parallax, as explained by Civera et al. (2007), are converted to 3D cartesian points. Features with insufficient parallax are marginalised out from the local map.

Accuracy is evaluated by comparing the estimated trajectory to the extended ground truth solution (only indoors) or GPS data with a precision of 0.9m (outdoors). The Absolute Trajectory Errors (ATE) are calculated for each timestamps in the ground truth (GT). Poses from our final estimation are interpolated to the available timestamps in GT. These are computed using the *Rawseeds Metrics Computation Toolkit* provided by the RAWSEEDS Project.

PR Learning Stage: Bovisa_2008-09-01_Static

Our place recognition system uses a vocabulary and a vector of weights for the potentials in CRF-matching as explained in Chapter 3. The parameters used in place recognition are summarised in Table 4.1

Table 4.1: Parameters for RAWSEEDS datasets

	α^+	α^-	β_{3D}	β_{Im}
Indoor	0.6	0.15	1.0	1.3
Mixed	0.6	0.15	1.5	1.7
Outdoor	0.6	0.15	1.5	1.7

Statistics of the cost per step for the place recognition system are shown in Table 4.2.

Table 4.2: Computational times for PR (in s)

	SURF extraction	BoW	CRF Matcher		Whole System
			$\mathcal{G}_{3D}$	$\mathcal{G}_{Im}$	
Average	0.15	0.01	0.15	0.15	0.47
Maximum	0.30	0.04	0.36	0.65	1.04

Indoor: Bicocca_2009-02-25b

This is a dataset in a static environment with artificial illumination. The stereo images were collected during 30min along a path of 760m.

In total, 169 local maps are built. The final result is a map of 5426 features and 169 poses, a state vector of 17292 components and an information matrix with 4277307 non zero entries, 1.3% density. The final map can be seen in Fig. 4.5.

We show in Fig. 4.6 (left) the cost per step to carry out each process in the CF SLAM algorithm: local mapping and joining submaps, and data association for submaps. Local mapping includes the cost of its internal data association (solid light-blue line). The joining submap cost (dashed orange line) and data association of submaps (dash-dot pink line) could be amortised during the next $2^l 10$ seconds as we show in Fig. 4.6 (bottom-left). The peak in the last step corresponds to the computation of the global map required at the end of the experiment. That cost is only 10.8s for all the pending submap joins and the most of the time the cost is dominated by the local mapping that is constant. In Fig. 4.6 (right) we show the cumulative cost for the same variables.

Fig. 4.7(a) shows the estimated trajectory (solid blue line), the odometry (dashed green line) and the GT (solid red line). They are aligned using the Rawseeds Metrics Computation Toolkit. The histogram of errors in the trajectory is shown in Fig. 4.7(b). Our solution achieves a mean absolute error of 1.18m with 0.47m of standard deviation. Note that the maximum error is as only 2.5m, 0.33% of the 760m travelled.

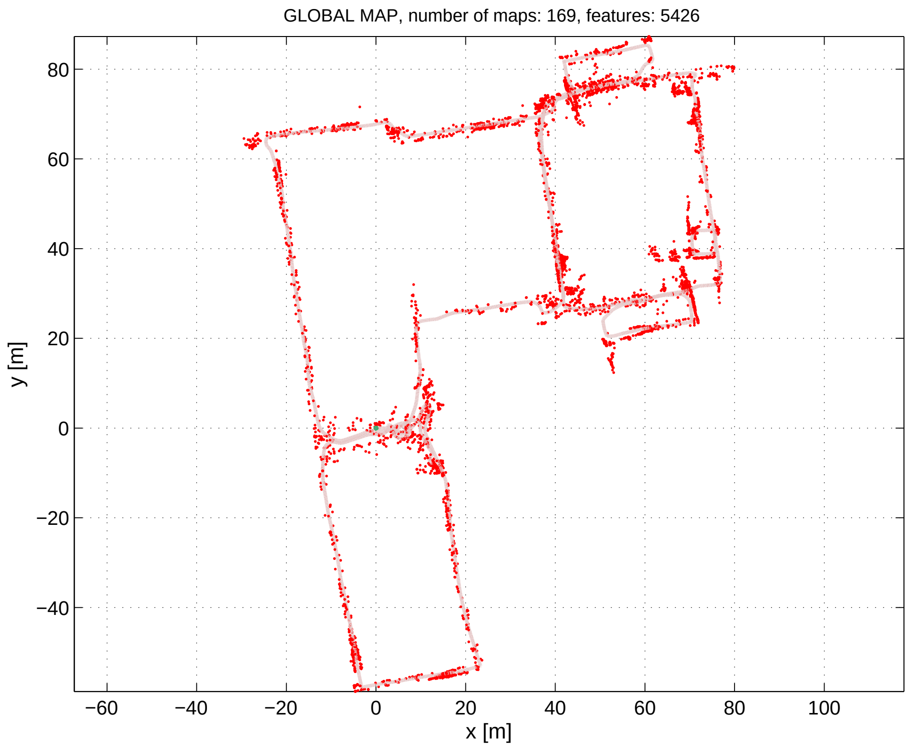

Figure 4.5: Final map for the Bicocca_2009-02-25b dataset after running our SLAM system.

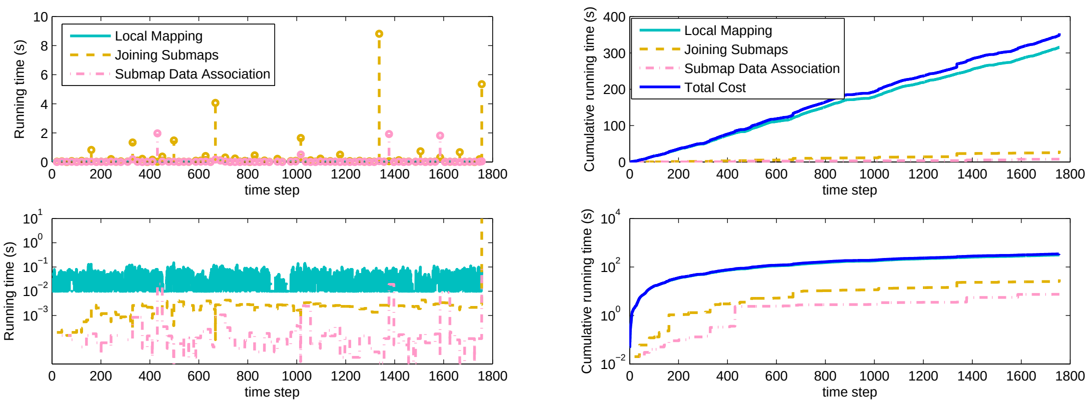

Figure 4.6: Running times for Local Mapping, Joining submaps and Data Association between submaps. On the left, top: running times per step for our system; bottom in semi-log scale: The same running times that would result from amortising the costs of joining and DA between submaps. On the right, top: the cumulative running times including the total cost; bottom: the same cumulative times in semi-log scale.

Mixed: Bovisa_2008-10-06_Dynamic

This dataset was taken in a dynamic environment in a combination of indoors and outdoors with natural illumination. The stereo images were collected during 35 min along a path of 1.89km.

In total 212 local maps are built. The result is one final map of 10056 features and

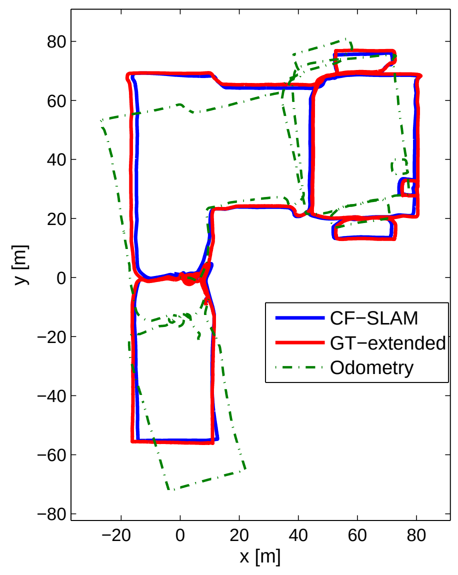

(a) Trajectory.

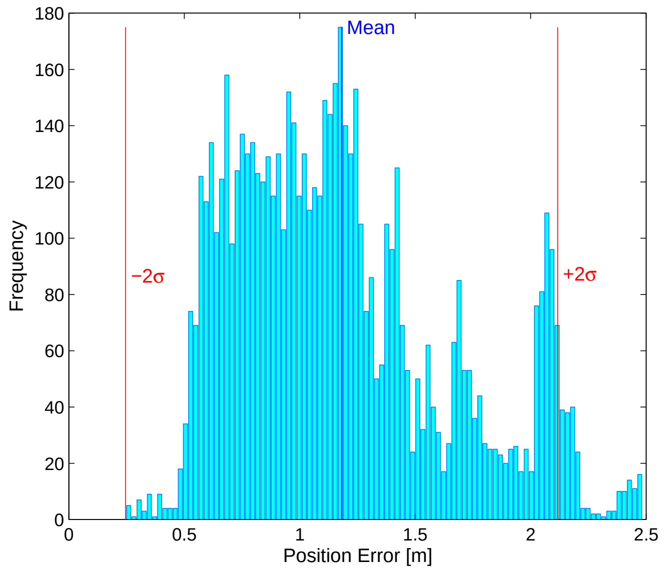

(b) Histogram of ATE.

Figure 4.7: Estimated trajectory compared against the extended ground truth and the odometry on the left. Robot pose error histogram with 2σ error bounds on the right.

212 poses, a state vector of 31440 components and an information matrix with 8841177 non zero entries, 0.36% density. The final map can be seen in Fig. 4.8.

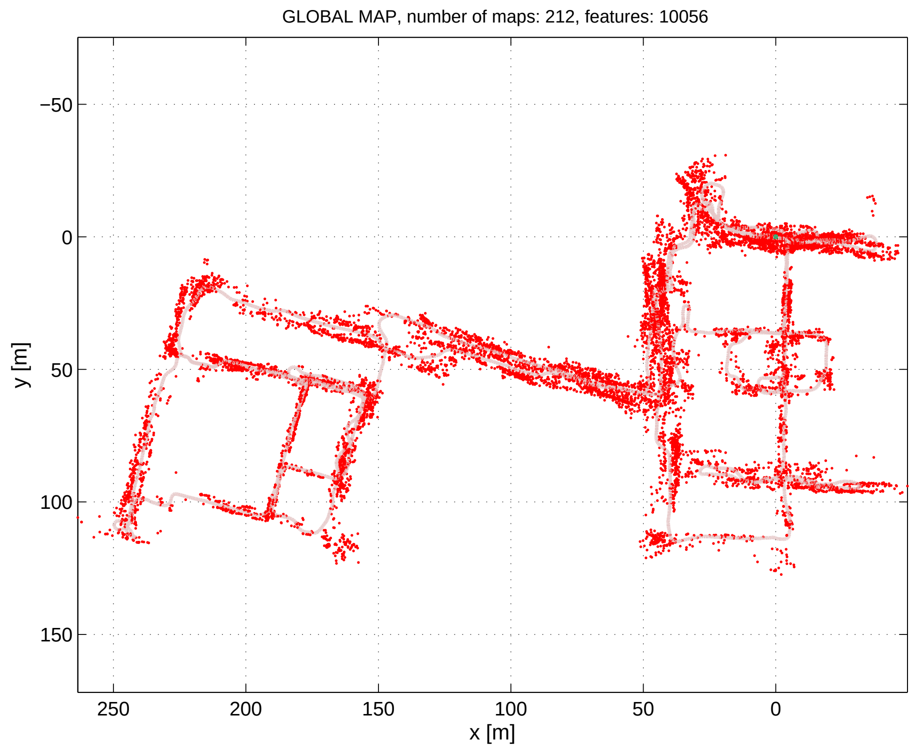

Figure 4.8: Final map for the Bovisa_2008-10-06 dataset after running our SLAM system.

We show in Fig. 4.9 (left) the cost per step to carry out each process in the CF SLAM algorithm. We can see that for partial outdoor trajectories, local mapping includes more features in inverse depth parametrisation, with the associated increased cost due to the greater number variables in the parametrisation.

Local mapping includes the cost of its internal data association (solid light-blue line). Again, the joining submap cost (dashed orange line) and data association of submaps (dash-dot pink line) could be amortised as we show in Fig. 4.9 (bottom-left). The peak in the last step is 38s for all the pending submap joins and the most of the time the cost is dominated by the local mapping, less than 0.1s. The length of the trajectory is more twice than in the indoor experiment, doubling the size of the final map and increased the cost of the joining process. In Fig. 4.9 (right) we show the cumulative cost for the same variables.

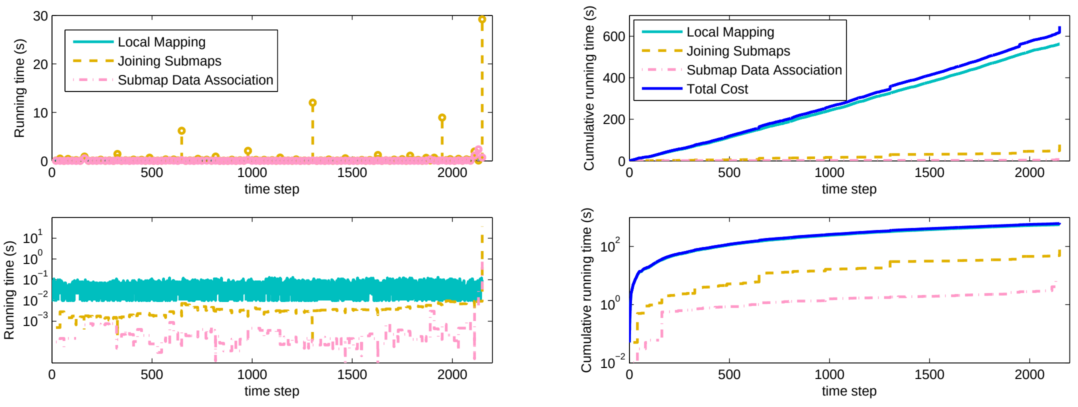

Figure 4.9: Running times for Local Mapping, Joining submaps and Data Association between submaps. On the left, top: running times per step for our system; bottom in semi-log scale: The running times that would result from amortising the costs of joining and DA between submaps. On the right, top: the cumulative running times including the total cost; bottom: the same cumulative times in semi-log scale.

Fig. 4.10(a) shows the estimated trajectory (solid blue line), the odometry (dashed green line) and the GT (solid red line). They are aligned using the Rawseeds Metrics Computation Toolkit. The histogram of errors in the trajectory is shown in Fig. 4.10(b). Our solution achieves a mean absolute error of 2.31m with 1.62m of standard deviation.

Outdoor: Bovisa_2008-10-04_Static

This dataset is taken in a static environment with natural illumination. The stereo images were collected during 38 min along a path of 1.72km. For this dataset, a partial visual odometry solution is available as a “Rawseeds Benchmark Solution” covering 1.3km of the

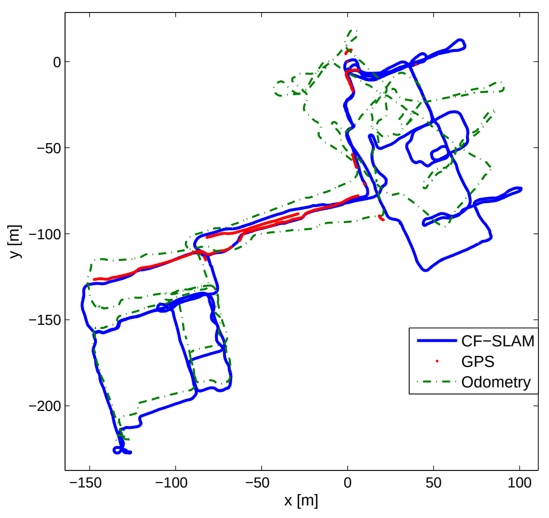

(a) Trajectory.

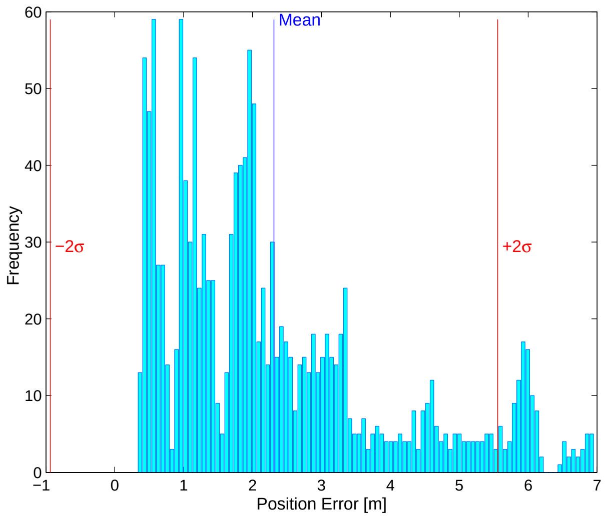

(b) Histogram of ATE.

Figure 4.10: Estimated trajectory compared against the ground truth given by the GPS and the odometry (left). Robot pose error histogram with 2σ error bounds (right).

trajectory. The visual odometry was obtained and published by Civera et al. (2010). They use the frontal camera (320x240) and their EKF + 1-point RANSAC algorithm, using the wheel odometry to observe the scale. We use this visual odometry in the timestamps where it is available, when it is not, we use the simple wheel odometry, see Fig 4.11.

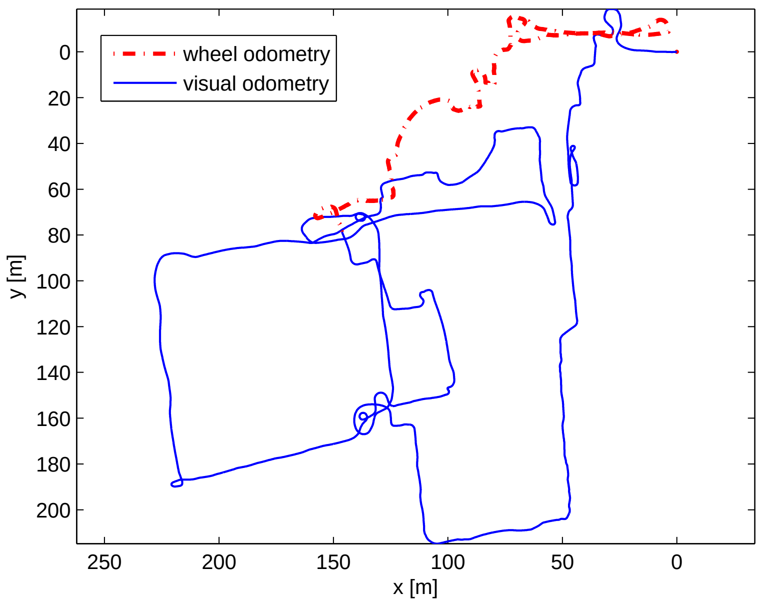

Figure 4.11: Odometry used in this dataset. Visual odometry covers 1.3km and the wheel odometry the remaining 0.4km.

In total 223 local maps are built. The result is one final map of 10170 features and 223 poses, a state vector of 31848 components and an information matrix with 9876676 non zero entries, 0.32% of density. The final map can be seen in Fig. 4.12.

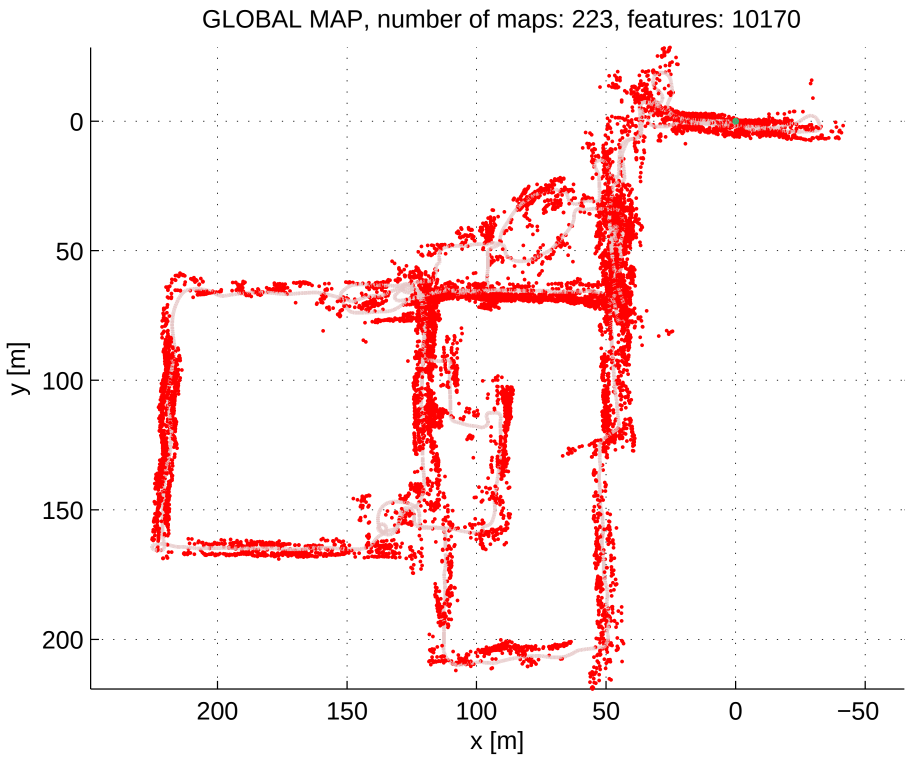

Figure 4.12: Final map for the Bovisa_2008-10-04 dataset after running our SLAM system.

We show in Fig. 4.13 (left) the cost per step to carry out local mapping and joining submaps, and data association for submaps. In outdoor experiments, the local mapping adds more features in inverse depth parametrisation, increasing again the cost due to having more features with greater number components in the parametrisation.

Local mapping includes the cost of its internal data association (solid light-blue line). The joining submap cost (dashed orange line) and data association of submaps (dash-dot pink line) could be amortised as we show in Fig. 4.13 (bottom-left). The peak in the last step is 38.5s for all the pending submap joins. The cost is dominated by the local mapping, less than 0.1s the most of the time. As in the mixed experiment, the length of the trajectory is more twice than in the indoor experiment, doubling the size of the final map and increasing the cost of the joining process. In Fig. 4.13 (right) we show the cumulative cost for the same variables.

Fig. 4.14(a) shows the estimated trajectory (solid blue line), the odometry (dashed green line) and the GT (solid red line). They are aligned using the Rawseeds Metrics Computation Toolkit. The histogram of errors in the trajectory is shown in Fig. 4.14(b). Our solution achieves a mean absolute error of 1.58m with 0.66m of standard deviation.

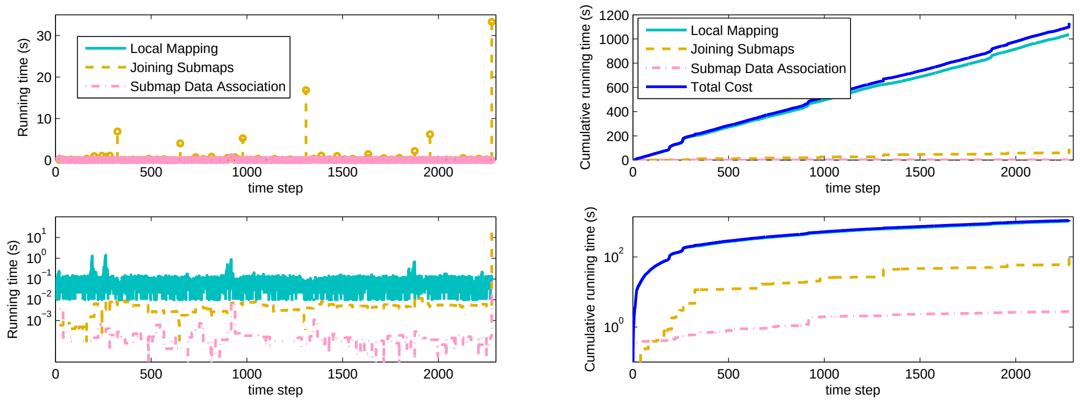

Figure 4.13: Running times for Local Mapping, Joining submaps and Data Association between submaps. On the left, top: running times per step for our system; bottom in semi-log scale: The running times that would result from amortising the costs of joining and DA between submaps. On the right, top: the cumulative running times including the total cost; bottom: the same cumulative times in semi-log scale.

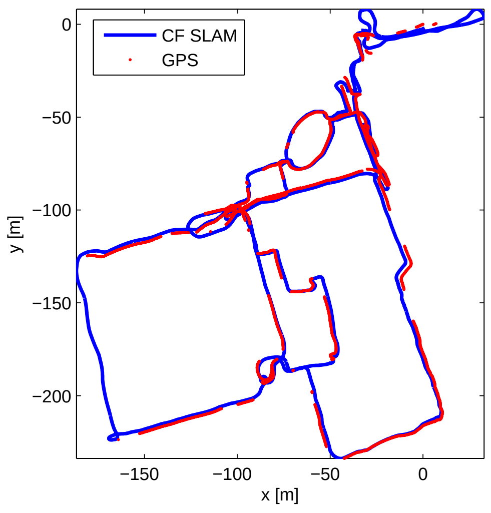

(a) Trajectory.

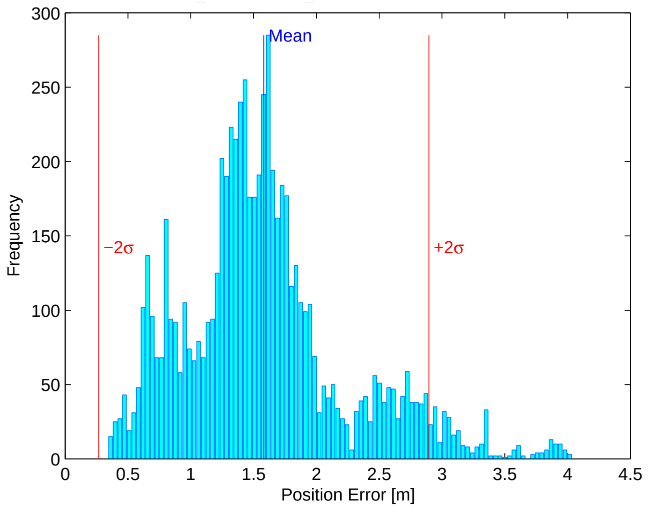

(b) Histogram of ATE.

Figure 4.14: Estimated trajectory compared against the ground truth given by the GPS on the left. Robot pose error histogram with 2σ error bounds on the right.

4.2.2 With Omidirectional Cameras + 3D LIDAR

In this experiment, we evaluate our SLAM system on an autonomous ground vehicle, a modified Ford F-250 pickup truck equipped with several sensors. We use the PointGrey Ladybug3 omnidirectional camera system to obtain the images and the Velodyne three-dimensional lidar scanner for 3D information. Pandey et al. (2011) provide the data between these two sensors already calibrated. We use the five calibrated images from the ladybug cropped to 788x1236 each one.

Two datasets are available, the first one (Ford-1) was taken in downtown Dearborn, MI (USA), in a trajectory of 1.44km during $\sim$ 6 min with a single large loop. The second one (Ford-2) was taken in the Ford Research campus, also in Michigan. The trajectory of Ford-2 is a two large loops path of 4km during $\sim$ 10 min.

PR Learning Stage: Ford-1

Our place recognition system is based on information of texture and 3D, and these dataset provide us with both. The learning process is carried out using Ford-1 in the same way as for the stereo camera datasets, but taking into account the five images for the 360° of field of view and the 3D information directly from the 3D laser. We show in Table 4.3 the resulting weights learned from 200 randomly chosen pairs of scenes separated 0.1 seconds between them in Ford-1.

		SURF	*geo*			*PCA*			*curv*	*pair*	*outlier*	
			k=1	*k*=2	*k*=3	1^{st}	2^{nd}	3^{rd}		*local*	*pair*	
$\mathcal{G}_{3D}$	**w**	-13.65	0.27	-0.14	-0.45	-0.19	-0.48	-1.24	1.04	-12.08	-2.66	-1.88
$\mathcal{G}_{Im}$	**w**	-15.98								-34.48	-1.90	-1.38

Table 4.3: Weights obtained in the learning process in the Ford-1 dataset.

The vocabulary for the BoW stage was trained here with all the image of Ford-1 with $k = 10$ and $l = 6$ given us a dictionary of 1 million of words. We carry out our place recognition system first using Ford-1 for adjusting the α and β parameters. With respect to the α parameters used in the previous experiments, the change was minor. Ford-1 was taken in an open urban area, no tall neither distinctive buildings. Parameter α^- increased from 0.15 to 0.2 and α^+ from 0.6 to 0.7, in order to be little more strict in the generation of candidates and the confidence to accept them as true, respectively. The β parameters work as they were in the previous outdoors configuration, we also increased them to $\beta_{3D} = 3.0$ and $\beta_{Im} = 3.0$ without obtaining false positives. This is expected from highly discriminative normalised scores η_{3D} and η_{Im} due to greater overlap between consecutive scenes, k and $k - 1s$, in 3D (long-range sensor) and image (full field of view) of this experiment. Despite this, we decide to be conservative and keep the β parameters as before, false positives are dire. The final parameters selected are in Table 4.4.

Table 4.4: Parameters for Ford datasets

α^+	α^-	β_{3D}	β_{Im}
0.7	0.2	1.5	1.7

Evaluation with Ford-2

We process the dataset at 10 frames per second in our local mapping and at 1 fps in our place recognition system. In local mapping we select $f_{min} = 100$ and $s_{min} = 50$ steps resulting in at least $5s$ per local map.

In the local mapping we use features parametrised in 3D Euclidean coordinates when the SURF-points have corresponding 3D information from the 3D lidar. Here we do not use any odometry information. We apply a constant velocity model in which we represent the pose with twelve components in the state vector: three Euclidean coordinates, three roll-pitch-yaw angles and six parameters for linear and angular velocities. When the local map is closed and another must be initialised, the velocity components are marginalised out from the local map.

With the vocabulary, weights and parameters selected, we run the place recognition over Ford-2 at 1 fps. The loops detected in this process are shown in Fig. 4.15(a). In Table 4.5 we can see the average and maximum computational times for this process. Excluding the SURF extraction cost, we plot the histograms of time per step in Fig.4.15(b). We can see that only one place recognition verification consumes more than 1 second.

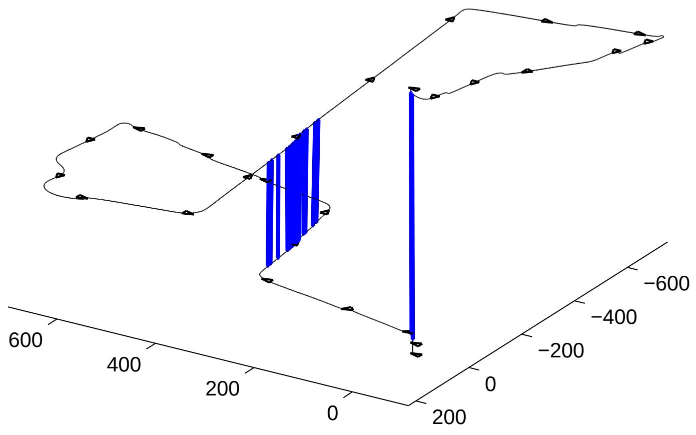

(a) Revisited places.

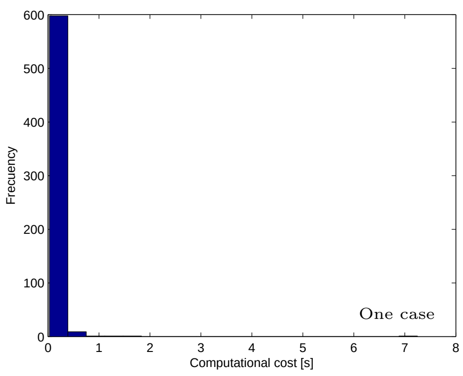

(b) Costs.

Figure 4.15: (a) Loops detected by our place recognition system in Ford-2. The ground truth trajectory in black and the loop closures in blue. Axis is in meters and the height represents the time of the experiment. (b) Histogram for the total computational cost without the SURF extraction cost.

Accuracy is evaluated by comparing the estimated trajectory to the position given by an Applanix POS-LV INS with Trimble GPS on board. The absolute trajectory errors were computed in the same way than before with the same toolkit.

In total 122 local maps are built. The result is one final map of 5980 features and 122

Table 4.5: Computational times for our place recognition system (in s) over Ford-2

	SURF	BoW	CRF Matcher		Whole
	extraction		$\mathcal{G}_{3D}$	$\mathcal{G}_{Im}$	System
Mode	1.82	0.07	0.01	0.11	1.92
Average	1.94	0.09	0.19	0.17	2.08
Maximum	3.11	0.32	0.45	6.83	9.39

poses, a state vector of 18672 components and an information matrix with 9466558 non zero entries, 2.7% of density. The final map can be seen in Fig. 4.16.

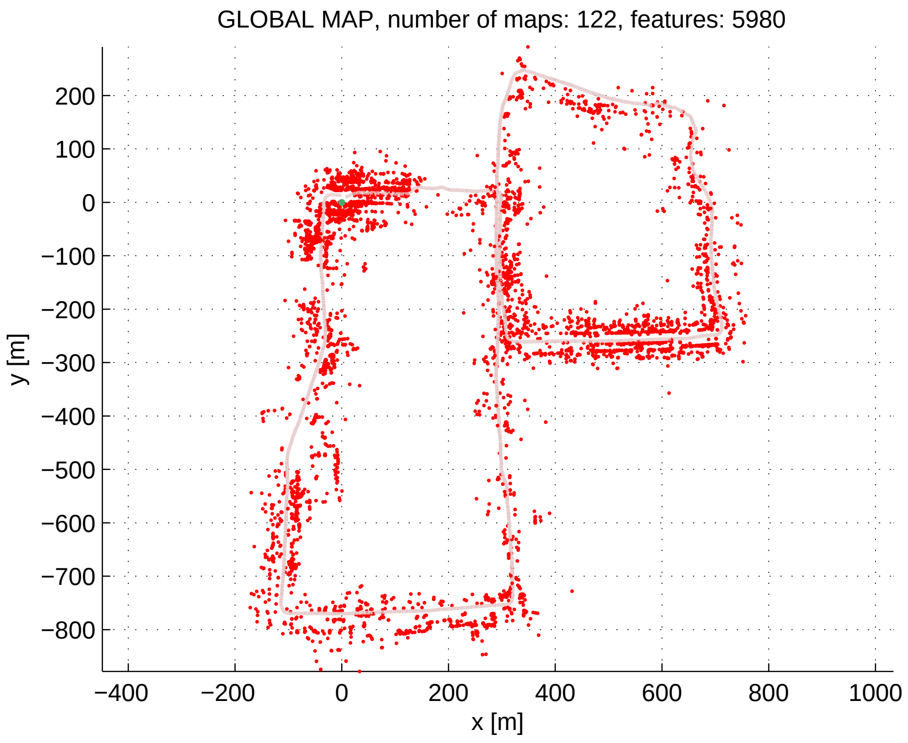

Figure 4.16: Final map for Ford-2 dataset after running our SLAM system.

We show in Fig. 4.17 (left) the cost per step to carry out each process in the CF SLAM algorithm: local mapping and joining submaps, and data association for submaps. Local mapping includes the cost of its internal data association (solid light-blue line). The joining submap cost (dashed orange line) and data association of submaps (dash-dot pink line) could be amortised during the next $2^l 5$ seconds as we show in Fig. 4.17 (bottom-left). The peak in the last step is 39s and 38s for all the pending submap joins and data associations, respectively. The cost is dominated by the local mapping and data association between submaps. That is because the LIDAR has a longer range with many more observations per step, increasing the cost of internal data associations and updates in the local mapping. For the same reason, the overlap between adjacent local maps is much larger, and the data association for submaps increases in cost, even though it is constant with respect to the size of the experiment. In Fig. 4.17 (left) we can see periods of time where the cost of these two processes increase. These periods correspond to moments when the vehicle stopped or is moving at reduced speed. With a slightly more specialised criteria to decide when execute a step of the filter based on the estimated velocity rather than only time between frames we can easily avoid that overhead. In Fig. 4.17 (right) we show the cumulative cost for the same variables.

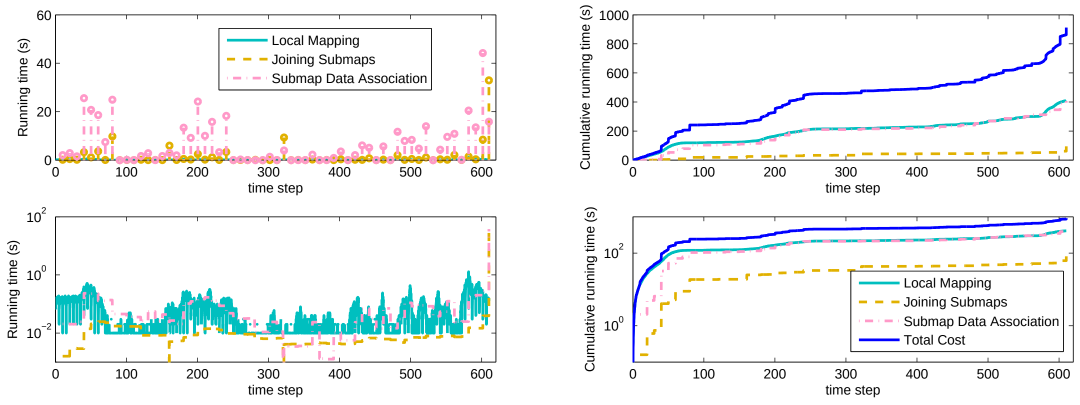

Figure 4.17: Running times for Local Mapping, Joining submaps and Data Association between submaps. On the left, top: running times per step for our system; bottom in semi-log scale: The same running times that would result from amortising the costs of joining and DA between submaps. On the right, top: the cumulative running times including the total cost; bottom: the same cumulative times in semi-log scale.

Fig. 4.18(a) shows the estimated trajectory (solid blue line) and the ground truth (GT, solid red line). They are aligned using the Rawseeds Metrics Computation Toolkit. The histogram of errors in the trajectory are shown in Fig. 4.18(b). Our solution achieves a mean absolute error of 15.89m with 8.85m of standard deviation. The main increment in the trajectory error is placed in the upper-right corner area in Fig. 4.16. It is an open area with only a few trees and some forest in the sensor range. With a scarce extraction and tracking of features it is more difficult for the filter to properly estimate the trajectory. This source of error could be avoided using some odometric information, for example from simple scan-matching with the other 2D Lidar sensors mounted in the vehicle.

4.3 Discussion

In this chapter we have shown that the CF SLAM and the BoW-CRF place recognition algorithms can work together in a computationally efficient and robust SLAM system in

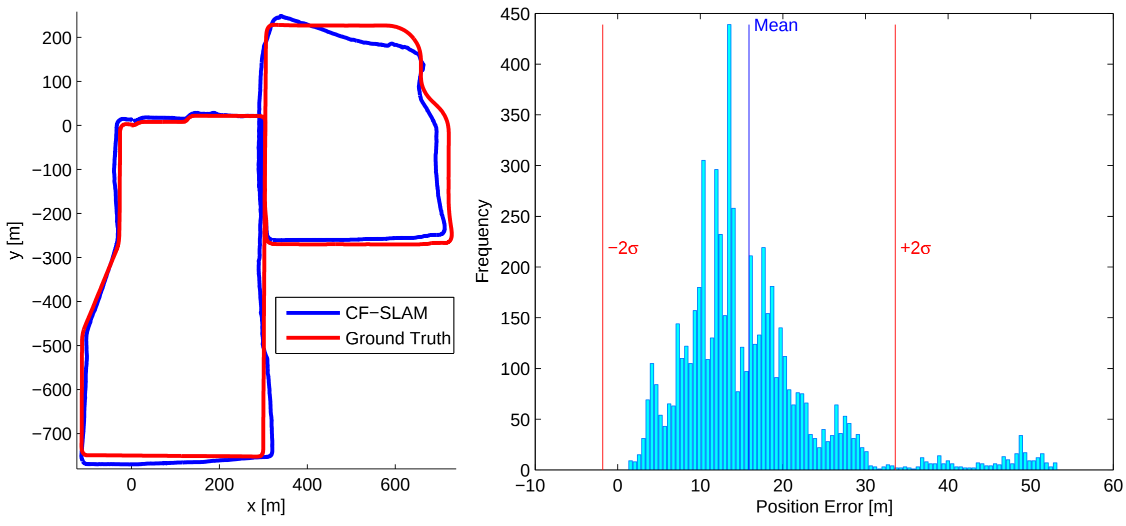

(a) Trajectory. (b) Histogram of ATE.

Figure 4.18: Estimated trajectory compared against the ground truth given by the Applanix on the left and robot pose error histogram with 2σ error bounds on the right.

real environments. Thanks to the place recognition system, we can compute the data association only between contiguous local maps, limiting the computational cost and making it constant with the size of the final map.

With our approach we obtain mean ATEs (percentage of the trajectory) of 1.18m (0.16%), 2.31m (0.12%) and 1.58m (0.09%) in the indoor, mixed and outdoor RAWSEEDS datasets, respectively. Piniés et al. (2010) use the trinocular system to also solve the same indoor and outdoor datasets with their CI-Graph algorithm, processing them at 15fps. They obtain a mean ATE of 1.64m in the indoor dataset, and 6.96m in the outdoor dataset. We think our results are better because of our improved place recognition system, rather than because of the feature detector used. We both use a submap-filter-based approach as the estimation core, thus it is expected to have similar precision performance. Features from a Shi-Tomasi detector at 15fps have better precision tracking performance than our SURF detector. The computational times reported in Piniés et al. (2010) are given by step, between 0.5s to 2s approx. in local submaps building, as compared to max. 0.1s in our case.

As we said above, Civera et al. (2010) report a partial (1.3km) visual odometry solution, using the monocular frontal camera and the wheel odometry in order to avoid the scale drift. In the partial trajectory they obtain a mean ATE of 9.8m. This solution has the advantage of working in constant time at 30fps but suffers from drift in the trajectory. Using this solution as odometry input in our system has proven be very beneficial for the final SLAM solution.

In the Ford-2 dataset, our solution achieves a mean ATE of 15.89m, a mean error of 0.4% of the length of the trajectory. The main reason for this increased error is low feature visibility in certain parts of the trajectory. We could easily improve the trajectory precision using odometric information, such as in the RAWSEEDS outdoor dataset, for example from a simple scan-matcher using the other 2D Lidar sensors mounted in the vehicle.

We think that a full implementation in C++ of the system can run at real time easily in these experiments with the same configurations and at a higher frame rate. Also, this system can easily accommodate visual odometry or scan-matching at higher frame rate.

Chapter 5

Conclusions

The ability to understand its environment and know its place within it, simultaneously and automatically, is essential in a robotic platform to adequately navigate, carry out path planning and make decisions. The sensor measurements that the robot obtains to perceive its own motion and the environment are inherently imperfect, since both the sensors and actuators on board are noisy. Environments where mobile robots are expected to operate are increasingly large, unstructured and changing. In such environments perceptual ambiguity is highly probable. Some current SLAM systems are able to work in environments up to a certain scale and a tolerance to noise and ambiguity. When that scale or level of ambiguity are overcome, these systems can become inefficient, make mistakes or altogether fail. The contributions of this thesis are focused on extending the boundaries of current SLAM systems in scale and robustness.

Among the many issues to address in SLAM, we have addressed two that stand as crucial, map estimation and place recognition. The estimation should find the most precise configuration for the map elements and robot poses that satisfy the constraints given by data association. Place recognition imposes constraints on the estimation which are usually strong, and greatly informative to achieve higher accuracy. They are so crucial, that an error in one of these constraints can damage the estimation completely.

5.1 Contributions

In this thesis we have described improvements in these two topics, estimation and place recognition, in efficiency and robustness.

5.1.1 Efficient Estimation

The first contribution of the thesis is focused on the efficiency of the estimation process. We have proposed a state estimation algorithm with sub-linear computational cost per step, the Combined Filter SLAM algorithm, the most efficient filtering up to now to work on large scale environments. CF SLAM does not sacrifice any information to achieve such efficiency, and its memory requirement remains linear with the size of the environment.

We limit the computational complexity thanks to the combination of four different ideas that have been tested before with their own pros and cons. Our combination takes advantage of their pros and tries to minimise their cons.

Extended Kalman Filter

The well-known EKF has demonstrated the ability to solve SLAM problems countless times in environments of limited size. It is consistent in small scale environment where the linearisation errors are limited. One of its nicest properties is the state covariance is directly available always. When we have access to the state covariance we can carry out robust data association methods with statistical tests to keep the estimation consistent. The main drawback is its poor scalability, thus we only use it in the smallest local maps.

Extended Information Filter

EIF with its canonical parametrisation of the state vector and covariance leads us to handle the information vector and information (or precision) matrix. The pros of this filter are: updating the filter is carried out with simple addition operations; new evidence only needs to be locally propagated, and if we keep all the poses in the state vector the information matrix has a sparse structure with linear memory requirements. The cons are: it requires recovery of the state vector to compute the Jacobians, and the size of the state vector grows even without increasing the size of the environment.

We have not used the EIF for local mapping, rather we have used it to fuse the information between submaps, where the EIF is more efficient than the EKF. Instead of keeping or marginalising out all previous poses, we keep only one pose per local map. That leads us to a sparse structure that also allows smoothing a sampled trajectory. With the sparseness of the information matrix we achieve great efficiency in the state recovery, and also attain linear memory requirements.

Local Mapping

Submapping techniques have demonstrated to be the best choice for high scalability. They are perfectly suitable for local navigation tasks, with bounded computational complexity and linearisation errors. However, they can still duplicate information between local maps still when the robot is in same area. This implies an increase in memory requirements. Also, old local maps are usually not updated with new evidence.

We duplicate information only before the joining step between submaps is carried out. This information is then associated and fused, and therefore all available information appears in the final map. We think that for local navigation tasks, e.g. obstacle avoidance or object handling, the most important information is the information in the current local map. And, for long term tasks, e.g. persistent SLAM, we can delay the joining to fuse the new with the old evidence. Eliminating out of date information is not currently considered in our SLAM system.

Divide and Conquer in a Tree Fashion

When a problem is difficult, the best strategy to solve it in most cases is to split it into smaller problems, solve each of them, and then combine these solutions into one unified solution. This is also the case in the SLAM problem. In addition, the strategy to split and merge implies computational savings and better consistency properties. The binary tree fashion has been demonstrated to be the best computational cost saving strategy, while having better consistency properties than the sequential fashion.

The drawback of this strategy is the high computational cost to find correspondences between two sub-maps of large size. We have eliminated this problem by delegating that task to other two processes, one is the sequential data association with the smallest local maps, and the other is finding the correspondences with the place recognition system.

We think that the main ideas of our contribution can be applied to other approaches with beneficial effects to the final result taking the new pros and trying to avoid or to solve the new cons. For instance, we can change EKF in local mapping by an incremental optimisation of pose graphs. One pro: the local maps will be the non-linear maximum likelihood solution. One drawback: the covariance in not directly available for data association.

As a final thought, we believe that the best achievable computational efficiency to solve a global-metric SLAM problem, without approximations, is **sublinear** with the size of the environment, as is achieved in this thesis. The goal of **constant** computational complexity in the estimation process is **hardly** possible, achievable only though approximations, by ignoring information or keeping consistency and precision only at a local level, without propagating the information to the complete state vector.

5.1.2 Robust Place Recognition

The second contribution is related to the detection of places revisited by the robot, or loop closing. The system we have proposed is based on the very fast selection of place candidates and very robust verification of these with probabilistic graphical models. Our place recognition system works with image and distance sensors, and makes use of all the information available in a unified framework of inference on probabilistic graphs.

Through different experiments with different sensors and configurations we have observed that the selected features and parameters of our place recognition are appropriate and stable. We have considered a certain set of features in our system, but CRFs are amenable to the use of different or additional features that might become available through other sensors or sensing modalities. With little effort of analysing the kind of scenes considered, and the selected sensors and their configuration, we can attain full precision, detecting the most revisited places. We believe that this effort can be transferred to a learning process. If we can determine by sliding windows the discriminative power of our place recognition system in consecutive scenes, we would be able to adapt the parameters accordingly. We think that this kind of system, with the capacity to adapt to changing environments is the right way for long term operations.

Our contributions have been evaluated in different real scenarios and compared with the state of the art. The efficiency of the CF SLAM has been tested in indoor environments with artificial and natural features, and outdoor environments with natural features. The robustness of our place recognition system has been tested using different stereo cameras on various robotic platforms, and even with hand-held stereo cameras, in diverse environments, and also using omnidirectional cameras in conjunction with a 3D LIDAR. Both contributions have been tested together as part of a prototype of a complete SLAM system.

5.2 Future Work

Our contributions allow a robot to operate in larger and perceptually more complex environments. Immediate improvements in our system include taking more advantage of the effort that has already been made to compute the graph structures and potentials in the conditional random fields, by incorporating semantic information in the map. The identification of objects such as vehicles, lamp posts, trees, walls, buildings, pedestrians, cyclists, and place classes such as parks, roads, corridors, kitchens, will allow a better understanding of the environment and also data association via a higher level of abstraction.

Now that the problem of modeling large-scale environments is better understood, there are at least three major technical challenges ahead:

- Maintaining a representation of the environment which changes over long periods of time. This problem is known as Life-Long Learning or Persistent SLAM.
- The ability to work in dynamic environments. Rather than deal with dynamic objects as outliers, recognize them as active agents of the map with different kinds of dynamics and levels of interaction.
- The ability to detect that past data association decisions related to place recognition were incorrect, and to recover the accuracy of state estimation once they are removed.

Efforts along these lines will place us closer to the goal of having safe and useful autonomous robotic systems.

Conclusiones

La localización de un robot y el mapeo del ambiente en el que interactúa de manera simultánea y automática es esencial para el correcto funcionamiento de otras tareas, como los sistemas de navegación, la planificación de trayectorias o la toma de decisión sobre el ambiente a explorar. Los entornos en los que se espera que la robótica móvil sea aplicable son cambiantes, no estructurados y probablemente de gran ambigüedad. Adicional a ello las mediciones que puede hacer el robot sobre su movimiento y su entorno son inherentemente imperfectas, tanto los sensores como los actuadores abordo son ruidosos.

A día de hoy se han propuesto ya sistemas que son capaces de trabajar en este tipo de ambientes hasta una escala y hasta un nivel de tolerancia al ruido y a la ambigüedad de los datos. Cuando dicha escala o nivel de ambigüedad son superados dejan de funcionar, se vuelven ineficientes o cometen errores. Las contribuciones de esta tesis están enfocadas a extender esas fronteras en escala y robustez.

Entre las muchas cuestiones que se deben abordar en el problema del SLAM resaltan dos como las más cruciales, la estimación y el reconocimiento de lugares. La estimación debe encontrar la mejor configuración para el mapa y para las posiciones del robot que satisfagan las restricciones dadas por la asociación de datos. El reconocimiento de lugares impone también restricciones en la estimación y normalmente son restricciones más fuertes, pero así mismo son mas informativas para alcanzar mayor precisión. Son tan cruciales que un error en una sola de estas restricciones puede dañar por completo la estimación.

Contribuciones

Es esta tesis hemos descrito mejoras en estos dos tópicos, estimación y reconocimiento de lugares, en eficiencia y en robustez.

Proceso de Estimación Eficiente

La primera contribución de la tesis está enfocada a la eficiencia del proceso de estimación. Hemos propuesto un algoritmo de estimación de estados con costo computacional sublineal por paso, el Combined Filter SLAM, el algoritmo de filtrado más eficiente a día de hoy para trabajar en entornos a gran escala. CF SLAM no sacrifica ninguna información para lograr tal eficiencia y mantiene un consumo de memoria lineal con el tamaño del entorno. Hemos reducido la complejidad computacional principalmente gracias a la combinación de cuatro ideas básicas. Cada una de ellas ha sido evaluada con anterioridad con sus pros y contras.

Extended Kalman Filter

El bien conocido EKF ha sido utilizado de manera exitosa en innumerables sistemas de SLAM en entornos de tamaño limitado. Es consistente en pequeña escala donde los errores debido a las linealizaciones están acotados. Y tal vez, una de sus mejores propiedades es que la covarianza del estado esta accesible siempre, sin cálculos adicionales. Esto es bueno porque nos da la posibilidad de utilizar técnicas de asociación de datos robustas basados en pruebas estadísticas que preservan la consistencia del filtro. La principal contra es la complejidad computacional, la cual evitamos usándolo solo en los mapas locales más pequeños.

Extended Information Filter

El EIF con su parametrización canónica del vector de estado y su covarianza nos lleva a manejar el vector y la matriz de información. Los pros de este filtro son: la actualización del filtro se reduce a adiciones de información, una evidencia nueva solo necesita propagarse localmente, y si mantenemos todas las localizaciones del robot en el vector de estados entonces la matriz de información tendrá una estructura dispersa consumiendo memoria lineal con el tamaño del vector de estados. Los contras son: el filtro necesita recuperar el vector de estados para evaluar los jacobianos, y el tamaño del vector de estado siempre crecerá aun sin que el tamaño del ambiente modelado aumente.

Para minimizar esas desventajas no usamos el EIF en el mapa local, mejor lo hemos usado para fusionar la información entre submapas donde el EIF es más eficiente que el EKF. Y, en lugar de mantener o eliminar toda la historia de localizaciones del robot, mantenemos solo una localización por mapa local. Con esto conseguimos una estructura dispersa con solo un muestreo de la trayectoria. Con la estructura dispersa de la matriz de información podemos recuperar el vector de estados muy eficientemente y un consumo de memoria lineal.

Mapas Locales

Las técnicas de submapas han demostrados ser la mejor escogencia in términos de escalabilidad. Son perfectamente usables para las tareas navegación local con un costo computacional y unos errores de linealización acotados.

Pero pueden duplicar información en diferentes mapas locales aun cuando el robot se encuentre físicamente en la misma área, esto implica un incremento en los requerimientos de memoria y no actualizar el mapa local anterior con la nueva evidencia adquirida. En nuestro sistema duplicamos la información solo hasta que la fusión de los submapas, entonces la información duplicada en diferentes mapas locales es asociada como y fusionada, por lo tanto usamos toda la información con la que contamos en la actualización.

Además, para las tareas locales de navegación, por ejemplo, la evitación de obstáculos o la manipulación de objetos, la información crucial está contenida en el mapa local actual. Para tareas a largo plazo, como persistent SLAM, es posible esperar a unir los submapas para fusionar la evidencia nueva con la antigua sobre el mismo espacio.

Divide and Conquer en Árbol

En la mayoría de los casos, cuando un problema es muy difícil, la mejor estrategia es dividirlo en pequeños problemas, solucionar cada uno, y después encontrar la solución completa desde las soluciones pequeñas. Este es el caso del SLAM en grandes entornos, y adicionalmente la estrategia escogida para dividir y fusionar implica más o menos ahorro computacional y más o menos consistencia. Un árbol binario como estrategia ha demostrado mejor consistencia y mayor ahorro computacional que las estrategias secuenciales.

La contra de esta estrategia es el costo elevado de encontrar las correspondencias entre dos submapas de gran tamaño, la cual hemos eliminado delegando esta tarea a otros dos procesos, una asociación de datos secuencial con los mapas locales más pequeños y otra encontrar las demás correspondencias con el sistema de reconocimiento de lugares.

Note que las principales ideas de nuestra contribución pueden ser aplicadas con otras aproximaciones aprovechando los nuevos pros y lidiando con los nuevos contras en beneficio del resultado final. Por dar un ejemplo, podríamos cambiar el EKF para construir los mapas locales por una optimización incremental de grafos de poses.

Un nuevo pro: el mapa local no sufrirá de linealizaciones. Un nuevo contra: la covarianza no está disponible para la asociación de datos. Como una reflexión final en la parte de estimación, pensamos que la mayor eficiencia computacional para solucionar el SLAM métrico y global, sin aproximaciones, es sublineal con el tamaño del entorno, como el alcanzado por nosotros en esta tesis.

A medida que el entorno se hace más grande tanto el problema como la solución aumentan de tamaño, entonces el objetivo de alcanzar una complejidad computacional constante no es posible. Solo será alcanzable haciendo aproximaciones, descartando información o manteniendo una consistencia y precisión solo a nivel local sin propagar la información a todo el vector de estados.

Reconocimiento de Lugares Robusto

La segunda contribución está enmarcada en el problema de asociación de datos, específicamente en la detección de lugares del entorno ya visitados por el robot. El sistema que hemos propuesto está basado en la muy rápida selección de candidatos y en la muy robusta verificación de estos con modelos gráficos probabilísticos. Nuestro sistema de reconocimiento trabaja con sensores de imagen y de distancia y hace uso de toda la información en un marco unificado de inferencia sobre grafos probabilistas.

A través de los diferentes experimentos con diferentes sensores y configuraciones hemos podido observar los parámetros de nuestro sistema de reconocimiento de lugares es estable, con muy poco esfuerzo analizando el tipo de escenas producida por los sensores y la configuración seleccionada hemos encontrado los parámetros para tener 100% de precisión. Ese esfuerzo puede ser transferido a un proceso de aprendizaje, si podemos determinar en ventanas deslizantes el poder discriminativo de nuestro sistema en escenas consecutivas, podríamos adaptar los parámetros de manera adecuada. Esta clase de sistemas, con la capacidad de adaptarse en entornos cambiantes están en el camino correcto para operaciones a largo plazo.

Nuestras contribuciones han sido evaluadas en diferentes escenarios reales y comparadas con el estado del arte. La eficiencia del CF SLAM ha sido probada en entornos de interiores, con características artificiales y naturales, y en entornos exteriores con características naturales extraídas con sensores laser. La robustez de nuestro sistema de reconocimiento de lugares ha sido probada usando diferentes sistemas estéreo sobre diferentes plataformas robóticas, e incluso llevados en la mano, en diferentes y variados entornos; también usando cámaras omnidireccionales en conjunción con un laser 3D.

Aún mas, las dos han sido evaluadas en conjunto como parte de un prototipo de sistema completo de SLAM.

Trabajo Futuro

Nuestras contribuciones permiten a un robot operar en entornos más grandes y difíciles perceptualmente. Mejoras inmediatas en nuestro sistema incluyen aprovechar aún más todo el esfuerzo que ya se ha hecho construyendo y calculando los modelos gráficos y los potenciales en los conditional random fields, con toda la información ya disponible pasaremos a un etiquetado semántico del mapa, detectar objetos como: vehiculos, arboles, paredes, edificios, petaones, ciclistas y clases de lugares como parques, caminos, corredores, cocinas, etc. Esto nos permitirá un mejor entendimiento del entorno e incluso una vía de asociación de datos en un nivel más alto de abstracción.

Pero ahora que el problema de modelar ambientes de gran escala está bien entendido, hay al menos tres grandes retos técnicos por afrontar:

- Ser capaz de mantener una representación del ambiente válida sobre largos periodos de tiempo. Este problema es conocido como Life-Long Learning o Persistent SLAM.
- Ser capaz de trabajar en ambientes dinámicos. Más que tratar los objetos dinámicos como outliers reconocerlos como agentes activos del mapa con diferentes clases de dinámica y de nivel de interacción con él.
- Ser capaz de recuperar la estimación de estados después de restricciones erróneas.

Esfuerzos en este sentido se nos acercan más a la meta de contar con sistemas robóticos autónomos seguros y útiles.

Bibliography

Angeli, A., Filliat, D., Doncieux, S., & Meyer, J. (2008). A fast and incremental method for loop-closure detection using bags of visual words. *IEEE Transactions On Robotics, Special Issue on Visual SLAM*, 24:1027–1037.

Anguelov, D., Srinivasan, P., Koller, D., Thrun, S., Rodgers, J., & Davis, J. (2005). SCAPE: shape completion and animation of people. *ACM Trans. Graph.*, 24(3):408–416.

Bailey, T. & Durrant-Whyte, H. (2006). Simultaneous localization and mapping (SLAM): Part II. *IEEE Robotics & Automation Magazine*, 13(3):108–117.

Bar-Shalom, T. & Fortmann, T. (1988). *Tracking and Data Association.* Academic Press In.

Bar-Shalom, Y., Li, X. R., & Kirubarajan, T. (2001). *Estimation with Applications to Tracking and Navigation.* John Willey and Sons.

Bay, H., Tuytelaars, T., & Gool, L. V. (2006). SURF: Speeded up robust features. In: *Proceedings of the 9th European Conference on Computer Vision*, volume 3951, pages 404–417. Springer LNCS.

Bibby, C. & Reid, I. (2007). Simultaneous localisation and mapping in dynamic environments (slamide) with reversible data associa. In: *Proceedings of Robotics: Science and Systems.*

Bishop, C. M. (2006). *Pattern Recognition and Machine Learning.* Springer.

Bosse, M., Newman, P. M., Leonard, J. J., & Teller, S. (2004). SLAM in large-scale cyclic environments using the atlas framework. *Int. J. Robotics Research*, 23(12):1113–1139.

Bryson, M. & Sukkarieh, S. (2008). Observability Analysis and Active Control for Airborne SLAM. *IEEE Transactions on Aerospace Electronic Systems*, 44:261–280.

Burgard, W., Fox, D., Hennig, D., & Schmidt, T. (1996). Estimating the absolute position of a mobile robot using position probability grids. In: *Proc. of the Fourteenth National Conference on Artificial Intelligence (AAAi-96).*

Cadena, C., Gálvez-López, D., Ramos, F., Tardós, J., & Neira, J. (2010). Robust place recognition with stereo cameras. In: *IEEE Int. Conf. on Intelligent RObots and Systems.*

Cadena, C., Gálvez-López, D., Tardós, J., & Neira, J. (2011a). Robust place recognition with stereo sequences. *IEEE Trans. Robotics.* submitted.

Cadena, C., McDonald, J., Leonard, J., & Neira, J. (2011b). Place recognition using near and far visual information. In: *18th World Congress of the International Federation of Automatic Control (IFAC).*

Cadena, C. & Neira, J. (2009). SLAM in O(log n) with the Combined Kalman - Information Filter. In: *IEEE Int. Conf. on Intelligent RObots and Systems.*

Cadena, C. & Neira, J. (2010). SLAM in O(log n) with the Combined Kalman-Information Filter. *Robotics and Autonomous Systems*, 58(11):1207–1219.

Chli, M. & Davison, A. (2008). Active matching. In: *European Conference on Computer Vision ECCV 2008*, D. Forsyth, P. Torr, & A. Zisserman, ed., volume 5302 of *Lecture Notes in Computer Science*, pages 72–85. Springer Berlin / Heidelberg.

Christensen, H. & Hager, G. (2008). Sensing and Estimation. In: *Springer Handbook of Robotics*, B. Siciliano & O. Khatib, ed., Springer Handbooks, chapter 4, pages 87–107. Springer.

Civera, J., Davison, A., & Montiel, J. (2007). Inverse Depth to Depth Conversion for Monocular SLAM. In: *Proc. IEEE Int. Conf. Robotics and Automation.*

Civera, J., Grasa, O., Davison, A., & Montiel, J. (2009). 1-point ransac for ekf-based structure from motion. In: *Intelligent Robots and Systems, 2009. IROS 2009. IEEE/RSJ International Conference on*, pages 3498 –3504.

Civera, J., Grasa, O. G., Davison, A. J., & Montiel, J. M. M. (2010). 1-point ransac for extended kalman filtering: Application to real-time structure from motion and visual odometry. *J. Field Robot.*, 27:609–631.

Clemente, L., Davison, A. J., Reid, I. D., Neira, J., & Tardós, J. D. (2007). Mapping large loops with a single hand-held camera. In: *Proc. Robotics: Science and Systems*.

Cohn, T. (2007). *Scaling Conditional Random Fields for Natural Language Processing*. PhD thesis, University of Melbourne.

Cummins, M. & Newman, P. (2008). FAB-MAP: Probabilistic Localization and Mapping in the Space of Appearance. *The International Journal of Robotics Research*, 27(6):647–665.

Cummins, M. & Newman, P. (2010). Appearance-only SLAM at large scale with FAB-MAP 2.0. *The International Journal of Robotics Research*.

Dellaert, F. & Kaess, M. (2006). Square Root SAM: Simultaneous Localization and Mapping via Square Root Information Smoothing. *Int. J. Robotics Research*, 25(12).

Dissanayake, M. W. M. G., Newman, P., Clark, S., Durrant-Whyte, H. F., & Csorba, M. (2001). A solution to the simultaneous localization and map building (SLAM) problem. *IEEE Trans. Robotics and Automation*, 17(3):229–241.

Douillard, B., Fox, D., Ramos, F., & Durrant-Whyte, H. (2011). Classification and semantic mapping of urban environments. *Int. J. Rob. Res.*, 30:5–32.

Durrant-Whyte, H. & Bailey, T. (2006). Simultaneous localization and mapping: part I. *IEEE Robotics & Automation Magazine*, 13(2):99–110.

Eliazar, A. & Parr, R. (2004). Dp-slam 2.0. In: *Robotics and Automation, 2004. Proceedings. ICRA '04. 2004 IEEE International Conference on*, volume 2, pages 1314–1320 Vol.2.

Eustice, R., Walter, M., & Leonard, J. (2005). Sparse extended information filters: Insights into sparsification. In: *IEEE Int. Conf. on Intelligent RObots and Systems*.

Eustice, R. M., Singh, H., & Leonard, J. J. (2006). Exactly Sparse Delayed-State Filters for View-based SLAM. *IEEE Trans. Robotics*, 22(6):1100–1114.

Fenwick, J., Newman, P., & Leonard, J. (2002). Cooperative concurrent mapping and localization. In: *Robotics and Automation, 2002. Proceedings. ICRA '02. IEEE International Conference on*, volume 2, pages 1810 – 1817 vol.2.

Fischler, M. A. & Bolles, R. C. (1981). Random sample consensus: A paradigm for model fitting with applications to image analysis and automated cartography. *Commun. ACM*, 24(6):381–395.

Frese, U. (2006). Treemap: An O(log n) algorithm for indoor simultaneous localization and mapping. *Autonomous Robots*, 21(2):103–122.

Gilbert, J. R., Moler, C., & Schreiber, R. (1992). Sparse matrices in matlab: Design and implementation. *SIAM Journal on Matrix Analysis and Applications*, 13:333–356.

Grimson, W. E. L. (1990). *Object Recognition by Computer: The Role of Geometric Constraints*. The MIT Press.

Grisetti, G., Grzonka, S., Stachniss, C., Pfaff, P., & Burgard, W. (2007a). Efficient Estimation of Accurate Maximum Likelihood Maps in 3d. In: *IROS*.

Grisetti, G., Rizzini, D. L., Stachniss, C., Olson, E., & Burgard, W. (2008). Online Constraint Network Optimization for Efficient Maximum Likelihood Mapping. In: *ICRA*.

Grisetti, G., Stachniss, C., & Burgard, W. (2009). Nonlinear constraint network optimization for efficient map learning. *Intelligent Transportation Systems, IEEE Transactions on*, 10(3):428 –439.

Grisetti, G., Tipaldi, G., Stachniss, C., Burgard, W., & Nardi, D. (2007b). Fast and accurate slam with rao-blackwellized particle filters. *Robotics and Autonomous Systems*, 55(1):30–38.

Handa, A., Chli, M., Strasdat, H., & Davison, A. (2010). Scalable active matching. In: *Computer Vision and Pattern Recognition (CVPR), 2010 IEEE Conference on*, pages 1546 –1553.

Hartley, R. (1997). In defense of the eight-point algorithm. *IEEE Transactions on pattern analysis and machine intelligence*, 19(6):580–593.

He, X., Zemel, R. S., & Carreira-Perpiñán, M. Á. (2004). Multiscale conditional random fields for image labeling. In: *Computer Vision and Pattern Recognition, IEEE Computer Society Conference on*, volume 2, pages 695–702. IEEE Computer Society.

Huang, S. & Dissanayake, G. (2007). Convergence and Consistency Analysis for Extended Kalman Filter Based SLAM. *IEEE Trans. Robotics*, 23(5):1036–1049.

Huang, S., Wang, Z., & Dissanayake, G. (2008a). Sparse local submap joining filters for building large-scale maps. *IEEE Trans. Robotics*, 24:1121–1130.

Huang, S., Wang, Z., Dissanayake, G., & Frese, U. (2008b). Iterated slsjf: A sparse local submap joining algorithm with improved consistency. In: *Proceedings of the Australasian Conference on Robotics and Automation.*

Ila, V., Porta, J., & Andrade-Cetto, J. (2010). Information-based compact pose slam. *Robotics, IEEE Transactions on*, 26(1):78 –93.

Kaess, M. & Dellaert, F. (2009). Covariance recovery from a square root information matrix for data association. *Robotics and Autonomous Systems*, 57(12):1198 – 1210. Inside Data Association.

Kaess, M., Johannsson, H., Roberts, R., Ila, V., Leonard, J., & Dellaert, F. (2011). iSAM2: Incremental smoothing and mapping with fluid relinearization and incremental variable reordering. In: *IEEE Intl. Conf. on Robotics and Automation, ICRA*.

Kaess, M., Ranganathan, A., & Dellaert, F. (2008). iSAM: Incremental Smoothing and Mapping. *IEEE Trans. on Robotics, TRO*, 24(6):1365–1378.

Kim, B., Kaess, M., Fletcher, L., Leonard, J., Bachrach, A., Roy, N., & Teller, S. (2010). Multiple relative pose graphs for robust cooperative mapping. In: *IEEE Intl. Conf. on Robotics and Automation, ICRA*, pages 3185–3192.

Klasing, K. (2010). *Aspects of 3D Perception, Abstraction, and Interpretation in Autonomous Mobile Robotics.* PhD thesis, Massachusetts Institute of Technology.

Klein, G. & Murray, D. (2007). Parallel tracking and mapping for small ar workspaces. In: *Proceedings of the 2007 6th IEEE and ACM International Symposium on Mixed and Augmented Reality*, ISMAR '07, pages 1–10. IEEE Computer Society.

Koller, D. & Friedman, N. (2009). *Probabilistic Graphical Models: Principles and Techniques.* MIT Press.

Konolige, K. & Agrawal, M. (2008). Frameslam: From bundle adjustment to real-time visual mapping. *Robotics, IEEE Transactions on*, 24(5):1066 –1077.

Konolige, K., Bowman, J., Chen, J., Mihelich, P., Calonder, M., Lepetit, V., & Fua, P. (2010a). View-based maps. *The International Journal of Robotics Research*, 29(8):941–957.

Konolige, K., Grisetti, G., K
"ummerle, R., Burgard, W., Limketkai, B., & Vincent, R. (2010b). Efficient sparse pose adjustment for 2d mapping. In: *Intelligent Robots and Systems (IROS), 2010 IEEE/RSJ International Conference on*, pages 22 –29.

Kümmerle, R., Grisetti, G., Strasdat, H., Konolige, K., & Burgard, W. (2011). g2o: A general framework for graph optimization. In: *Proc. of the IEEE Int. Conf. on Robotics and Automation (ICRA)*.

Lafferty, J., McCallum, A., & Pereira, F. (2001). Conditional Random Fields: Probabilistic models for segmenting and labeling sequence data. In: *Proc. 18th International Conf. on Machine Learning*, pages 282–289. Morgan Kaufmann, San Francisco, CA.

Leonard, J. & Feder, H. (2001). Decoupled stochastic mapping. *IEEE Journal of Oceanic Engineering*, 26(4):561–571.

Leonard, J. & Newman, P. (2003). Consistent, convergent and constant-time SLAM. In: *Int. Joint Conf. Artificial Intelligence*.

Liao, L., Fox, D., & Kautz, H. (2007). Extracting places and activities from gps traces using hierarchical conditional random fields. *The International Journal of Robotics Research*, 26(1):119.

Lim, E. H. & Suter, D. (2007). Conditional random field for 3d point clouds with adaptive data reduction. In: *Cyberworlds, 2007. CW '07. International Conference on*, pages 404 –408.

Lowe, D. G. (2004). Distinctive Image Features from Scale-Invariant Keypoints. *International Journal of Computer Vision*, 60(2):91–110.

Maimone, M., Cheng, Y., & Matthies, L. (2007). Two Years of Visual Odometry on the Mars Exploration Rovers. *Journal of Field Robotics*.

McDonald, J., Kaess, M., Cadena, C., Neira, J., & Leonard, J. (2011). 6-DOF Multi-session Visual SLAM using Anchor Nodes. In: *European Conference on Mobile Robotics, ECMR*.

Mei, C., Sibley, G., Cummins, M., Newman, P., & Reid, I. (2011). Rslam: A system for large-scale mapping in constant-time using stereo. *International Journal of Computer Vision*, 94:198–214. 10.1007/s11263-010-0361-7.

Montemerlo, M., Thrun, S., Koller, D., & Wegbreit, B. (2002). FastSLAM: A Factored Solution to the Simultaneous Localization and Mapping Problem. In: *Proceedings of the AAAI National Conference on Artificial Intelligence*. AAAI.

Montemerlo, M., Thrun, S., Koller, D., & Wegbreit, B. (2003). FastSLAM 2.0: An Improved Particle Filtering Algorithm for Simultaneous Localization and Mapping that Provably Converges. In: *Int. Joint Conf. Artificial Intelligence*.

Montiel, J. M. M., Civera, J., & Davison, A. J. (2008). Unified inverse depth parametrization for monocular SLAM. *IEEE Trans. Robotics*. To appear.

Murphy, K. P., Weiss, Y., & Jordan, M. I. (1999). Loopy belief propagation for approximate inference: An empirical study. In: *In Proceedings of Uncertainty in AI*, pages 467–475.

Mutambara, A. (1994). *Decentralized estimation and control with applications to a modular robot*. PhD thesis, University of Oxford.

Mutambara, A. & Al-Haik, M. (1997). State and information space estimation: a comparison. *American Control Conference, 1997. Proceedings of the 1997*, 4:2374–2375 vol.4.

Neira, J. & Tardós, J. D. (2001). Data association in stochastic mapping using the joint compatibility test. *IEEE Trans. Robotics and Automation*, 17(6):890–897.

Newman, P., Sibley, G., Smith, M., Cummins, M., Harrison, A., Mei, C., Posner, I., Shade, R., Schroeter, D., Murphy, L., Churchill, W., Cole, D., & Reid, I. (2009). Navigating, recognizing and describing urban spaces with vision and lasers. *The International Journal of Robotics Research*, 28(11-12):1406–1433.

Ni, K. & Dellaert, F. (2010). Multi-Level Submap Based SLAM Using Nested Dissection. In: *IEEE Int. Conf. on Intelligent RObots and Systems*.

Ni, K., Steedly, D., & Dellaert, F. (2007). Tectonic SAM: Exact, Out-of-Core, Submap-Based SLAM. In: *2007 IEEE Int. Conf. on Robotics and Automation*.

Nister, D. & Stewenius, H. (2006). Scalable recognition with a vocabulary tree. In: *Computer Vision and Pattern Recognition, 2006 IEEE Computer Society Conference on*, volume 2, pages 2161–2168.

Olson, E. (2009). Recognizing places using spectrally clustered local matches. *Robotics and Autonomous Systems*, 57(12):1157–1172.

Olson, E., Leonard, J., & Teller, S. (2006). Fast iterative optimization of pose graphs with poor initial estimates. In: *Proc. IEEE Int. Conf. Robotics and Automation*, pages 2262–2269.

Pandey, G., McBride, J. R., & Eustice, R. M. (2011). Ford campus vision and lidar data set. *The International Journal of Robotics Research*.

Paul, R. & Newman, P. (2010). FAB-MAP 3D: Topological mapping with spatial and visual appearance. In: *Proc. IEEE Int. Conf. Robotics and Automation*, pages 2649 –2656.

Pauly, M., Gross, M., & Kobbelt, L. (2002). Efficient simplification of point-sampled surfaces. In: *Visualization, 2002. VIS 2002. IEEE*, pages 163 –170.

Paz, L. M., Guivant, J., Tardós, J. D., & Neira, J. (2007). Data association in *O(n)* for divide and conquer SLAM. In: *Proc. Robotics: Science and Systems*.

Paz, L. M., Tardós, J. D., & Neira, J. (2008). Divide and conquer: Ekf slam in O(n). *IEEE Trans. Robotics*, 24(5):1107–1120.

Pearl, J. (1988). *Probabilistic reasoning in intelligent systems: networks of plausible inference*. Morgan Kaufmann Publishers Inc.

Piniés, P., Paz, L. M., Gálvez-López, D., & Tardós, J. D. (2010). Ci-graph simultaneous localization and mapping for three-dimensional reconstruction of large and complex environments using a multicamera system. *Journal of Field Robotics*, 27:561–586.

Pinies, P., Paz, L. M., & Tardos, J. D. (2009). Ci-graph: An efficient approach for large scale slam. In: *Robotics and Automation, 2009. ICRA '09. IEEE International Conference on*, pages 3913 –3920.

Quattoni, A., Wang, S., Morency, L.-P., Collins, M., & Darrell, T. (2007). Hidden conditional random fields. *Pattern Analysis and Machine Intelligence, IEEE Transactions on*, 29(10):1848–1852.

Ramos, F., Fox, D., & Durrant-Whyte, H. (2007). CRF-Matching: Conditional Random Fields for Feature-Based Scan Matching. In: *Robotics: Science and Systems (RSS).*

Ramos, F., Kadous, M. W., & Fox, D. (2008). Learning to associate image features with CRF-Matching. In: *ISER*, pages 505–514.

Ranganathan, A. & Dellaert, F. (2011). Online probabilistic topological mapping. *The International Journal of Robotics Research*, 30(6):755–771.

RAWSEEDS (2009). Robotics advancement through Webpublishing of sensorial and elaborated extensive data sets (project FP6-IST-045144). http://www.rawseeds.org/rs/datasets.

Scharstein, D. & Pal, C. (2007). Learning conditional random fields for stereo. In: *Computer Vision and Pattern Recognition, IEEE Computer Society Conference on*, volume 0, pages 1–8. IEEE Computer Society.

Sibley, G., Mei, C., Reid, I., & Newman, P. (2009). Adaptive relative bundle adjustment. In: *Robotics Science and Systems (RSS).*

Sivic, J. & Zisserman, A. (2003). Video Google: A text retrieval approach to object matching in videos. In: *Proceedings of the International Conference on Computer Vision*, volume 2, pages 1470–1477.

Smith, M., Baldwin, I., Churchill, W., Paul, R., & Newman, P. (2009). The new college vision and laser data set. *The International Journal of Robotics Research*, 28(5):595–599.

Smith, R., Self, M., & Cheeseman, P. (1988). A Stochastic Map for Uncertain Spatial Relationships. In: *Robotics Research, The Fourth Int. Symposium*, O. Faugeras & G. Giralt, ed., pages 467–474. The MIT Press.

Steder, B., Grisetti, G., & Burgard, W. (2010). Robust place recognition for 3d range data based on point features. In: *Proc. IEEE Int. Conf. Robotics and Automation*, pages 1400 –1405.

Strasdat, H., Davison, A., Montiel, J., , & Konolige, K. (2011). Double window optimisation for constant time visual SLAM. In: *IEEE International Conference on Computer Vision (ICCV)*.

Strasdat, H., Montiel, J. M. M., & Davison, A. (2010). Scale drift-aware large scale monocular slam. In: *Proceedings of Robotics: Science and Systems*.

Tappen, M. F., Liu, C., Adelson, E. H., & Freeman, W. T. (2007). Learning gaussian conditional random fields for low-level vision. In: *Computer Vision and Pattern Recognition, IEEE Computer Society Conference on*, volume 0, pages 1–8. IEEE Computer Society.

Tardós, J. D., Neira, J., Newman, P. M., & Leonard, J. J. (2002). Robust Mapping and Localization in Indoor Environments using Sonar Data. *Int. J. Robotics Research*, 21(4):311–330.

Thrun, S. (2002). Particle Filters in Robotics. In: *Proceedings of Uncertainty in AI (UAI)*.

Thrun, S., Burgard, W., & Fox, D. (2005). *Probabilistic Robotics*. The MIT Press.

Thrun, S. & Leonard, J. (2008). Simultaneous Localization and Mapping. In: *Springer Handbook of Robotics*, B. Siciliano & O. Khatib, ed., Springer Handbooks, chapter 37, pages 871–889. Springer.

Tipaldi, G. & Ramos, F. (2009). Motion clustering and estimation with conditional random fields. In: *Intelligent Robots and Systems, 2009. IROS 2009. IEEE/RSJ International Conference on*, pages 872 –877.

Törnqvist, D., Schön, T. B., Karlsson, R., & Gustafsson, F. (2009). Particle filter slam with high dimensional vehicle model. *J. Intell. Robotics Syst.*, 55(4-5):249–266.

Triggs, B., McLauchlan, P., Hartley, R., & andrew Fitzgibbon (2000). Bundle adjustment – A modern synthesis. In: *Vision Algorithms: Theory and Practice*, W. Triggs, A. Zisserman, & R. Szeliski, ed., LNCS, pages 298–375. Springer Verlag.

Valgren, C. & Lilienthal, A. J. (2007). SIFT, SURF and seasons: Long-term outdoor localization using local features. In: *Proceedings of the European Conference on Mobile Robots (ECMR)*, pages 253–258.

Valgren, C. & Lilienthal, A. J. (2010). Sift, surf & seasons: Appearance-based long-term localization in outdoor environments. *Robotics and Autonomous Systems*, 58(2):149 – 156. Selected papers from the 2007 European Conference on Mobile Robots (ECMR '07).

Williams, B., Cummins, M., Neira, J., Newman, P., Reid, I., & Tardós, J. (2009). A comparison of loop closing techniques in monocular slam. *Robotics and Autonomous Systems*.

Williams, B., Klein, G., & Reid, I. (2007). Real-time SLAM relocalisation. In: *Proc. International Conference on Computer Vision*.

Williams, S. B., Dissanayake, G., & Durrant-Whyte, H. (2002). An efficient approach to the simultaneous localisation and mapping problem. In: *Proc. IEEE Int. Conf. Robotics and Automation*, volume 1, pages 406–411.